INFORMATION TO USERS

The most advanced technology has been used to photograph and reproduce this manuscript from the microfilm master. UMI films the original text directly from the copy submitted. Thus, some dissertation copies are in typewriter face, while others may be from a computer printer.

In the unlikely event that the author did not send UMI a complete manuscript and there are missing pages, these will be noted. Also, if unauthorized copyrighted material had to be removed, a note will indicate the deletion.

Oversize materials (e.g., maps, drawings, charts) are reproduced by sectioning the original, beginning at the upper left-hand corner and continuing from left to right in equal sections with small overlaps. Each oversize page is available as one exposure on a standard 35 mm slide or as a 17″ × 23″ black and white photographic print for an additional charge.

Photographs included in the original manuscript have been reproduced xerographically in this copy. 35 mm slides or 6″ × 9″ black and white photographic prints are available for any photographs or illustrations appearing in this copy for an additional charge. Contact UMI directly to order.

Accessing the World's Information since 1938

300 North Zeeb Road, Ann Arbor, MI 48106-1346 USA

Order Number 8810702

Properties of stellar activity in F stars

Varsik, John Roger, Ph.D.

University of Hawaii, 1987

U·M·I
300 N. Zeeb Rd.
Ann Arbor, MI 48106

PLEASE NOTE:

In all cases this material has been filmed in the best possible way from the available copy. Problems encountered with this document have been identified here with a check mark __✓__.

1. Glossy photographs or pages _____
2. Colored illustrations, paper or print _____
3. Photographs with dark background _____
4. Illustrations are poor copy _____
5. Pages with black marks, not original copy _____
6. Print shows through as there is text on both sides of page _____
7. Indistinct, broken or small print on several pages ✓
8. Print exceeds margin requirements _____
9. Tightly bound copy with print lost in spine _____
10. Computer printout pages with indistinct print _____
11. Page(s) _____ lacking when material received, and not available from school or author.
12. Page(s) _____ seem to be missing in numbering only as text follows.
13. Two pages numbered _____. Text follows.
14. Curling and wrinkled pages ✓
15. Dissertation contains pages with print at a slant, filmed as received _____
16. Other _____

_____

_____

PROPERTIES OF STELLAR ACTIVITY IN F STARS

A DISSERTATION SUBMITTED TO THE GRADUATE DIVISION OF THE
UNIVERSITY OF HAWAII IN PARTIAL FULFILLMENT
OF THE REQUIREMENTS FOR THE DEGREE OF
DOCTOR OF PHILOSOPHY
IN ASTRONOMY
DECEMBER 1987

By
John Roger Varsik

Dissertation Committee:
James N. Heasley, Chairman
Thomas A. Schroeder
Barry J. LaBonte
Walter K. Bonsack
J. Patrick Henry

ACKNOWLEDGEMENTS

This dissertation would never have been possible without the help of many individuals. First of all I would like to thank Jim Heasley for providing support, advice and encouragement through all phases of this project. I would also like to thank Barry LaBonte for his insights into stellar activity, and Sidney Wolff for her expertise in stellar spectroscopy. Comments and suggestions from Pat Henry, Frank Orrall, Walter Bonsack, and Tom Schroeder are gratefully acknowledged. I would also like to thank Charlie Lindsey, Eric Pilger, and John MacKenty for much help and useful discussions.

I would especially like to thank the Canada-France-Hawaii Telescope Corporation for granting me observing time essential for the completion of this project. Steadily improving computing facilities were made possible by George Miyashiro, Richard Wolff, and Pui-Hin Rhoads. Valuable assistance during observations was provided by Bob Hlivak and Bill Heacox. This research was supported by existing grants from the National Science Foundation and by the ARCS Foundation.

Numerous friends and colleagues have supported me in other ways over the course of this work; it would be impossible to list them all here. Most of all, I would like to thank my parents, without whom this project would not have been possible, and who have never yet told me I should have studied engineering.

ABSTRACT

This dissertation is an investigation of the evolution of chromospheric activity in stars from F2 to G2 as measured by Ca II flux as a function of stellar age, for a large sample of nearby field stars. Ages are estimated from theoretical isochrones using Strömgren colors to obtain effective temperatures, absolute magnitudes, and metallicities. These data are combined with measurements from the literature for the Pleiades, Hyades, and Coma clusters, and allow chromospheric activity and rotation to be traced for stars with masses in the range 1.05 $M_{\odot}$ to 1.45 $M_{\odot}$.

The main-sequence F stars of solar composition with $M_{*} < 1.325 M_{\odot}$ follow an exponential chromospheric activity law, with an e-folding time of 2.04 Gyr. There appears to be little change in e-folding time with mass in these essentially solar-type stars. For $M_{*} \geq 1.325 M_{\odot}$ the change in activity with age is small but is consistent with an exponential dependence with an e-folding time of 3.12 Gyr. The exponential age dependence and slow change in the rate of decay of activity with mass are consistent with an overall quadrupole magnetic field as proposed by Gill and Roxburgh (1984), rather than the generally assumed radial field geometry. The majority of F stars appear similar in their activity–age behavior to G stars on the high activity side of the Vaughan-Preston gap. The number of solar-composition stars observed below the Vaughan-Preston gap was too small to come to any conclusions concerning any change in the activity–age relation.

However, when a sample of older late F stars below the Vaughan Preston gap somewhat below solar metallicity was examined, a different age dependence more like a power law was found. This is qualitatively consistent with the Gill and Roxburgh (1984) theory, which suggests that the geometry of the stellar magnetic field changes from quadrupole to dipole as a star crosses the Vaughan-Preston gap.

It has been suggested by Wolff, Boesgaard, and Simon (1986) that the lack of low activity early F stars indicates that there is another component of the chromospheric Ca II flux for stars with $M_* \geq 1.32 M_\odot$, which is independent of the magnetic field. However, it does not appear that purely acoustic heating can provide this component. If it is assumed that the "floor" in chromospheric activity seen in the early F stars is due to pure acoustic heating with acoustic flux proportional to T_{eff}^{11} as found by Stein (1981) then the amount of acoustic heating predicted for late F stars and in the Sun would be much greater than that which is observed.

The behavior of activity as a function of age for early F stars appears to be similar to that for late F and solar type stars, but with a somewhat longer decay time. These results suggest that acoustic heating does not provide the main energy source for activity in the low chromosphere in early F stars.

It has been predicted (Durney and Latour 1978) that the time required for significant angular momentum loss in F stars should increase by a large amount with increasing mass. This prediction is based on the assumption that the magnetic field in these stars is predominantly radial, and that the magnetic field is proportional to the angular velocity.

Observations do not agree with the radial field model. In fact, the $V \sin i$–age dependence for stars of solar composition appears best modeled by an exponential, and the observed e-folding time is slightly smaller for $M_* > 1.32 M_\odot$ than for $M_* < 1.32 M_\odot$. The observations are in better agreement with the theory of Gill and Roxburgh (1984) assuming a quadrupole magnetic field than with the standard radial field model.

Convective turnover times based on Ruciński and VandenBerg (1986) were estimated for each star. Tests of several rotation-convection parameters suggest that the best predictor of activity level in F stars is the dynamo number defined by Durney and Robinson (1982) $N_D = \Omega\tau_C(R_C/H_P)^{\frac{1}{2}}$. The relation between R'_{HK} and N_D appears best described by $R'_{HK} = 1.83 \times 10^{-6} N_D$ for solar-composition late F stars. Beyond $N_D \sim 30$ the activity level appears to saturate. The early F stars follow a similar but shallower relation. Comparison between the expected behavior for stars using this relationship and the quadrupole field geometry and observations yields good agreement for all stars above the Vaughan-Preston gap. The age–activity relations suggest that early F stars do not become old enough to cross the VP gap during their main-sequence lifetimes.

TABLE OF CONTENTS

LIST OF TABLES

LIST OF ILLUSTRATIONS

CHAPTER I

INTRODUCTION

The solar chromosphere is a region of gas above the visible surface of the Sun, approximately 10000 km thick. It is optically thin in nearly all visible wavelengths, and is only observed in visible light in the cores of strong lines such as Hα and Ca II H and K above the limb during solar eclipses or with a coronagraph. In the ultraviolet the chromosphere is seen in emission lines such as Si I 1682 Å. The ultraviolet continuum of the Sun shortward of 1525 Å comes from the chromosphere as well.

Solar astronomers have traditionally made a distinction between the "quiet" solar atmosphere and the "active" atmosphere, distinguished by the presence of sunspots, prominences, flares, and other short lived phenomena associated with the Sun's 22 year magnetic cycle. Over the past several decades astronomers have succeeded in observing the effects of similar activity in other stars. The most accessible indicator of activity used by stellar astronomers has been the emission strengths of the Ca II H and K line cores, which in stars similar to the Sun are believed to come from regions in the chromospheres of stars corresponding to solar plages, regions of enhanced brightness in Ca and many other chromospheric lines near sunspots. These plages are regions of enhanced chromospheric density caused by strong magnetic fields believed to be generated by an internal magnetic dynamo. In other stars the stellar disk cannot be resolved, but the strength of the line reversals seen in the spectrum from the entire star depends on the strength and coverage of the plages on the surface of the star.

The reversal of the core of the Ca II H and K lines was first noted by Schwarzschild and Eberhard (1913), and the first catalog of H and K line core strengths

was compiled by Joy and Wilson (1949). However, the dependence of Ca II line strength on age was first observed by Wilson (1963), who noted that the line strength of G0–K2 stars in young open clusters was greater than that seen in nearby field stars. Ever since that time, observers of activity in main sequence stars have concentrated on "solar type" stars in this spectral range. Skumanich (1972) placed this decay in activity with increasing age on a quantitative basis, and showed that Ca II activity appeared to be proportional to the rotational velocity of the star. Roberts (1974) showed that this relationship is plausible according to magnetic dynamo theory.

There are some indications that F stars, particularly those earlier than $B-V$ = 0.45, show a substantially different type of activity from the solar-type stars. The modulation of Ca II H and K flux (Baliunas *et al.* 1984), which has allowed the rotational periods of many slowly rotating G and K stars to be measured, is not seen in these objects. Other major differences include the lack of a $V \sin i$–X-ray flux relationship (Walter 1983) a $V \sin i$–UV flux relationship (Walter and Linsky 1985), or solar-type activity cycles (Vaughan 1980). On the other hand, there is flux present from these early F stars in X-rays, UV, and in the Ca II H and K lines which would not be present in completely inactive stars.

Today one can observe the effects of stellar activity in the entire spectral range from radio using the VLA to X-rays using spacecraft. In fact, for detailed analysis of stellar activity spectral lines in the ultraviolet, such as C IV 1548, 1551 Å (actually a transition region line), accessible with the *IUE* spacecraft are preferred over the Ca II lines because of the much lower continuum background. However, if the effects of the continuum and photospheric contributions are carefully allowed for the Ca II lines can be as useful as any other feature as a chromospheric activity

monitor. In fact, for survey work they are much more useful, since large ground-based telescopes can observe much fainter objects than spacecraft, and are much more accessible for such projects.

The most significant such survey project has been the Mt. Wilson HK survey (Wilson 1968, Vaughan and Preston 1979, Baliunas *et al.* 1984, Duncan 1983, 1985) an ongoing effort to monitor Ca II activity levels in several hundred nearby stars. The Mt Wilson S index, the ratio of the HK core flux to the flux of the surrounding continuum, is the basic product of this work. However, because of the higher photospheric temperatures in the F stars, the value of the S index is smaller than in later-type stars, which initially discouraged interest in F-star activity. In these F stars, Ca II chromospheric emission generally makes its appearance known by filling in, to a varying degree, the cores of the H and K lines, rather than producing obvious emission reversals. Although the Ca II line center contrast in F stars at first glance appears very low compared to later type stars, when corrected for the difference in photospheric line equivalent width it is in fact as large a fraction of the total luminosity of the star as it is in later type objects.

Because of the differences already noted between chromospheric activity in F stars and in those of solar type, it is apparent that we cannot expect to have a complete understanding of stellar activity without studying these objects. A first step, then, in such a study would be the determination of how chromospheric activity and rotation, presumably the source of the magnetic dynamo generating the activity, depend on each other and on the age of the star. Can a Skumanich-like relation be determined for these objects?

While young stars (generally less than 1 Gyr in age) of known age can be observed in nearby open clusters, determining the age dependence of activity and

rotation for F stars as well as later types requires ages older than can be obtained from nearby clusters. Generally, studies of chromospheric activity and rotation in solar-type stars have used age estimates based on Li abundances (Herbig 1965; van den Heuvel and Conti 1971; Duncan 1981). This method is based on the gradual destruction of Li in the convective zones of G stars. This process does not take place (at least not in the same way) in F stars.

However, F stars evolve sufficiently rapidly in the H-R diagram that provided that a means of estimating effective temperatures, luminosities, and compositions is available, it may be possible to estimate the mass and age of field F stars between the zero-age main sequence (ZAMS) and the main sequence turnoff point. Such a means is available for F stars in the Strömgren photometric indices.

Chapter II discusses the photometric age estimates for individual field stars, and compares ages based on Strömgren indices to ages based on absolute luminosities from parallaxes, cluster main sequence fitting, and lithium surface abundances. Good agreement is shown between the photometric estimates and parallax-based and cluster ages. Agreement is also seen between the photometric ages and those based on Li abundances where those methods overlap, if the same effective temperature scales are used. The photometric age estimates in this chapter are based on the stellar isochrones of Ciardullo and Demarque (1977).

Chapter III discusses the relation between Ca II activity in F stars and age. The models used here and in the remainder of the thesis are those of VandenBerg (1983). As stated in Chapter III, these models incorporate improved opacities and better treatment of the convective zone and surface layers than the Ciardullo and Demarque models. These factors are very significant in obtaining a good match between theoretical and observed quantities. The $Y = 0.25$, $Z = 0.0169$,

$\alpha = 1.6$ model of VandenBerg provides a much closer fit to the solar luminosity, temperature, and age than the Ciardullo and Demarque models. Chapter III shows that for stars of solar composition, the decay of activity with increasing age is best modeled by an exponential law for both low and high masses.

Chapter 4 explains a new method for obtaining measurements of the projected stellar rotational velocity $V \sin i$ using autocorrelation analysis. This method has several advantages over others of similar precision. It uses line broadening information from a number of spectral lines at once, reducing the uncertainty below that which would be obtained for a single line. It does not require any modification of a standard coudé spectrograph, and could also be used with an echelle for greater spectral coverage. The reduction process is fairly straightforward, although measurements of rotation velocity standards are required for calibration.

Chapter 5 combines rotational velocity measurements from the literature with those determined using the method of Chapter 4 in order to determine the relationships between age, activity, and rotation in F stars.

CHAPTER II

AGE ESTIMATES FOR F2–G2 MAIN-SEQUENCE FIELD STARS

1. Background

An important goal of stellar evolution modeling theory is to estimate the ages of stars. All methods of stellar age estimation are ultimately based on the comparison of the observed properties of stars to theoretical models. The fitting of stellar models to individual field stars generally has been avoided because of the difficulty in obtaining accurate absolute magnitudes for stars located beyond the immediate neighborhood of the Sun. Difficulties multiply on the lower main sequence (G stars and later) due to the slow evolution of these stars, and the position of their evolutionary tracks parallel to the main sequence for billions of years. In order to increase the accuracy of the luminosity determinations galactic clusters can be used. Fitting an isochrone to a cluster in which all stars are assumed to have formed simultaneously increases the confidence of the age estimate by reducing the effects of the errors in fitting individual stars. For many purposes, the relative rarity of old open clusters causes problems for the study of stellar properties and their age dependence. Clusters older than $\sim$2 billion years (the age of NGC 752) are generally distant and difficult to observe. Still, for purposes such as the study of solar-like activity in stars, one would like to have stars with a wide range of known ages.

The usual approach in studies of stellar activity in main-sequence stars has been to use some property other than the absolute magnitude, which is considered to vary with age. Most frequently this has been the lithium abundance, an approach first suggested by Herbig (1965) and by van den Heuvel and Conti (1971).

Lithium is easily destroyed at temperatures reached in (or just below) the convective envelopes of late-type stars. Thus, assuming all stars reach the zero-age main sequence (ZAMS) with a similar Li abundance, the measured Li abundance should be a function of the age and mass (and thus the depth and temperature of the convective zone) of the star. The lithium abundance method is especially attractive for G stars, since the range of Li abundance seen in these stars is large and more direct luminosity fitting methods fail for stars later than G2 due to the slow luminosity evolution expected in such stars.

Ages based on lithium abundance must be calibrated with stars of known age. For young stars this calibration depends on measurements of the young Pleiades and Hyades clusters and the Ursa Major association (Soderblom 1983). The calibration for older stars is based on measurements of the lithium abundance of the Sun, however Herbig (1965) has suggested that the Sun may not be a typical star for its age in regard to its lithium abundance. This possibility, also suggested by Skumanich (1972), indicates that lithium-age calibrations based on the Sun's lithium abundance may possibly not be valid. Nevertheless, several studies using Li-based age estimates of main-sequence field star ages have been made, for example, the studies of Ca II emission and lithium abundance by Duncan (1981) and the study of lithium abundance and stellar rotation by Soderblom (1982, 1983).

Recent results have shown some inconsistencies in the lithium abundance-age relation. Duncan (1981) studied the variation of the Ca II K line core emission flux using lithium-derived ages. He found several results which appear inconsistent with the assumptions behind the Li-age calibration. Some of the stars he observed (his group C stars) showed low Ca II line core emission (indicating an older age),

but high Li abundance (indicating young age). Some of these stars show large motion perpendicular to the galactic plane, indicating high age. The hotter stars in his sample (with $T_{eff} > 6200$ K) did not behave in the way expected if Li is simply correlated with age. Instead of having a uniform high Li abundance, a wide range in Li abundance was seen in these stars, indicating that there are other depletion mechanisms besides the one operating in later spectral types.

Spite and Spite (1982), considering mainly the same data set as Duncan (1981) and Soderblom (1982), made crude age estimates using the isochrones of Hejlesen (1980). They found that the Population I field stars fell into two groups, those with high Li abundance as in the Hyades cluster, and those with low Li abundance, as in the Sun. The mean ages for both subsamples were the same, and thus the age dependence of Li in older field stars was again called into question.

This chapter will examine ages obtained from direct isochrone modeling in luminosity and effective temperature, compare these estimates with ages determined from lithium abundances, and examine the Ca II activity-age relations. For stars in the spectral range F2 to G2 this should be possible, provided a method of obtaining the effective temperature, luminosity, and composition of an individual field star can be found. Such a technique would use the stellar properties best explained by current stellar evolution models–those which depend less strongly on the details of convection and circulation responsible for the Li abundance (and the Ca II core emission) in such stars. Of course, this method would be limited in that stars later than spectral type G2 could not be handled.

Twarog (1980) has developed such a direct method of placing stars in the theoretical HR diagram using uvbyβ colors. This method yields T_{eff} based on β or on $b-y$, [Fe/H] based on the δm_1 index, and δM_V, the distance in magnitudes

above the ZAMS, from the δc_1 index. Here δm_1 and δc_1 are the standard color differences defined as $\delta m_1 = m_{1\ std} - m_{1\ obs}$ and $\delta c_1 = c_{1\ obs} - c_{1\ std}$, with $c_1 = (u-v)-(v-b)$ and $m_1 = (v-b)-(b-y)$. In the present chapter this method will be applied to nearby field stars. To confirm the value of this method for dating individual stars and estimating the magnitude of the uncertainties involved, Strömgren photometry for the open cluster NGC 752 will be used to obtain age estimates for individual cluster stars, which will be compared to a cluster age from main-sequence fitting. Also, for those field stars with parallaxes available from the Gliese (1969) catalog, age estimates will be obtained by fitting isochrones to effective temperatures from β and luminosities from M_{bol} determined from stellar parallaxes. The age estimates based on δc_1 derived luminosities can then be compared to Li-abundance age estimates made by Duncan (1981). The dependence of Ca II line core emission on age will also be briefly discussed.

2. Age Determination Method

a. Program Stars and Photometry

Strömgren photometry for all field stars used in this study has been obtained from the catalog of Hauck and Mermilliod (1980). In all cases the stars had $0.22 < b-y < 0.41$ so that the δm_1-metallicity calibration of Crawford and Perry (1976) could be applied. However, it was later decided that stars with $T_{eff} < 6000$ K and $\log(L/L_\odot) < 0.25$ had to be excluded due to the large age uncertainty in such stars. The field star sample included 61 stars. Of these, 59 had Ca II and Li measurements from Duncan (1981), and for most of these Duncan has also made Li age estimates. Two additional stars were selected from the Gliese catalog in

order to have a larger sample for the comparison of δc_1-derived ages with ages based on luminosities from parallaxes. Absolute magnitude for those stars with parallaxes came from the Gliese (1969) catalog. Bolometric corrections were taken from Schlesinger (1969).

As a further demonstration of Twarog's age dating method, Strömgren data for 29 stars in NGC 752 were obtained from Crawford and Barnes (1970) and dereddened according to the method described by the authors.

b. Isochrone Fitting

The most direct method of age estimation is the comparison of effective temperature and luminosity observations to the predictions of models of the correct composition. As we have seen, there are difficulties in the direct approach, especially in the determination of M_{bol} for stars which have small parallaxes.

As in Twarog's (1980) dating procedure, the effective temperature for the cluster stars were obtained from Hβ photometry. This has the advantages of being essentially independent of reddening, metallicity, and surface gravity for F and early G stars. These properties make the Hβ index preferable to the $b-y$ index so long as the T_{eff}–Hβ calibration is valid. The temperature calibration used here is that of Hauck and Magnenat (1975), based on the Oke and Conti (1966) T_{eff} calibration for $B-V$.

For the field star sample, effective temperature was obtained from the b—y color for each star. A number of the field stars have $b-y$ colors redder than 0.36. For these stars the Hβ line becomes too weak for reliable temperature determination (Strömgren 1966) so for consistency $b-y$ was used for the entire field star sample.

Reddening for these nearby stars is extremely small. In order to select the correct model isochrone for comparison with a star, the composition of the star must be known. As *ubvyβ* measurements are available for all of the stars in the data sample of this chapter, it is simplest to use the Strömgren δm_1 index to estimate the metallicity for these stars. In this way, all [Fe/H] estimates will be on the same scale. For consistency with the T_{eff} determinations, calibrations based on $H\beta$ will be used for the cluster stars, while calibrations based on $b-y$ will be used for the field stars. The choice of [Fe/H] calibration is important, however. If [Fe/H] values obtained spectroscopically (Morel *et al.* 1976) are plotted against δm_1 substantial scatter (0.3 in [Fe/H]) is seen. Calibrations from Crawford and Perry (1976) and Duncan (1981) were examined, but the equations from Crawford and Perry (1976)

$$[\mathrm{Fe/H}] = 0.15 - 11\delta m_1(\beta) \qquad 1a$$

for the cluster stars, and

$$[\mathrm{Fe/H}] = 0.15 - 13\delta m_1(b-y) \qquad 1b$$

for the field stars will be used here, as they appear to fit the spectroscopic data better.

The absolute magnitude calibration for the cluster stars was done as in Twarog (1980). Using the Strömgren δc_1 index, Crawford (1975) determined

$$M_V = M_V(ZAMS,\beta) - f\delta c_1(\beta) \qquad 2$$

where

$$f = 9 + 20(2.720 - \beta) \qquad 3$$

and where $M_V(ZAMS)$ is Crawford's empirically determined main sequence. Following Twarog (1980) the separation from the ZAMS, $\delta M_V = \delta M_V(ZAMS) - M_V$

will be used. The luminosity L_* will be found by setting $\delta M_{bol} \approx \delta M_V$. Then $\log(\delta L/L_\odot) = \delta M_{bol}/2.5$, and $L/L_\odot = (L_{ZAMS,T}/L_\odot) + (\delta L/L_\odot)$, avoiding uncertainties in the empirically calibrated ZAMS of Crawford and reducing the effects of metallicity differences between the empirical ZAMS and the particular star under consideration. For the field stars the similar equation (Crawford, 1975)

$$M_V = M_V(ZAMS, b-y) - f[\delta c_1(b-y) + 1.5\delta m_1(b-y)] \qquad 2a$$

will be used, with $f = 10.0$.

The model isochrones used here are those of Ciardullo and Demarque (1977) for the compositions $Y = 0.30$; $Z = 0.004$, 0.010, and 0.040. The isochrones were derived assuming the mixing length to scale height ratio $\alpha = 1.0$ in the convection zone. I have used only $Y = 0.30$ throughout for several reasons. First, it is consistent with measurements in solar prominences (Heasley and Milkey 1978) and in young Population I stars (Norris 1971). Second, from Twarog's results on the galactic age- metallicity relation, it appears that the relative ages of stars are not greatly affected by varying the helium abundance used to model them, at least in the sense of making one star previously thought older than another appear younger than the other. Also, because the luminosity is determined relative to a model ZAMS, the effect on the age estimates of the movement of the isochrones in the temperature-luminosity plane is reduced.

The value of α has a large effect on the positions of model isochrones in the H-R diagram for late-type stars. Varying α essentially varies the depth of the convection zone for the model star. For example, Perrin *et al.* (1977) estimated the age of the oldest halo stars in their solar neighborhood sample, HD 19445 and HD 140283, as being greater than 25 Gyr, using $\alpha = 2.0$. This is clearly in conflict with virtually all recent estimates of the age of the universe. On the

other hand, using the values of $\log T_{eff}$ and M_{bol} given by Perrin *et al.* and the $\alpha = 1.0$ isochrones for the same metal abundance by Ciardullo and Demarque (1977), one obtains an age of about 16 Gyr for these stars. Ciardullo and Demarque (1979) describe a method for adjusting the value of α in their isochrones without recomputing their stellar models. Using this approach, the age of these two stars can be estimated for different values of α. Using $\alpha = 2.0$, the age becomes roughly 22 Gyr; with $\alpha = 1.5$ one obtains about 18 Gyr. The models used by Perrin *et al.* still yield ages somewhat older than the Ciardullo and Demarque models, but varying removes most of the discrepency.

In order to match the observed run of differential rotation in the Sun (smooth monotonic decrease of rotational velocity from equator to poles) recent models of differential rotation in the Sun (Gilman 1981) require that the stellar rotation time (the inverse of the angular frequency) be less than the convective turnover time. This convection turnover time depends on the ratio of the mixing length to the convective velocity at the base of the convective zone. Using a value of the convective velocity derived from a model of the convective zone described in Durney and Latour (1978), Gilman found that his solar differential rotation model required $\alpha \geq 2.0$ to match observations. If the convective velocity is actually somewhat lower than Gilman's value then a smaller value of α could also provide adequate agreement. VandenBerg (1983) was able to fit globular clusters of widely varying metallicities with model isochrones with $\alpha = 1.6 \pm 0.1$. In more recent work VandenBerg and Bridges (1984) have shown that young galactic clusters are best fit by $\alpha = 1.5$ using their model isochrones. Clearly the best value of α is probably greater than one, the value used in this chapter, but less than two (unless the Universe is really more than 25 Gyr old), and is most likely near 1.5. In future work more up-to-date isochrones will be used. It should be

pointed out that near the main sequence the main effect of a change in α on the theoretical isochrones is a shift to higher T_{eff} ($\Delta T_{eff} \approx 50$ K for a change in α from 1.0 to 1.5 on the main sequence (Ciardullo and Demarque 1979)) and this change is largely compensated for by the Hβ–logT_{eff} calibration used (Hauck and Magnenat 1975), which yields slightly cooler temperatures than others (e.g. Bessell 1979). The effect of metallicity on age estimates cannot be overlooked. Figure 1 shows isochrones at 0.5, 1.0, and 3.0 Gyr for three different compositions: $Z = 0.004$, $Z = 0.010$, and $Z = 0.020$. The size of the (1σ) uncertainties in effective temperature and luminosity (see below) are also shown.

An interpolation program has been developed in order to generate model isochrones not available in Ciardullo and Demarque (1977). The interpolation is based on the assumption that for small changes logT_{eff}, log($L/L_{\odot}$), log$M$, log$Z$, and log$A$ (where M is the mass and A is the age of the star) are approximately linearly related. Sets of isochrones have been computed for $Y = 0.30$; $Z = 0.0055$, 0.0080, 0.0120, 0.0150, 0.0200, 0.0250, and 0.0325.

Fitting of the *ubvyβ* data for individual stars in NGC 752 as well as in the field is done as in Twarog (1980), except for the use of $b-y$ instead of β as the temperature indicator for the field stars, as noted above. The composition is found from the δm_1 measurements. An age is first found for the star using isochrones most closely matching the value of Z found from δm_1. For this metallicity the two individual isochrone curves which most closely match the calculated logT_{eff} and log($L/L_{\odot}$) for the star are found. The age estimate for the star at this metallicity value is then found by linear interpolation in logT_{eff} at constant log($L/L_{\odot}$) if the star is at or below the main-sequence turnoff for the older isochrone curve. If the star is above this point the interpolation is in log($L/L_{\odot}$) at constant logT_{eff}.

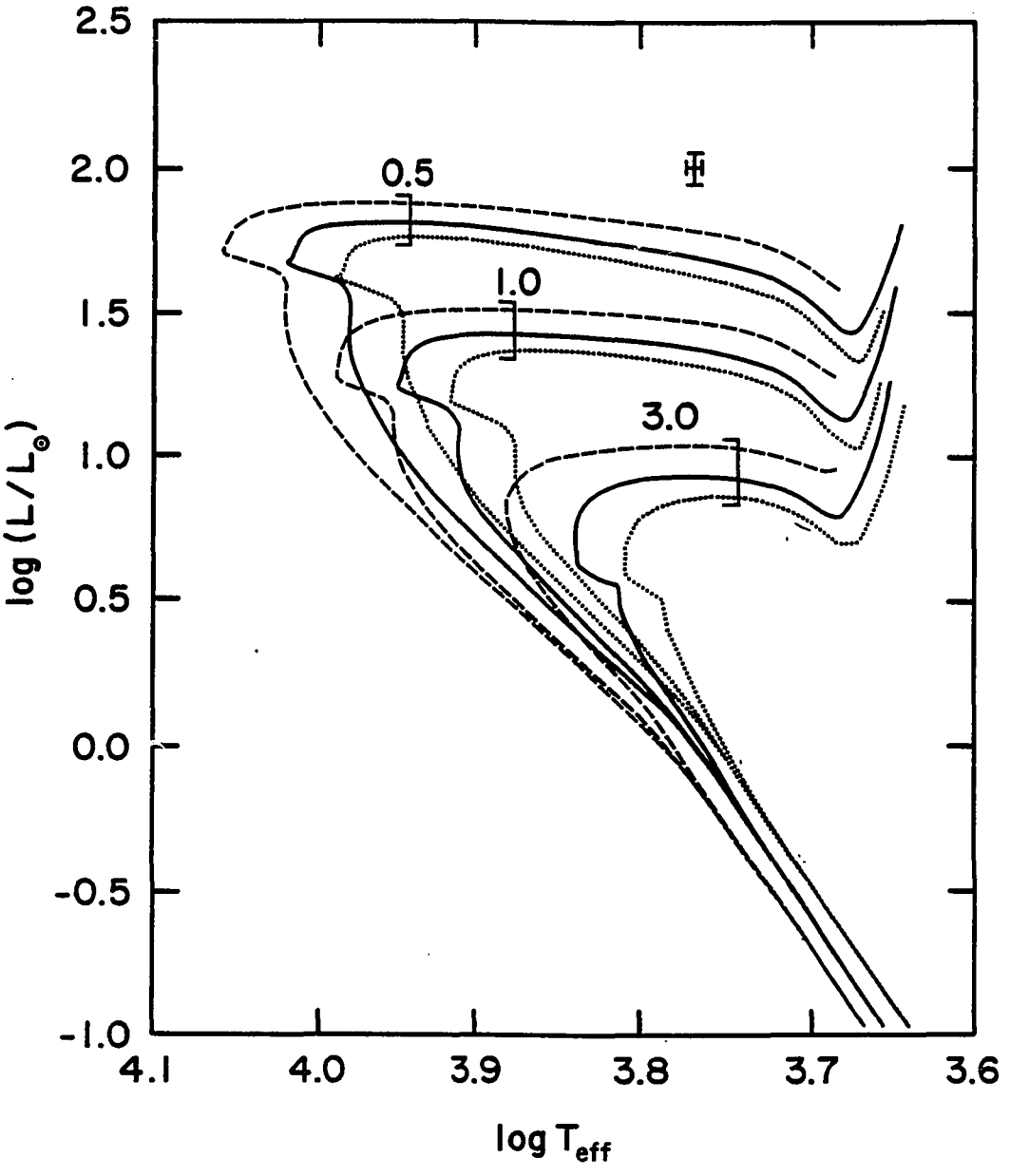

Figure 1. Isochrones from Ciardullo and Demarque (1977) for 0.5, 1.0, and 3.0 Gyr with $Y = 0.30$. Dashed curves have $Z = 0.004$, solid curves have $Z = 0.01$, and dotted curves have $Z = 0.02$. A 1σ error box resulting from uncertainties in δc_1 and β is shown.

This age estimate is called the nominal age (A^N) . Then age estimates are made in the same way at metallicities which bracket the value measured for the star. The final age estimate is found by interpolating in metallicity between the bracketing values using the Z derived from the photometry. Age estimates for NGC 752 are given in Table 1 and for the field stars in Table 2. Table 3 gives ages based on Li abundance from Duncan (1981) and ages derived using the luminosity obtained from trigonometrically determined M_{bol}, where available.

c. Age Uncertainties

The uncertainty in the photometric colors for a single star measurement will have two effects on the age determination. First, it results in uncertainty in the position in the HR diagram. This is due to uncertainty in β or $b-y$ affecting the effective temperature and uncertainty in δc_1 affecting the luminosity. Second, uncertainty in m_1 affects the metallicity estimate, introducing possible error in the choice of the set of isochrones used to model the star.

The data in the Hauck-Mermilliod catalog are homogenized, mean values compiled from all available sources. No uncertainties are given for individual stellar colors. Therefore typical mean uncertainty values were estimated, based on Crawford (1975), one of the sources for the Hauck-Mermilliod catalog. There, the mean errors for one observation of a star were: $b-y$, ± 0.010; m_1, c_1, and β, ± 0.012. Three observations were made of each star, yielding uncertainties of ± 0.006 for $b-y$ and ± 0.007 for m_1, c_1, and β. Since the data in the Hauck-Mermilliod catalog are mean values, we adopted these uncertainties as typical of good $ubvy\beta$ measurements.

Table 1

NGC 752 Age Estimates

Star	β	δc_0	δm_0	δM_V	[Fe/H]	T_{eff} (K)	Age (Gyr)
(1)	(2)	(3)	(4)	(5)	(6)	(7)	(8)
58	2.699	0.089	0.015	0.843	−0.01	6690	2.5±0.7
61	2.700	0.134	0.009	1.260	0.05	6700	2.1 0.3
62	2.694	0.027	0.016	0.257	−0.03	6650	1.4 0.9
66	2.643	0.080	0.025	0.843	−0.12	6200	4.4 0.6
88	2.646	0.027	0.013	0.283	0.01	6220	1.9 1.1
96	2.714	0.144	0.000	1.313	0.15	6830	1.5 0.7
105	2.684	0.185	0.009	1.798	0.05	6550	1.8 0.6
126	2.676	0.180	0.022	1.778	−0.10	6480	2.1 0.5
135	2.682	0.030	0.003	0.293	0.12	6530	1.3 0.6
139	2.664	0.031	0.046	0.314	−0.35	6370	3.2 1.9
171	2.672	0.197	0.008	1.962	0.06	6440	1.7 0.2
187	2.687	0.064	0.019	0.618	−0.06	6480	2.4 1.0
189	2.684	0.036	0.017	0.350	−0.04	6550	1.9 1.0
196	2.677	0.157	−0.008	1.543	0.24	6490	1.6 0.6
197	2.670	0.033	0.018	0.330	−0.05	6420	2.0 1.0
205	2.684	0.078	0.006	0.758	0.08	6550	2.3 0.9
206	2.666	0.163	0.019	1.643	−0.06	6390	2.2 0.3
217	2.689	0.147	0.007	1.414	0.07	6600	2.0 0.2
218	2.673	0.150	0.018	1.496	−0.05	6450	2.5 0.5
222	2.713	0.023	0.006	0.210	0.09	6820	0.9 0.5
234	2.698	0.046	0.022	0.434	−0.09	6680	2.0 0.8
235	2.659	0.003	0.010	0.036	0.04	6330	$<$ 1.1
238	2.658	0.193	0.026	1.976	−0.13	6320	2.2 0.5
254	2.705	0.102	0.009	0.949	0.05	6750	2.3 0.4
259	2.688	0.028	0.016	0.270	−0.02	6590	1.5 1.0
261	2.663	0.001	0.003	0.015	0.12	6360	$<$ 0.9
263	2.707	0.076	−0.006	0.704	0.21	6770	1.8 0.5
266	2.694	0.012	0.011	0.114	0.03	6650	0.8 0.6
300	2.684	0.165	0.016	1.604	−0.03	6550	2.1 0.2

NOTES.

Column (1): NGC 752 members from Heinemann (1926).

Column (2): Strömgren β index from Hauck and Mermilliod (1980).

Column (3) and (4): Strömgren luminosity and metallicity indices using β to find the ZAMS values.

Column (5): Estimated magnitude difference between the star and the ZAMS.

Column (6): Metallicity estimated from δm_0.

Column (7): Effective temperature from β.

Column (8): Photometric age estimates for individual stars.

Table 2

Observed Parameters for Field Star Age Comparisons

Name	HR	$b-y$	δc_1	δm_1	[Fe/H]	T_{eff} (K)	R_K $\times 10^{-6}$	$\log N_{Li}$ Observed	Estimated	Adjusted
(1)	(2)	(3)	(4)	(5)	(6)	(7)	(8)	(9)	(10)	(11)
6 Cet	33	0.328	0.035	0.053	−0.54	6110	< 3.9	2.51		
ϕ^2 Cet	235	0.334	0.003	0.029	−0.23	6080				
	244	0.346	0.064	−0.003	0.19	6000	< 5.5	< 1.67	2.2±0.3	< 1.54
υ And	458	0.344	0.059	0.010	0.02	6020	< 4.9	2.18	2.1 0.3	1.98
α Tri	544	0.316	0.115	0.023	−0.15	6180	21.4	1.92		
	672	0.368	0.083	0.011	0.01	5870	< 2.3	2.57	1.3 0.5	2.54
ϵ Cet	781	0.297	0.036	0.015	−0.04	6280	< 7.7	2.13		
	784	0.331	−0.003	0.016	−0.06	6090	13.2	2.86	2.5 0.3	2.87
θ Per	799	0.326	0.000	0.017	−0.08	6120	< 4.9	2.48	2.6 0.3	2.54
τ^1 Eri	818	0.320	0.025	0.013	−0.02	6160	16.9	2.13		
94 Cet	962	0.361	0.095	0.013	−0.02	5910	< 6.7	< 1.75	1.4 0.4	< 1.47
10 Tau	1101	0.360	0.045	0.022	−0.14	5920	< 4.6	2.25	1.1 0.5	2.16
	1249	0.321	−0.009	0.013	−0.02	6150				
50 Per	1278	0.334	0.010	0.005	0.08	6080	21.0	2.62		
π^3 Ori	1543	0.298	−0.003	0.010	0.02	6280	14.4	2.57		
68 Eri	1673	0.300	0.034	0.030	−0.23	6270				
λ Aur	1729	0.389	0.067	0.005	0.08	5740	< 8.3	< 1.57	0.0 0.9	< 1.09
γ Lep A	1983	0.317	0.019	0.025	−0.18	6170	< 7.5	2.54	2.6 0.2	2.50
74 Ori	2241	0.284	−0.002	0.018	-0.08	6350	13.5	< 2.30		
ξ Gem	2484	0.288	0.119	0.005	0.09	6330	17.1	< 2.19		
63 Gem	2846	0.286	0.030	0.005	0.08	6340		< 2.39		
α CMi	2943	0.272	0.069	0.003	0.11	6410	< 7.6	< 1.95		
μ^2 Cnc	3176	0.406	0.125	0.015	−0.04	5640	< 4.2	2.23	0.0 1.0	2.07
18 Pup	3202	0.338	0.037	0.039	−0.35	6050	< 6.3	< 1.93		
	3499	0.336	0.002	0.002	0.12	6060	22.3	2.90		
	3579	0.286	0.063	−0.002	0.17	6340	9.2	< 2.13		

Table 2 (Continued) Observed Parameters for Field Star Age Comparisons

Name	HR	$b-y$	δc_1	δm_1	[Fe/H]	T_{eff} (K)	R_K $\times 10^{-6}$	$\log N_{Li}$ Observed	Estimated	Adjusted
(1)	(2)	(3)	(4)	(5)	(6)	(7)	(8)	(9)	(10)	(11)
τ^1 Hya	3759	0.296	0.029	0.010	0.03	6290	11.3	< 2.10		
θ UMa	3775	0.314	0.074	0.025	−0.18	6190	< 3.0	3.09		
	3862	0.338	0.016	0.023	−0.15	6050	7.3	2.35	2.1±0.3	2.32
	3881	0.390	0.087	0.009	0.04	5740	< 4.9	< 1.69	0.1 0.8	< 1.43
40 Leo	4054	0.297	0.042	0.003	0.11	6280	5.9	< 1.67		
89 Leo	4455	0.297	0.006	0.002	0.13	6280	10.8	2.68		
β Vir	4540	0.354	0.076	0.006	0.07	5960	< 5.9	< 1.90	1.7 0.4	< 1.27
α Com AB	4968/9	0.309	0.012	0.027	−0.20	6220	15.9	< 2.37		
53 Vir	4981	0.313	0.083	0.031	−0.25	6200	< 6.5	3.23		
59 Vir	5011	0.376	0.072	0.013	−0.01	5820	22.8	2.92	0.4 0.7	2.45
τ Boo	5185	0.319	0.057	0.001	0.14	6160	8.1	2.35		
η Boo	5235	0.376	0.165	0.001	0.14	5820	< 6.2	< 1.75	1.7 0.4	< 0.83
ι Vir	5338	0.341	0.094	0.025	−0.17	6040	8.5	< 1.93		
θ Boo	5404	0.334	0.056	0.029	−0.23	6080	15.4	< 2.15		
α^1 Lib	5530	0.262	0.011	0.016	−0.05	6450	< 8.2	3.20		
45 Boo	5634	0.285	0.011	0.006	0.07	6340	8.6	< 2.30		
5 Ser	5694	0.349	0.081	0.018	−0.09	5990	4.0	2.15	1.9 0.3	1.57
λ Ser	5868	0.385	0.053	0.010	0.02	5770	< 5.5	< 1.70	0.4 0.9	< 1.25
γ Ser	5933	0.319	0.019	0.029	−0.23	6160	< 5.2	< 1.91		
θ Dra	5986	0.354	0.123	0.019	−0.10	5960		< 2.25		
18 Sco	6060	0.397	0.054	−0.005	0.22	5690	8.1	1.41	0.8 0.9	1.04
ζ Her	6212	0.415	0.138	0.019	−0.10	5600	< 8.3	< 1.40	0.0 1.0	< 0.72
11 Aql	7172	0.350	0.112	0.018	−0.08	5980	7.5	< 1.66		
	7354	0.309	0.028	0.040	−0.37	6220	11.9	< 2.20		
	7451	0.320	0.040	0.034	−0.30	6160	< 2.7	2.87		

Table 2 (Continued) Observed Parameters for Field Star Age Comparisons

Name	HR	$b-y$	δc_1	δm_1	[Fe/H]	T_{eff} (K)	R_K $\times 10^{-6}$	$\log N_{Li}$ Observed	Estimated		Adjusted
(1)	(2)	(3)	(4)	(5)	(6)	(7)	(8)	(9)	(10)		(11)
	7496	0.298	0.088	0.012	−0.01	6280	15.0	< 2.04			
16 Cyg A	7503	0.410	0.103	0.011	0.01	5610	< 6.9	< 1.50	0.0	1.1	< 0.77
17 Cyg A	7534	0.316	0.049	0.024	−0.16	6180	< 5.0	2.37			
o Aql	7560	0.356	0.069	0.006	0.07	5940	< 4.9	2.14	1.6	0.4	1.78
	7793	0.338	−0.016	0.025	−0.17	6050	9.0	2.29	2.5	0.3	2.39
ψ Cap	7936	0.271	0.016	0.013	−0.02	6410	13.3	< 2.11			
ι Peg	8430	0.296	0.027	0.015	−0.04	6290	7.6	2.53			
ξ Peg	8665	0.330	0.039	0.037	−0.33	6100	< 6.1	1.89	2.0	0.4	2.06
σ Peg	8697	0.320	0.052	0.031	−0.26	6160	< 3.6	2.34	2.5	0.3	2.64
ι Psc	8969	0.329	0.026	0.019	−0.10	6100	5.0	1.90	2.4	0.3	2.19
	9074	0.347	0.002	0.014	−0.04	6000	11.3	2.17	2.1	0.5	2.04

NOTES.

Column (2): Yale Bright Star Catalog number (Hoffleit 1964).

Column (3): Strömgren $b-y$ color from Hauck and Mermilliod (1980).

Column (4) and (5): Strömgren luminosity and metallicity indices, using $b-y$ to find the corresponding ZAMS values.

Column (6): Metallicity estimated from δm_1.

Column (7): Effective temperature estimated from $b-y$.

Column (8): CaII K line relative surface flux from Duncan (1981).

Column (9): $\log N_{Li}$ observed by Duncan (1981).

Column (10): $\log N_{Li}$ estimated using the photmetric ages and Duncan's relationship between Li abundance and age.

Column (11): Duncan's observed Li abundance adjusted to reflect the difference between Duncan's T_{eff} and that used here.

Table 3

Comparison of Field Star Age Estimates

Name	HR	Parallax	Ages (Gyr) δc_1	Orig. Li	Adj. Li
(1)	(2)	(3)	(4)	(5)	(6)
6 Cet	33		6.9±1.4		
ϕ^2 Cet	235	4.3±3.8	5.3 1.5		
	244		3.3 1.4	> 6.8	> 5.5
υ And	458	3.7 0.9	4.1 1.3	5.0±2.0	4.1
α Tri	544		3.6 0.6		
	672		5.0 0.9	0.9 0.5	0.7
ϵ Cet	781		3.5 1.4		
	784		2.7 2.1	0.0 0.7	0.1
θ Per	799	3.8 1.4	2.7 2.0	3.3 1.5	2.8
τ^1 Eri	818		3.8 1.7		
94 Cet	962	5.8 1.3	5.3 0.8	> 5.2	> 4.6
10 Tau	1101	5.1 1.2	6.4 1.1	2.5 1.0	2.0
	1249	< 2.9	1.9 1.6		
50 Per	1278		1.6 1.3		
π^3 Ori	1543	1.8 1.1	1.0 0.9		
λ Aur	1729	6.6 1.3	6.7 1.8	> 3.9	> 3.8
γ Lep A	1983	2.7 2.4	4.1 1.0	5.1 2.2	3.8
74 Ori	2241		1.8 1.3		
ξ Gem	2484		2.9 0.6		
63 Gem	2846		2.2 1.0		
α CMi	2943	2.2 0.2	2.3 0.9		
μ^2 Cnc	3176		6.9 1.4	1.1 0.4	1.0
18 Pup	3202		7.3 1.4		
	3499		< 1.1		
	3579	1.9 0.9	2.2 0.9		
τ^1 Hya	3759		2.3 0.9		
θ UMa	3775		4.4 0.6		
	3862		4.7 1.2	3.5 1.5	2.6
	3881	4.9 3.4	6.2 1.3	> 3.1	> 2.7
40 Leo	4054	1.9	1.0		
89 Leo	4455		0.8 0.7		
β Vir	4540	4.8 1.3	4.9 0.8	> 6.8	> 8.0
α Com AB	4968/9	3.6 1.6	3.5 1.3		
53 Vir	4981		4.6 0.8		
59 Vir	5011	< 5.0	6.7 1.3	0.9 0.5	0.1
τ Boo	5185		2.5 0.8		
η Boo	5235	2.7 0.6	3.0 0.9	> 5.5	> 8.0
ι Vir	5338		4.7 0.8		
θ Boo	5404	5.3 1.0	6.0 1.0		
α^1 Lib	5530		2.1 1.0		
45 Boo	5634		1.4 0.9		
5 Ser	5694		4.6 0.7	6.3 3.9	7.0
λ Ser	5868	4.7 2.8	5.8 2.0	> 3.7	> 3.5

Table 3 (Continued) Comparison of Field Star Age Estimates

Name	HR	Ages (Gyr)					
		Parallax	δc_1		Orig. Li		Adj. Li
(1)	(2)	(3)	(4)		(5)		(6)
γ Ser	5933	5.4±0.7	5.3±0.4				
θ Dra	5986		3.7	0.8			
18 Sco	6060	< 4.1	3.9	1.8	3.1±1.1		3.3
ζ Her	6212	3.7 0.7	5.8	1.5	> 3.4		> 3.4
11 Aql	7172		4.0	0.6			
	7354		5.9	1.2			
	7451		6.8	1.2			
	7496		3.1	0.5			
16 Cyg A	7503		7.5	1.4	> 3.5		> 3.4
17 Cyg A	7534	4.6 0.6	4.7	0.6			
o Aql	7560		5.0	1.1	4.3	1.9	3.6
	7793		2.6	2.0	3.1	1.2	2.6
ψ Cap	7936		2.4	1.0			
ι Peg	8430		3.2	1.2			
ξ Peg	8665		7.1	1.3	4.9	2.2	4.9
σ Peg	8697		5.3	0.8	3.0	1.5	2.7
ι Psc	8969	4.3 0.7	3.6	1.7	5.3	1.8	4.0
	9074		3.6	2.7	4.1	1.7	3.3

NOTES.

Column (2): Yale Bright Star Catalog number (Hoffleit 1964).

Column (3): Age estimate using luminosities based on parallaxes (Gliese 1969).

Column (4): Photometric age estimate using the Ciardullo and Demarque isochrones.

Column (5): Age estimates based on Li abundances (Duncan 1981).

Column (6): Age estimates using Li abundances adjusted to reflect the temperature scale used in Chapter II of this dissertation.

The uncertainties in T_{eff} and δM_V are obtained as follows: for the clusters, if f is known exactly in equation 2*a* (errors in β should have little effect on the value of f), $\sigma(\delta M_V) \approx \pm 0.08$ mag. The uncertainty in β will produce a T_{eff} uncertainty $\approx$ 60K. For the field stars, $\sigma(\delta M_V) \approx \pm 0.13$, and $\sigma T_{eff} \approx$ 40K.

An estimate of the uncertainty in age caused by uncertainties in c_1 and β (which I will call $\sigma(A^N_{obs})$, since it is an uncertainty in the age of the star at the nominal metallicity caused by uncertainties in c_1 and β) can be found by calculating the age at the positions in the effective temperature-luminosity diagram given by applying the above uncertainties to the observed position of the star. The average age difference between these ages found for the ends of the 1σ error bars and the nominal age is then $\sigma(A^N_{obs})$.

The metallicity uncertainty can be estimated similarly. For the cluster stars, [Fe/H] $= 0.15 - 11\delta m_1$, so the effect of uncertainty in β can also be neglected here. Then, σ([Fe/H]) $= \pm 0.08$, while for the field sample σ([Fe/H]) $= \pm 0.09$. This is roughly one metallicity step in the model grid, so the uncertainty in age due to metallicity can be found by estimating the age of the star given by models one metallicity step higher and one step lower than the nominal [Fe/H] (that is, A^H and A^L), and finding the average age difference between those ages and the nominal age A^N. That is,

$$\Delta A_{[Fe/H]} = \frac{|A^L - A^N| - |A^N - A^H|}{2} \qquad 4$$

The final estimate of the uncertainty is found to be

$$\sigma(A) = [\sigma^2(A^N_{obs}) + (\Delta A_{[Fe/H]})^2]^{\frac{1}{2}} \qquad 5$$

These uncertainties are listed in Tables 1 and 3 for NGC 752 and the field stars. Note that these calculations do not consider the effects of errors in the T_{eff}–β or

T_{eff}–$b-y$ calibration, the calibration of the c_1 standards, the δM_V–δc_1 calibration or the δm_1–[Fe/H] calibration. These problems, although very important, are clearly beyond the scope of this dissertation. Examination of these uncertainties show that in many cases it is possible to make meaningful age estimates for individual field stars, although clearly this becomes more difficult as one proceeds down the main sequence.

d. Age Estimates for Individual Stars in NGC 752

One way to test the reasonableness of age estimates for individual stars is to derive an age for each suitable star in a nearby well observed open cluster and compare these ages with a cluster age obtained by main-sequence fitting. It would be best to have a number of open clusters with a wide range in age for comparison, but good quality Strömgren measurements are available only for nearby young to intermediate age clusters. It would be particularly desirable to perform this test for older clusters, where the evolutionary effects are largest.

Strömgren photometry for the intermediate age open cluster NGC 752 was obtained from Crawford and Barnes (1970) and age estimates for the individual stars within the acceptable temperature range were made using δc_1 as for the field stars. A temperature–luminosity diagram for the cluster is shown in Figure 2. Note that in this case the upper temperature limit near 6900 K does not allow the actual turnoff point for the cluster to be seen. The composition used in this plot is $Y = 0.30, Z = 0.020$, which corresponds to the mean metallicity of 0.0 ± 0.1. While this result agrees with that of Nissen (1980) of -0.02 ± 0.02, it differs significantly from the value of -0.30 obtained by Janes (1979) from D.D.O. photometry. Best agreement with the observed stellar distribution is seen with the 2.0 Gyr isochrone,

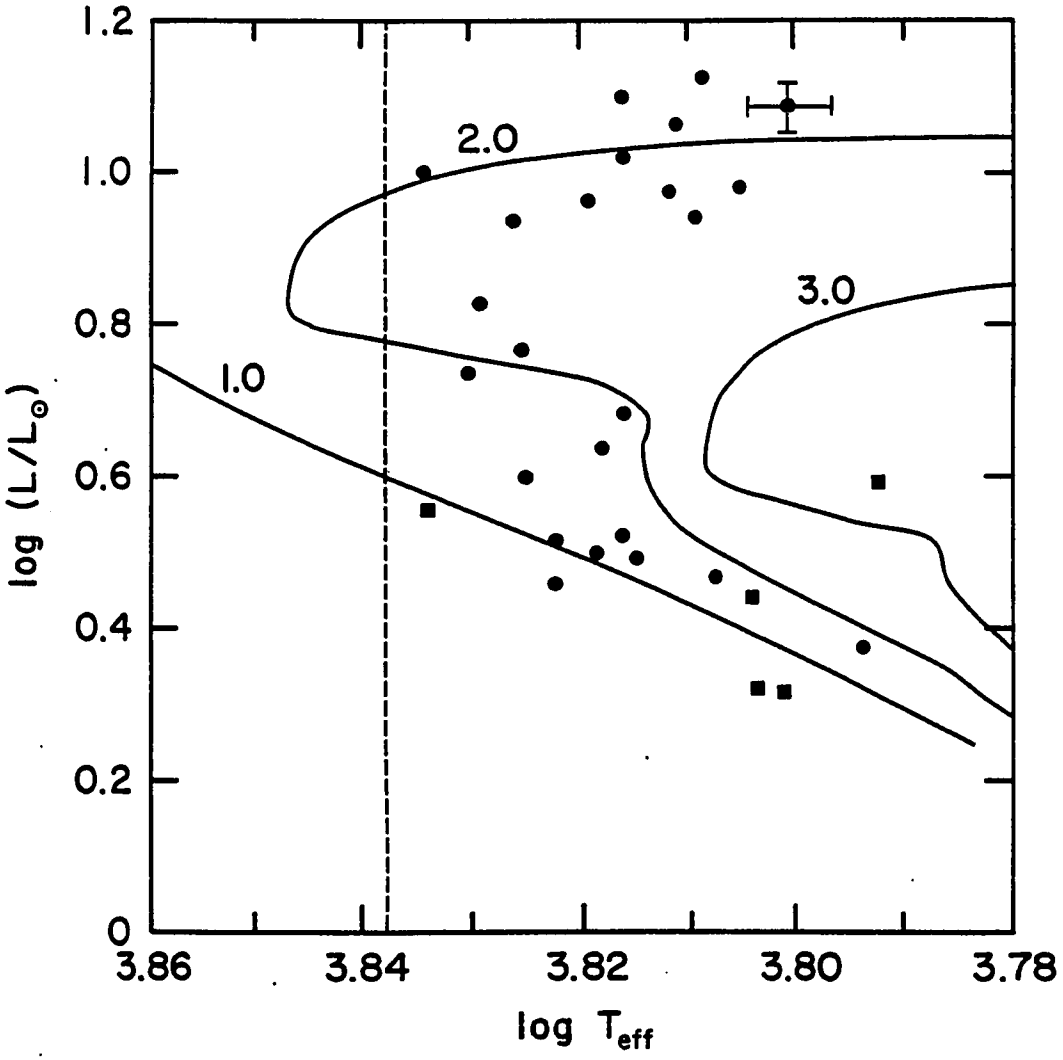

Figure 2. Comparison of NGC 752 stars with isochrones for 1.0, 2.0 and 3.0 Gyr with composition $Y = 0.30$, $Z = 0.020$. The dashed line shows the upper limit in temperature of the Crawford and Perry (1976) metallicity calibration. Stars indicated by boxes have the most discrepant final age estimates.

with an estimated error of 0.2 Gyr based on an "eyeball" fit to the cluster as a whole. This value is consistent with the weighted mean of the individual stellar ages of 2.0 Gyr with a standard deviation for a single star of ± 0.6 Gyr.

Analysis of the available data for NGC 752 indicates that the ages and uncertainties obtained for the individual stars are consistent with those obtained for the cluster as a whole. The estimated mean of the individual stellar ages for all cluster members is 1.9 Gyr with an uncertainty of ± 0.9 Gyr for an individual star using the Kaplan-Meier estimator method for censored data (Feigelson and Nelson 1985). One star (Heinemann 66) clearly appears to have a discrepant Hβ index when compared to its $b-y$ and $B-V$ (Johnson 1953) colors. Omitting this star (which is legitimate since this discrepancy could also be determined for a field star) produces a mean age of 1.9 Gyr with an uncertainty of ± 0.6 Gyr for an individual star. This result is consistent with the appearance of an age histogram for the NGC 752 members (Figure 3).

Twarog (1983) has recently reobserved NGC 752 using Strömgren photometry. Among the most interesting of the results are that six stars in the cluster are probable binaries. Omitting these stars yields a new mean age of 1.9 Gyr with an uncertainty of ± 0.5 Gyr for an individual cluster member. His work also indicates that the main sequence is bimodal with the more luminous branch due partially to the binaries noted above and partially due to a difference in rotation velocity. The difference in rotational velocity amounts to < 45 km s^{-1}. If the rotational velocity were not known, as is generally the case with field stars, the luminosity difference would be interpreted as an age difference of $\sim 3 \times 10^8$ yr. This difference is probably too small to have any effect on individual cluster member age estimates, which have uncertainties typically twice that value.

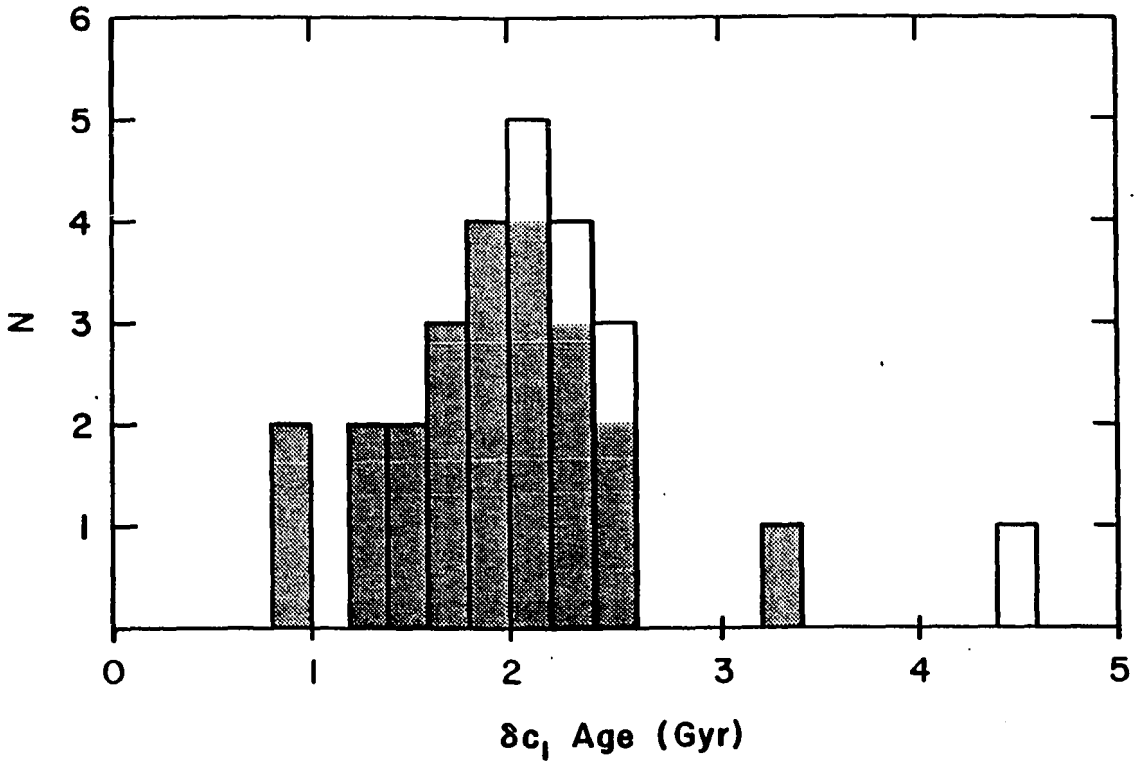

Figure 3. Histogram of individual stellar ages from isochrone fitting for 27 stars in NGC 752. The shaded region shows the distribution if four probable binaries (Twarog 1983) are omitted.

e. Comparison with Parallax-Based Age Determinations

The major reason for using δc_1 to obtain age estimates is that only a small sample of stars would be available if the sample had to be limited to those stars with well-measured parallaxes. However, stars with both parallaxes and Strömgren photometry provide another check on the photometric age estimates by determining how well the conversion of δc_1 to luminosity works. As a check on the absolute magnitude and age determinations, ages have been estimated for a subset of the field stars in Table 3 with luminosities determined from the parallaxes listed in the

Gliese (1969) catalog rather than δc_1. Absolute visual magnitudes based on parallaxes were taken from the catalog and bolometric corrections from Schlesinger (1969) were used. Otherwise, the age estimates using the absolute magnitude data were done in the same way, using the same effective temperature and metallicity calibrations as those based on δc_1. Although these two age estimates are not strictly independent, if one had a much larger scatter than the other, the whole idea of using the δc_1 index as a relative luminosity measure would be in doubt.

The ages derived by both methods of finding the luminosity for the 33 stars listed in Table 3 with parallaxes are compared in Figure 4. The scatter is consistent with errors in the photometry or parallax. Note that the uncertainty in a single star's parallax is frequently larger than the uncertainty resulting from the δc_1 measurement. The ages derived using Twarog's (1980) method appear to be as satisfactory as those obtained using parallactic luminosities.

Twarog (1980) originally applied the δc_1 method to a large sample of stars in a statistical fashion to determine the age-metallicity relation for the galactic disk. However, from the results for both open clusters and field stars it appears this method can, with caution, be used to determine ages for individual field stars in the F2- early G region near the main sequence, even those without parallax measurements.

3. Discussion

As discussed in the introduction, lithium has been used as an age indicator in late-type stars. Lithium is destroyed if the temperature near the base of the convection zone in greater than 3×10^6K. If surface lithium can be transported to

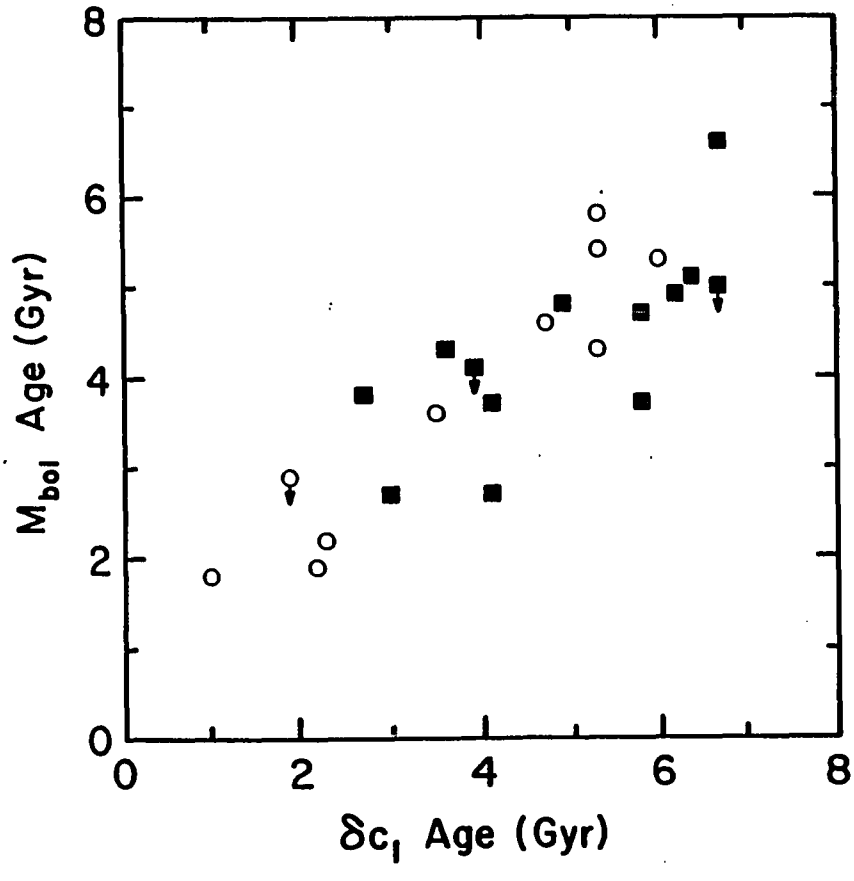

Figure 4. Comparison of age estimates for field stars based on M_{bol} from parallax measurements to Strömgren photometric ages. Stars with Li ages from Duncan (1981) are shown as boxes.

a region where this temperature is reached, then the surface Li abundance should exponentially decline (Herbig 1965). Duncan (1981) has used measurements of Li in stars in the Pleiades, Hyades, and the Sun to calibrate this decline for late F and G stars with $T_{eff} < 6200$K. Stars hotter than this are not expected to lose Li due to their shallow convection zones. The exact position of this break point is not well determined; Soderblom (1983) gives Li ages for stars up to 7000K. Figure 5 shows $\log N_{Li}$ (on the standard scale relative to the solar hydrogen abundance with $\log N_H = 12.0$) versus $\log T_{eff}$ for the field stars selected in this chapter. Stars

are shown with symbols according to their photometrically determined ages. The scatter in the F5-F6 region ($T_{eff} > 6200$K) has been noted by previous authors (Duncan 1981, Soderblom 1983) and has been attributed to another depeletion mechanism, such as turbulent diffusion (Schatzman 1977). Many stars in this temperature range with low Li abundance also show low Be abundance (Boesgaard 1976). The "lithium dip" observed in the Hyades and field stars by Boesgaard and Tripicco (1986*a*,*b*) occurs in stars warmer ($T_{eff} \sim$ 6500K) than those considered here. Some F5-F6 stars with relatively high Li abundances have large δc_1 ages. The stars with $T_{eff} < 6200$K on the whole show a decline of Li abundance with age, but there appear to be a few significant exceptions.

Stars with $T_{eff} < 6000$K and $\log(L/L_{\odot}) < 0.25$ have been excluded from the δc_1 isochrone fitting procedure due to their large age uncertainities. This increase in age uncertainty at low temperature and luminosity is simply caused by the small difference in luminosity between isochrones in this part of the HR diagram. The older stars which are present show low Li abundance, with the exceptions of μ^2 Cnc, HR 672, and 10 Tau. Two of these stars, (μ^2 Cnc and HR 672) have been classified as subgiants. The relatively high Li abundance of these stars is not surprising, since they are more massive than typical dwarfs of the same temperature, and thus came from a region of the main sequence where Li depletion is not as strong and universal. The star 10 Tau also appears to be evolved well away from its zero-age main sequence; both the parallax-based age and the δc_1 age are in reasonable agreement. A fourth star, 59 Vir, presents a more serious problem. It is classified as a dwarf, and has a δc_1 age of 6.7 Gyr. Parallax measurements only establish an upper limit of 5.3 Gyr for the age of this star, and this value is very uncertain and is such that any age from 0 to $\sim$8 Gyr could be obtained. It may be, however, that the Strömgren photometry for this

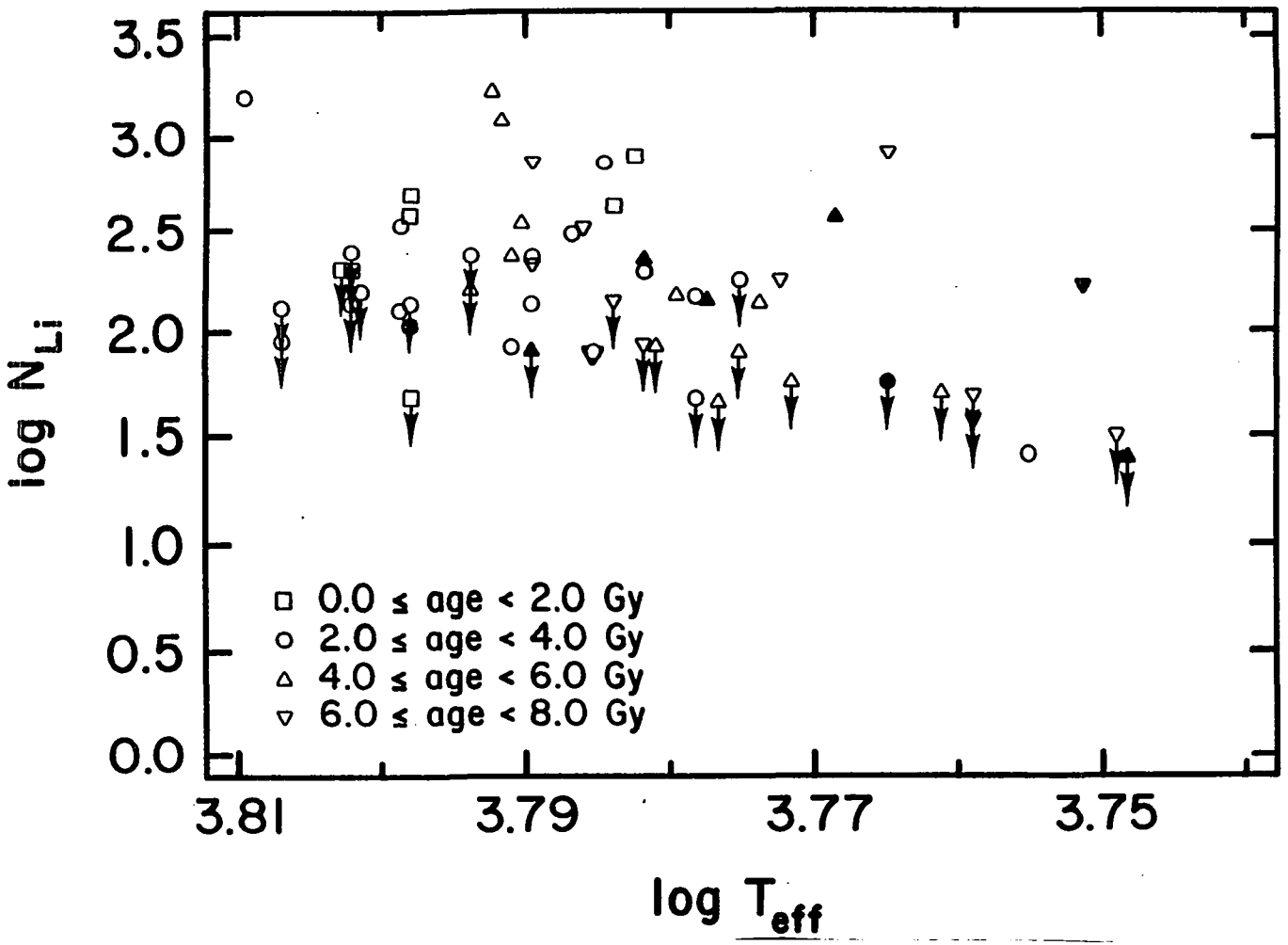

Figure 5. Plot of field star $\log N_{Li}$ and $\log T_{eff}$. Stars classified as subgiants shown as filled-in symbols.

star is not correct, and this star is actually much younger than it appears to be. If so, the photometric and Li-abundance age could be in agreement. This possibility will be discussed below. As will be shown later, this interpretation is consistent with other age indicators.

One way to examine these exceptions to the Li-age calibration is to estimate the Li abundance the field stars ought to have, if the photometric ages are correct and Duncan's Li–age relation applies. This was done by using Duncan's empirical zero-age Li abundances and *e*-folding times to generate a plot of Li abundance values versus temperature. Spline fits connecting points of the same age were made. The age for a particular star was interpolated between the curves and the Li abundance corresponding to a given temperature and age was found. The uncertainty of the estimated Li abundance was found as follows: Duncan indicates that the Li abundance isochrones were based on a quadratic least squares fit in $\log N_{Li}$–$\log T_{eff}$ space to the Hyades, scaled to the *e*-folding time established for the Sun. This gives the approximate relation

$$\log N_{Li} = 2.96 - (67.9 + 101t)(3.82 - \log T)^2 \qquad 6$$

for the field star Li abundance, where t is measured in Gyr. An estimate of the uncertainty in the Li abundance can be found using standard error propagation techniques, which yields

$$\sigma^2 \log N_{Li} = 10200(3.82 - logT)^4\sigma^2 t + [(136+202t)(3.82-\log T_{eff})]^2\sigma^2 \log T_{eff} \qquad 7$$

A plot of the estimated Li abundance versus Duncan's observed Li abundance is shown in Figure 6. A possible trend is seen if the stars with only Li abundance upper limits four older low temperature stars previously discussed, μ^2 Cnc, 59 Vir, 10 Tau, and HR 672, are excluded. There clearly is a correlation between the

observed and estimated Li abundances, but the slope of the least-squares line is clearly not 1.0.

There could be two basic sources for this discrepancy: either there are systematic differences in the observational parameters used to determine the Li abundance and photometric ages, or the model isochrones used could be producing stellar ages which generate incorrect Li abundance estimates. The observed Li abundance depends on several parameters: the observed effective temperature, metallicity, gravity, and the theoretical curve of growth. The observational parameters lend themselves most easily to comparison, since the photometric ages also require the same data.

There appears to be very little systematic difference between the abundances and gravities used by Duncan and those used here. However, the temperature scales are different. These scales are compared in Figure 7, which also shows a least-squares fit to Duncan's temperature scale:

$$T_{eff}(Duncan) = 0.573 T_{eff}(b-y) + 2570 \qquad 8$$

The systematic difference between the scales amounts to ~80 K at $T_{eff}(b-y) =$ 6200K and ~-90 K at $T_{eff}(b-y) =$ 5800K. If one then plots the Li abundance residual $\log N_{Li\ obs}$ - $\log N_{Li\ est}$, excluding the three evolved stars mentioned above, the discrepant star 59 Vir, and the stars with only Li upper limits, versus the temperature residual $T_{eff}(b-y)$ - $T_{eff}(Duncan)$ (see Figure 8) a trend is evident. There does appear to be a systematic difference in the Li residuals with T_{eff}. If the differences between the observed and estimated Li abundance were due to random photometric age errors, one would expect an essentially random Li residual distribution, although the scatter in the residual should decrease

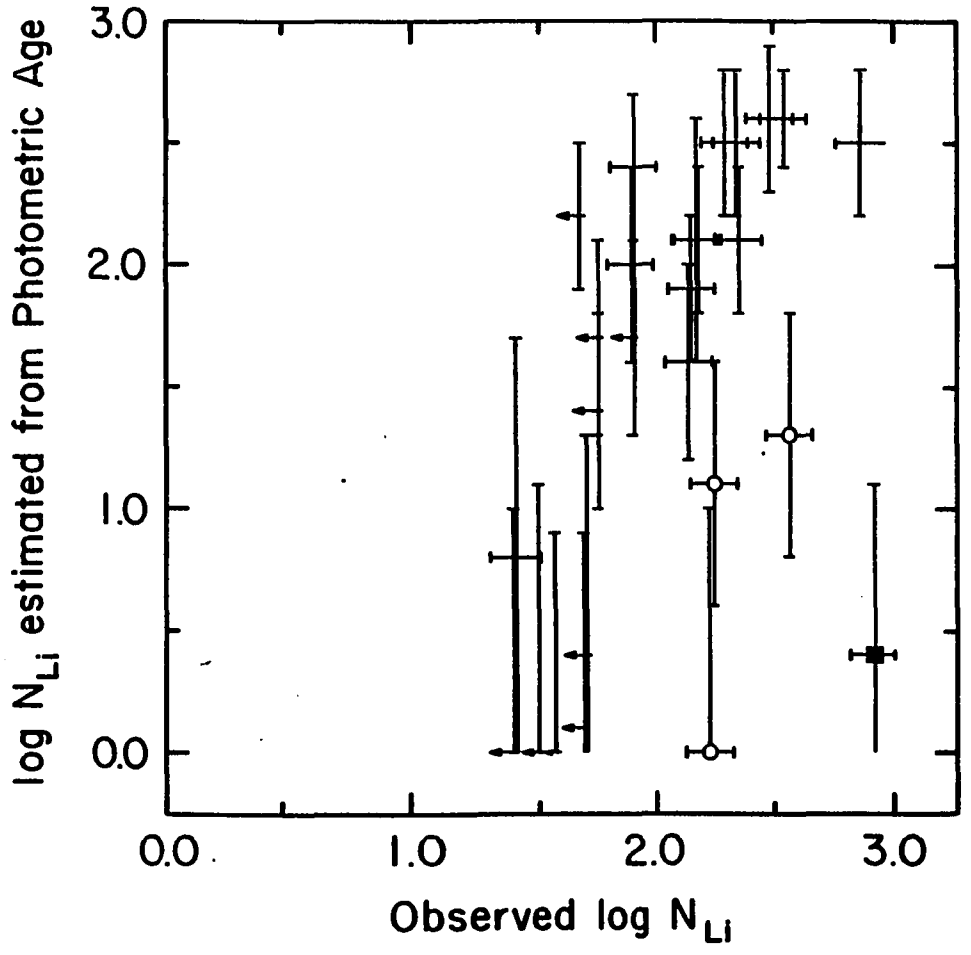

Figure 6. Plot of Li abundances based on estimates using the Li abundance–age relation of Duncan (1981) and Strömgren photometric ages for stars with $\log T_{eff} \leq 3.79$ versus observed Li abundances of Duncan (1981). The open symbols in the lower right-hand corner of the plot refer to stars which evolved from early F main-sequence stars. The filled box is the star 59 Vir, which appears to have discrepant Strömgren colors.

with increasing effective temperature due to the reduction of the photometric age uncertainty.

Very roughly, the abundance $\log N_{Li}$ according to the curves of growth given in Duncan (1981) is given by $\log N_{Li} \approx 1 \times 10^{-3} T_{eff} + F(W_{6707})$, and therefore if

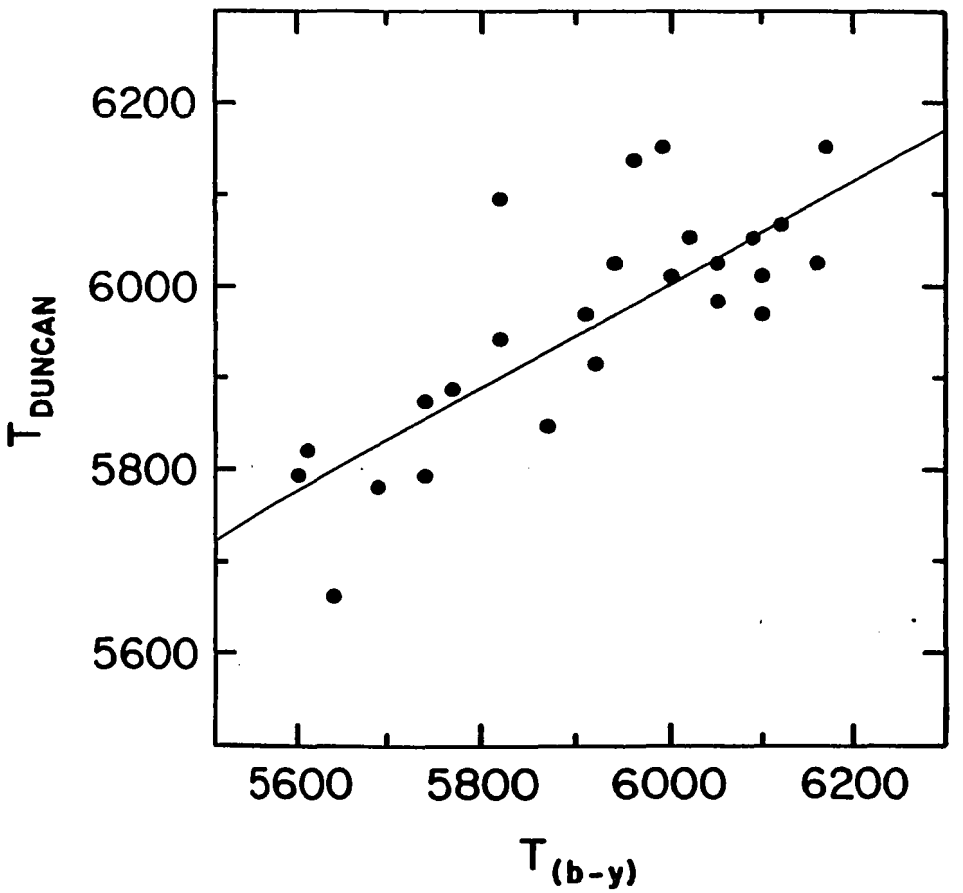

Figure 7. Comparison of the effective temperature scales of Duncan (1981) and this paper. The line is a least-squares fit of the Duncan temperatures to the temperatures used in this paper.

the difference between the observed and estimated Li abundances is simply due to the differing field star temperature calibrations used, and if the photometric ages are indeed correct, the difference in the observed and estimated Li abundances is given by

$$\delta \log N_{Li} \approx -0.001(T_{eff}(b-y) - T_{eff}(Duncan)) \qquad 9$$

This line is also shown in Figure 8. The correction expected from recomputing the Li abundances based on a temperature scale consistent with the photometric ages

photometric colors with age at lower temperatures. The resulting reduction of the estimated Li abundance, with a the larger reductions at lower temperatures, would be just opposite that required to bring the estimates into agreement with the observations.

Releya and Kurucz (1978) point out that Kurucz' models (1979), used by Duncan (1981), probably do not treat convection correctly in F and early G stars. Reducing the mixing length to scale height ratio, as they suggest, would have the effect of allowing a given $b - y$ color to correspond to a lower temperature atmosphere, which has the effect of lowering the Li abundance calculated from the curve of growth method. This result would reduce the difference between the observed Li abundance and that estimated from the photometric age.

In order to correct for the effect of the difference in the effective temperature scales on the Li abundance, the empirical linear least-squares fit for the Li abundance residual–effective temperature difference relation,

$$\delta \log N_{Li} = -0.003[T_{eff}(b-y) - T_{eff}(Duncan)] + 0.097 \qquad 10$$

is subtracted from Duncan's observed Li abundance. The result, as expected, significantly improves the correspondence between the actual and estimated Li abundances (Figure 9).

Revised Li-based age estimates for the field stars can then be made, using Duncan's relations between Li abundance, T_{eff}, and age. Comparison to the photometric ages (Figure 10) shows that the adjusted Li ages are consistent with the photometric ages for stars with observed Li abundances which are not too far from the main sequence. It is important at this point to consider the uncertainties in the two methods. The uncertainties in the photometric ages have been discussed

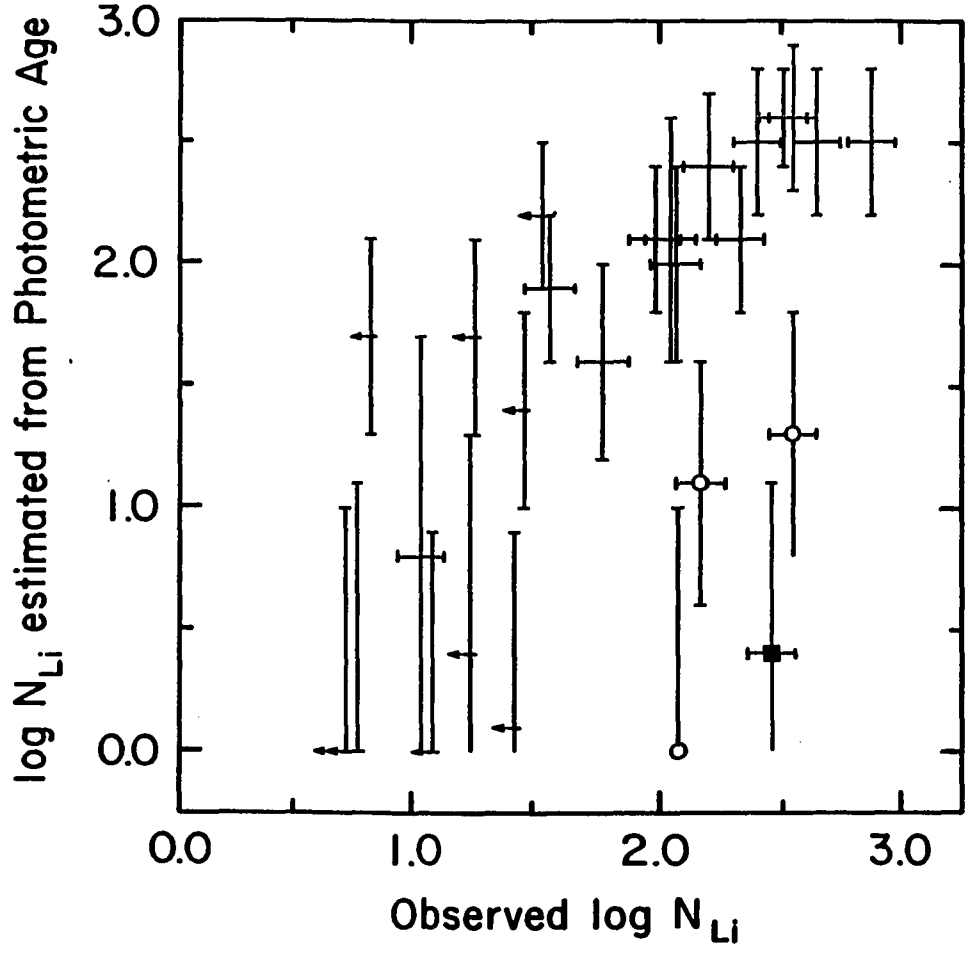

Figure 9. Same as Figure 6 except that the observed Li abundances are revised to correct for the systematic effect on the Li abundance of the difference in temperature scales.

in section (2c). The uncertainties in the Li-based ages can be obtained using the approximation discussed above for the Li abundance (Equation 6). Solving for t,

$$t \approx 9.9 \times 10^{-3}[(2.96 - \log N_{Li})/(3.82 - \log T)^2] - 0.672 \qquad 11$$

which, neglecting the cross terms, yields

$$\sigma_t^2 = \frac{\sigma^2 \log N_{Li}}{[10200(3.82 - \log T)^4]} + 3.92 \times 10^{-4} \frac{(2.96 - \log N_{Li})^2}{(3.82 - \log T_{eff})^6} \qquad 12$$

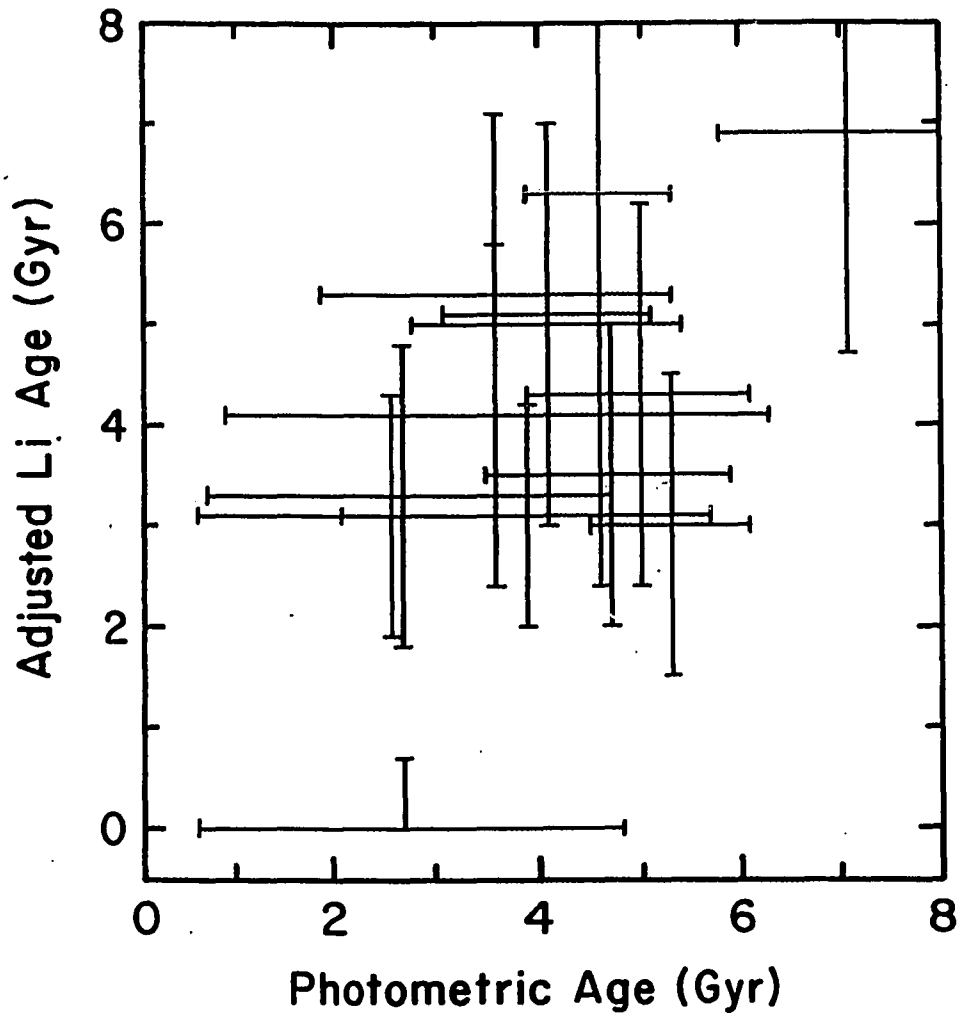

Figure 10. Plot of Li age versus photometric age. The Li age is based on the revised Li abudances corrected for the systematic Li abundance–effective temperature effect discussed in the text. The age scales appear to be consistent within their uncertainties. Stars excluded in Figure 8 (those with Li upper limits and those likely to be evolved beyond the main sequence) are also excluded here.

These uncertainties are included in Table 3. These uncertainties include the decline in significance of the T_{eff} uncertainty for hot stars (Soderblom 1983) but do not include the effect of uncertainty in T_{eff} on the Li abundances themselves.

Neither the Li abundance based ages nor the photometric ages work well for young stars. In both cases it becomes impossible to distinguish slightly evolved

stars from stars which are actually on the zero-age main sequence for their composition. However, young open cluster members can be used to complete age distributions for F and G stars.

We now briefly consider the effect of age on the Ca II K line emission in main-sequence field stars, using the R_K index of Duncan (1981). This index, which measures the chromospheric flux in the K line relative to the total surface flux of the star, is used because it removes the effect of differing continuum levels in stars of different effective temperatures on the visibility of the K line, and also attempts to remove the filling in of the inner wings of the line by nonradiative heating of the photosphere. This effect is described by Linsky *et al.* (1979) and by Kelch, Linsky, and Worden (1979). By allowing for these effects R_K better describes the level of chromospheric activity in these stars than the Mt. Wilson S index.

A plot of R_K versus stellar age for those stars with Li-based ages or lower limits determined by Duncan (1981) is shown in Figure 11a. The stars marked with open symbols are the evolved stars μ^2 Cnc, HR 672, and 10 Tau discussed earlier. The star in the upper right hand corner is 59 Vir, and probably the photometric age is in error for this object. This plot can be compared with Figure 11b, which shows R_K versus Duncan's Li ages, and Figure 11c, which shows the adjusted Li ages. The correspondence between the behavior of Ca II activity and age appears to be consistent with the errors in the two dating methods. Note that the evolved stars in the photometric age plot appear to have normal Ca II fluxes for their ages, while in both Li-age plots they appear as objects of lower Ca II flux than would be expected from the classical Skumanich (1972) $t^{-\frac{1}{2}}$ law. The lack of young stars prevents any conclusion from being drawn about the functional dependence of Ca II flux with age, except that stars older than $\sim$2 Gyr tend to have relatively low

Ca II flux, and that Duncan's group C stars (those with anomalously low Ca II flux for their Li ages) are probably actually evolved stars which have retained their Li, as Duncan proposed.

If stars with temperatures too high to have Li age estimates are considered (see Figure 11d) the picture changes. These stars all have $T_{eff} \gtrsim 6200$K, which corresponds to $B-V \lesssim 0.46$. Their photometric ages seem to indicate that a large fraction of these objects continue high Ca II activity levels to relatively large ages. In other words, the Ca II flux in these objects appears to be less age-dependent than that in later-type stars. This difference in Ca II flux activity appears to be consistent with other activity measures. Walter (1983) indicates that F dwarfs earlier than $B-V = 0.46$ show no relation between X-ray flux and rotation rate; all early F stars have roughly the same X-ray flux regardless of their $V \sin i$ values. This lack of correlation with rotation also appears in the ultraviolet C II and C IV lines observed with IUE (Walter and Linsky 1985), and in the He I 5876Å line (Wolff, Heasley, and Varsik 1985). The mass and age dependence of Ca II flux and rotation in the early F stars is investigated in Chapter III.

4. Conclusions

This chapter has attempted to calibrate a new method for determining ages for individual field stars using Strömgren photometry. This method of fitting Strömgren photometric indices to stellar isochrones was used by Twarog (1980) in a statistical way in his study of the age–metallicity relation in the galactic disk, and involves using Strömgren $ubvy\beta$ photometry to measure the effective temperature, metallicity, and difference in luminosity from the ZAMS for a particular

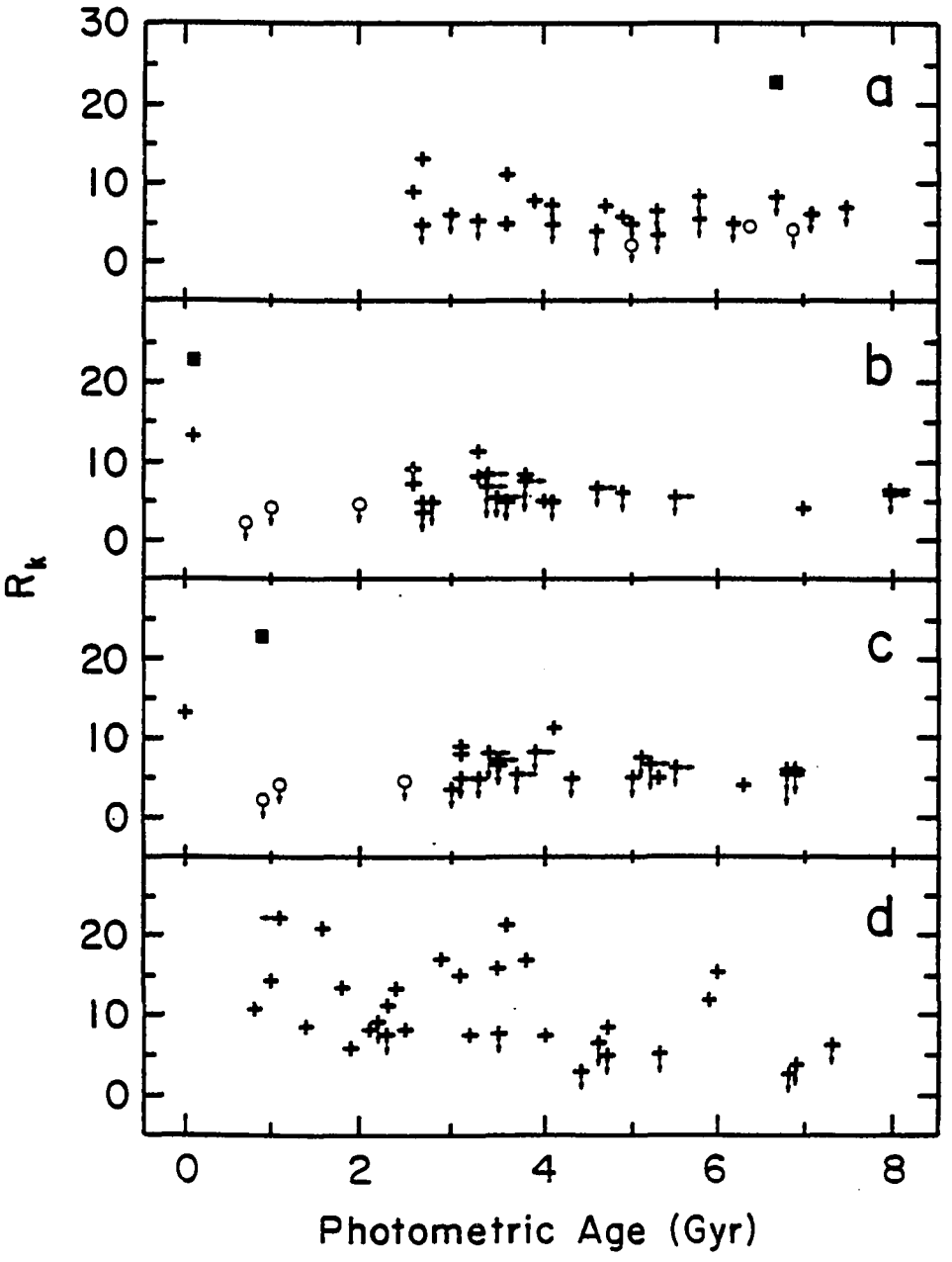

Figure 11. The Ca II relative flux index R_K (Duncan 1981) versus a) Strömgren photometric age for stars with Li age from Duncan (1981), b) Duncan's original Li ages, c) Li ages as adjusted in this paper, d) photometric ages for stars with $T_{eff} \geq 6200$K. The hot stars appear not to lose their Ca II activity as rapidly as the cooler stars.

metallicity. While Twarog used his method in a statistical fashion, here it is applied to individual field stars, with adequate measures of the uncertainty resulting from photometric errors. The ages are determined by comparison of the observed stellar positions in the theoretical H-R diagram to stellar model isochrones produced by Ciardullo and Demarque (1977). The resulting ages compare favorably to ages based on the same model isochrones but with absolute magnitudes derived from stellar parallaxes for a subset of the sample.

Data were also obtained for the open cluster NCG 752. Age estimates for the individual stars in the cluster were consistent with a mean age for the cluster obtained from main sequence fitting, even allowing for a possible bimodal cluster age distribution (Twarog 1983). The accuracy of the method, as in any such age determination method, is based on the effective temperature, metallicity, and luminosity calibrations, and on the accuracy of the stellar models. Given the uncertainties in these quantities, the relative ages for the stars given here are probably reliable, but the absolute age scale is less so.

The ages estimated from the photometric data were then compared to those by Duncan (1981) based on lithium abundance measurements. A systematic difference in the lithium abundance observed by Duncan and the abundance estimated for the field stars based on the photometric ages was found. This difference appears to depend on the difference in the temperature scales used, but is larger than what would be generated by comparing the Li abundances obtained by Duncan and those which would be obtained using the temperature calibration used for the photometric ages. The remaining difference may possibly be related to the known difference between the Kurucz (1979) models and observations for F and G stars.

When the observed Li abundances are adjusted to remove the dependence on the temperature calibration, good agreement is found between Li-based and photometric ages, except for a few cases of evolved stars retaining a high Li abundance.

Ca II fluxes corrected for photospheric nonradiative heating (R_K) were compared to both the photometric and Li-based field star ages. The behavior of stellar activity as a function of age was similar for both age scales, although the lack of young stars prevented a determination of the functional dependence of activity for field stars using either age scale. It appears that Duncan's (1981) group C stars have normal Ca II flux for their photometric ages.

Stars hotter than roughly 6200 K or $B - V \approx 0.46$ appear to retain much of their initial activity as main sequence stars for their main sequence lifetimes. This result, along with the lack of variation of other activity indicators as a function of rotation rate in the hotter F stars, suggests differences in the fundamental stellar activity mechanism in these stars.

CHAPTER III
STELLAR ACTIVITY IN F STARS I.
THE AGE DEPENDENCE OF CA II FLUX

1. Background

Most of the analysis of stellar activity over the past twenty years has been mainly concerned with the activity of solar-type stars. However, chromospheric activity has been observed in the Ca II *H* and *K* lines as early as F2 (Baliunas *et al.* 1983) in Mg II *h* and *k* and C IV as early as F2 (Böhm-Vitense and Dettman 1980), and to F0 in He I 5876 Å (Wolff, Heasley, and Varsik 1985). There are some indications that the behavior in early and mid-F stars of stellar activity is substantially different than in later-type objects. The modulation of Ca II *H* and *K* flux observed in G and K stars is generally not seen in early and mid-F stars (Baliunas *et al.* 1984, Giampapa and Rosner 1984), nor is cyclic activity observed (Vaughan 1980).

According to the early measurements of Wilson (1968) and Vaughan and Preston (1979), chromospheric activity (as measured on the Mt. Wilson *S* index) is quite low in the F stars, and only becomes very strong in the K and M dwarfs. Middelkoop (1982), however, showed that if the Ca II line core surface flux is considered, the F stars appear to have the highest levels observed in main sequence dwarfs. In an attempt to consider only the emission from the chromosphere, Noyes *et al.* (1984) developed an activity index R'_{HK}, which measures the chromospheric energy output in the cores of the Ca II lines as a fraction of the total energy output of the star. In this measure, the late F, G, and K stars show about the same range of activity (Soderblom 1985) regardless of effective temperature, while the activity

level in the early to mid-F stars declines. Thus the F stars offer the opportunity to examine chromospheric behavior in a group of stars with appreciable activity containing stars similar to the Sun and stars which are rather different from the Sun.

Another advantage of examining the evolution of activity in the F stars rather than G and K stars is that it becomes possible to estimate the ages of individual field stars by use of Strömgren photometric indices, at least in a relative sense (see Chapter II). This is especially useful since the method commonly used for obtaining age estimates of solar-type stars, the surface Li abundance, does not appear to work for the F stars (Duncan 1981).

The major difficulty of observing Ca II activity in F stars lies in the rapidly changing continuum level and photospheric contribution with spectral type. Although the Ca II *H* and *K* lines may not be ideal for measuring activity in these objects, a substantial amount of data is available in the literature, providing a larger statistical sample. Middelkoop (1982) has shown a method of correcting Mt. Wilson *S* index measurements for the differences in photospheric flux levels with temperature, thus allowing the Ca II flux relative to the total flux of the star to be calculated for stars of differing effective temperature.

In this chapter of the dissertation Ca II data for both a sample of field F stars with known ages (based on the Strömgren photometric indices) and for the Pleiades, Hyades, Praesepe, and Coma Berenices clusters will be examined, both as a whole and as samples of stars of specific masses.

2. Observations and Calibration

The early and mid-F stars have not been extensively observed for Ca II core emission, in spite of the vast amount of observations done on later type stars. The most extensive data set thus far available for these and later stars is that of the Mt. Wilson group (Wilson 1978; Vaughan and Preston 1980; Duncan 1983, 1985). This sample, moreover is somewhat biased toward more active stars, and has only a small number of early and mid-F stars. Therefore it was decided to combine the available data from the Mt. Wilson set and additional observations from Mauna Kea to form an essentially magnitude-limited sample which would include stars of all activity levels. The selection of the stars to be included was as follows. The Yale Bright Star Catalog (3rd edition, Hoffleit 1964) was searched for stars in the spectral type range F2–G2, luminosity classes V, IV-V, and IV. Stars which were later found (from the Strömgren photometry) to lie above the turnoff points of their isochrones were excluded. Only stars observable from Mauna Kea were included. This preliminary list was then examined to eliminate short-period spectroscopic binaries, close visual binaries where the period was either less than 10 years or unknown, and close binaries where the magnitude difference between components was small ($\lesssim$ 3mag.). Stars with faint M dwarf companions were not eliminated as the companions were typically 4-5 mag. fainter than the primary.

There were additional selection parameters to be considered, mainly relating to the Strömgren photometric calibrations. All stars selected had homogenized $ubvy\beta$ photometry available from the catalog of Hauck and Mermilliod (1979). In order to obtain consistent T_{eff}, [Fe/H], and luminosity values using the Strömgren index calibrations (see section (3)), only a subset of the above stars could be used. The [Fe/H] calibration of Crawford and Perry (1976) was only valid for

$2.720 > \beta \geq 2.590$; the temperature calibration problems noted below meant that all stars with $b - y > 0.370$ or $\beta < 2.600$ had to be eliminated. Additional stars with $\beta < 2.61$ and $\log(L/L_{\odot})$ (as calculated below) < 0.25 were eliminated due to the small evolutionary differences in luminosity in these low mass stars close to the ZAMS.

Finally, the choice of the VandenBerg (1985) isochrones for age and mass determinations limited the field star sample to objects of solar and lower metallicity, since a complete set of isochrones for metallicities greater than solar was not available. Additionally, to avoid ambiguities, of solar composition found lie in the region of isochrone overlap (the hydrogen exhaustion phase) and in the subgiant stage beyond that region were omitted. These selection parameters left a master list of 68 field stars, 20 of which had Mt. Wilson S index values. Of the remaining stars, 21 were observed with the 2.2m telescope.

In order to obtain photometric data which could be placed on the same scale as the Mt. Wilson data, spectra were obtained at the coudé focus of the 2.2m telescope using the I.f.A./Galileo virtual phase 800 × 800 pixel CCD detector (Hlivak, Henry, and Pilcher 1984; Hlivak *et al.* 1982). The #3 camera of the coudé spectrograph was used along with a 600 line mm^{-1} grating which allowed a dispersion of 6.9 Å mm^{-1} or 0.104 Å $pixel^{-1}$ at the detector. Two successful observing runs were obtained with this instrument, August 11-13 (UT) and October 17-19 (UT) 1984. Resolution was 2 pixels FWHM, as measured from the comparison lines. The signal to noise ratio in the continuum was typically 100, with exposures of approximately 30 minutes for a sixth magnitude star. In most cases, only a single measurement was made for each star. The spectra were not trailed.

Each raw image was rectified by subtracting a scaled bias frame and dividing the resulting image by a normalized flat field image. This normalized flat field image was obtained by uniformly illuminating the coudé spectrograph slit with light from an ordinary tungsten filament light bulb passed through a sheet of ground glass in order to produce a diffuse unfocused beam. After subtracting the bias level, the flat field image was normalized by dividing each pixel by the average level of a small region near the center of the image. A flat field image was obtained each night. The final spectrum was obtained by coadding all rows containing significant signal level. Examples of the resulting spectra are shown in Figure 12.

Measurements for the Pleiades, Hyades, Praesepe, and Coma Berenices clusters from the literature were used to provide a more complete sample for very young objects, since few of these were seen in the field. Mean R'_{HK} values were calculated using S index data for the Hyades stars obtained from Duncan *et al.* (1984), while mean S index data for the Pleiades, Praesepe, and Coma stars were from Duncan (1983). Conversions to the R'_{HK} scale were made using $B-V$ colors from Mendoza (1966) and Duncan *et al.* (1984) using the method described below.

For comparison with available data an instrumental Ca II HK spectral index was calculated based on the spectra observed at Mauna Kea. A region on the blue side of the HK region from 3895.0 to 3913.0 Å was used as a continuum reference. A continuum index V was found by integrating the counts in the spectrum in this region. It was impossible to use a corresponding band on the red side of the HK region due to the limited spectral range of the detector. Line indices H and K were found by integrating in 1.1 Å wide bands around the centers of the stellar H

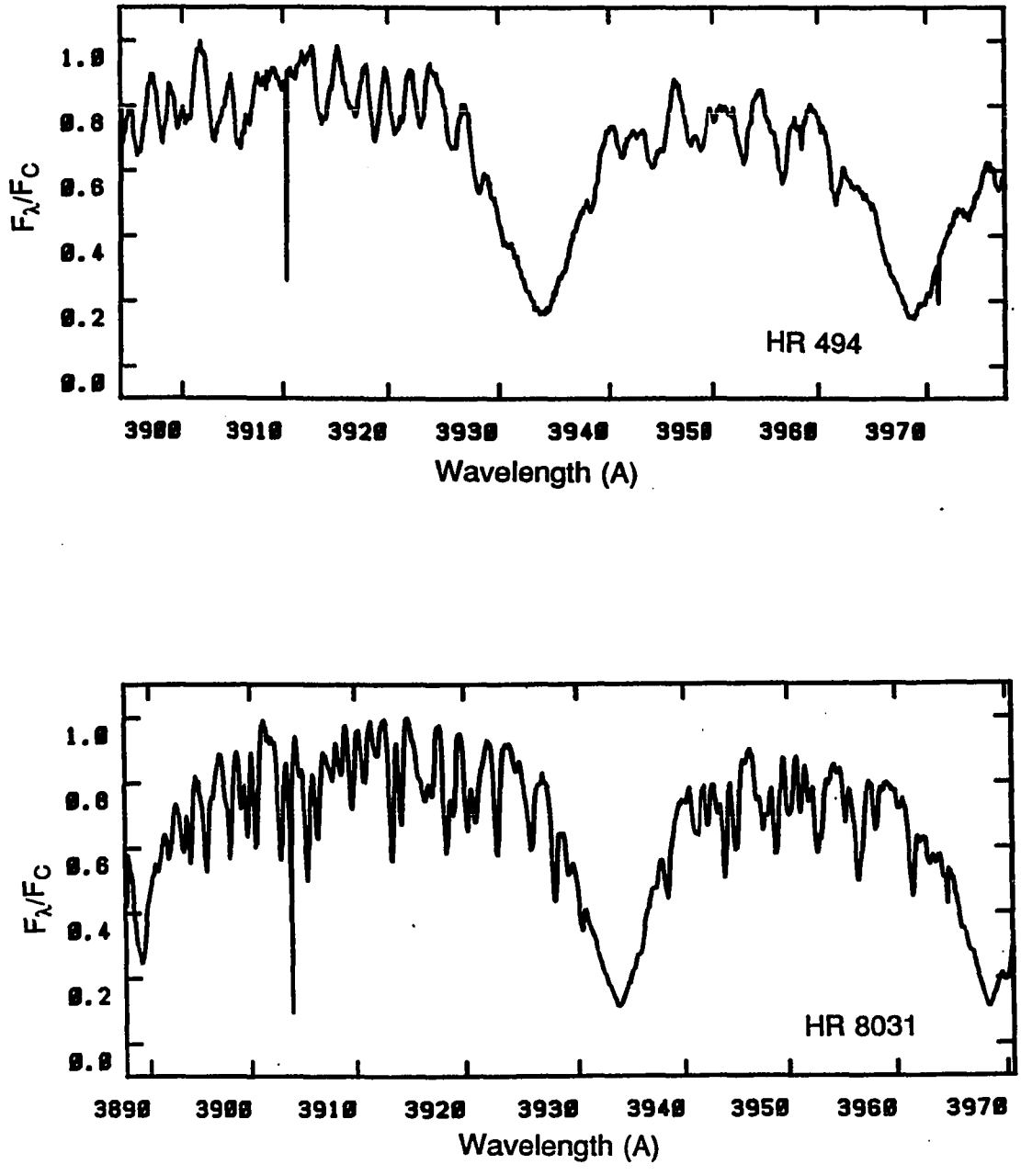

Figure 12. Examples of Ca II spectra. In early F stars chromospheric emission generally causes a filling-in of the cores of the H and K lines, rather than actual core emission reversals. a) HR 494, $\beta = 2.694$. b) HR 8031, $\beta = 2.688$.

and K lines. An instrumental HK index S' was found from

$$S' = (H + K)/2V. \qquad 13$$

In order to convert this index to the Mt. Wilson calibration, S' values for stars with known S values were computed and a satisfactory parabolic fit was obtained for the common stars, once two stars with low S/N were omitted. Figure 13 compares the S and S' values for the common stars, and shows that no systematic difference is seen between the early G and mid F stars used for calibration, indicating that the lack of a red continuum band is not introducing any bias in the calibration of S. Due to the limited spectral range used no color correction is necessary for the continuum levels. The resulting S values are listed in Table 4, along with those from the literature.

The uncertainty in these Ca II flux measurements can be traced to two causes: the difference between a single observation and the mean flux value for a star, and the instrumental uncertainty. The instrumental uncertainty of the MKO S determinations appears to be on the order of 1%; this is similar to the Mt. Wilson measurements. Far more significant is the real variation with time of the Ca II flux of the stars. According to the data presented in Baliunas *et al.* (1983), for stars in the range $0.42 \leq B-V \leq 0.65$, S appears to show a roughly 4 to 5 % variation over a three-month period, with little difference between hot and cool stars; this can be considered an uncertainty estimate for a single isolated measurement. This value is reasonable for the field stars, and similar to the variation seen in the Hyades F stars (see Duncan *et al.* 1984). However, the limited data available on the Pleiades cluster stars suggests that they may exhibit variations in S on the order of 20% (Hartmann *et al.* 1984, Duncan 1983 private comm.). Long term variations in early to mid-F stars ($B-V \approx 0.45$) are small, but late F stars may

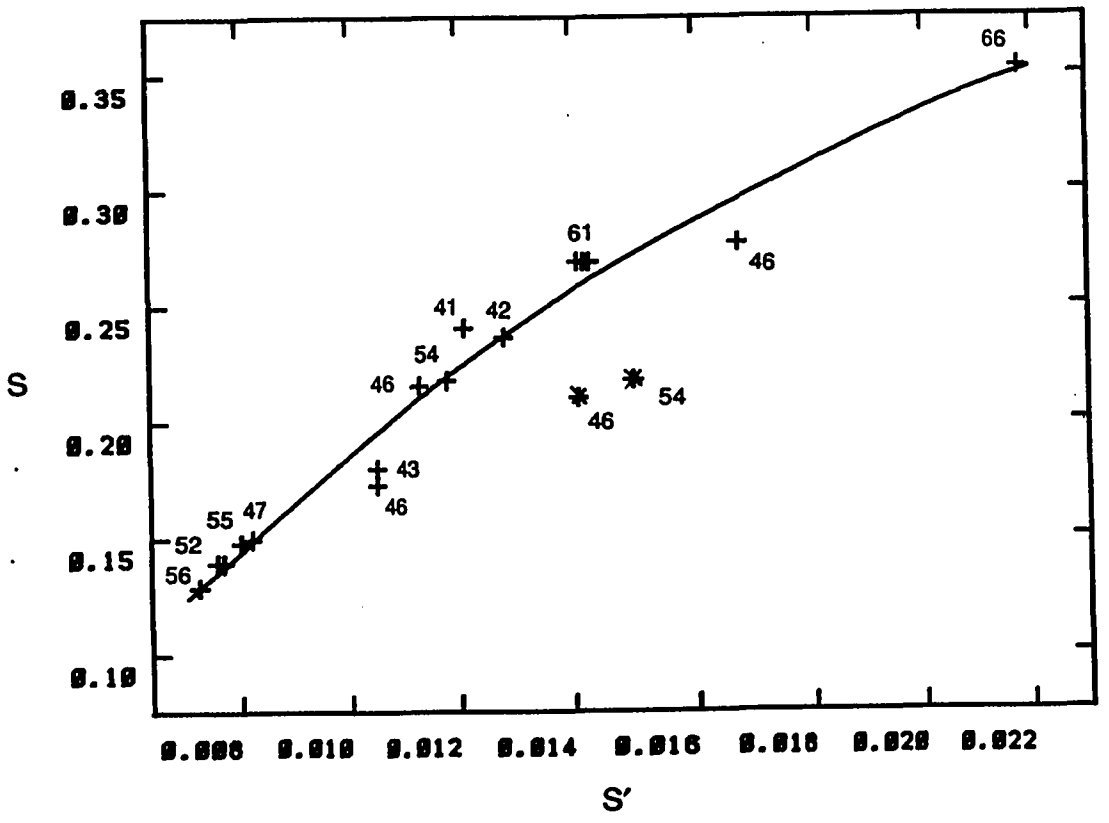

Figure 13. Calibration of the S' index of Ca II activity. The curve is a quadratic fit to the S' points with mean Mt. Wilson S values. The two points indicated by asterisks were omitted from the fit due to low S/N values. The legends for each point indicate the $B-V$ value for each star in hundredths of a magnitude. There is no obvious color dependence in the calibration.

have additional uncertainties on the order of 30% due to stellar activity cycles (Wilson 1978, Baliunas and Vaughan 1985, Baliunas 1985).

3. Field Star Sample Age Description

Chapter II described a first approach to the estimation of ages for F and early G field stars by fitting of model isochrones in the theoretical HR diagram

Table 4

Observed Parameters for Stars with Ca II Relative Surface Fluxes

Name	HR	HD	β	$\log T$		S Ref.	#	$B-V_c$	$\log C_{cf}$	R_{HK}	R_{phot}	R'_{HK}	F'_{HK}
(1)	(2)	(3)	(4)	(5)	(6)	(7)	(8)	(9)	(10)	(11)	(12)	(13)	(14)
θ Scl	35	739	2.652	3.812	0.1375	1	1	0.47	0.251	3.28	2.51	0.77±0.28	0.77
	251	5156	2.673	3.822	0.2086	1	1	0.43	0.286	5.41	2.83	2.58 0.35	2.84
77 Psc	313	6479	2.681	3.826	0.1934	1	1	0.40	0.312	5.31	3.22	2.09 0.37	2.38
30 Cet	329	6706	2.675	3.823	0.2285	1	1	0.41	0.303	6.16	2.92	3.24 0.37	3.60
	410	8673	2.651	3.812	0.1875	1	1	0.47	0.251	4.48	2.50	1.98 0.30	1.98
ω And	417	8799	2.672	3.822	0.2365	2	1	0.43	0.286	6.13	2.78	3.35 0.36	3.68
	494	10481	2.694	3.831	0.2809	1	1	0.38	0.328	8.01	3.97	4.04 0.49	4.84
ι^2 For	777	16538	2.656	3.814	0.1330	1	1	0.46	0.260	3.24	2.55	0.69 0.28	0.70
84 Cet	790	16765	2.646	3.809	0.2809	1	1	0.49	0.232	6.42	2.46	3.96 0.34	3.87
θ Per	799	16895	2.625	3.795	0.1587	2	2	0.54	0.182	3.24	2.27	0.97 0.26	0.83
10 Tau	1101	22484	2.610	3.780	0.1469	2	1	0.60	0.118	2.58	2.14	0.44 0.23	0.33
	1249	25457	2.645	3.808	0.3147	1	1	0.49	0.232	7.19	2.45	4.74 0.36	4.61
	2233	43318	2.646	3.809	0.1308	1	1	0.49	0.232	2.99	2.46	0.53 0.27	0.52
74 Ori	2241	43386	2.663	3.818	0.2258	2	11	0.44	0.278	5.74	2.62	3.12 0.33	3.30
α CMi	2943	61421	2.670	3.821	0.1891	2	1	0.43	0.286	4.90	2.69	2.21 0.32	2.41
	3079	64379	2.651	3.812	0.2249	1	1	0.47	0.251	5.37	2.50	2.87 0.32	2.87
	3499	75332	2.626	3.796	0.2766	2	188	0.54	0.182	5.64	2.28	3.36 0.31	2.90
40 Leo	4054	89449	2.654	3.813	0.1781	2	1	0.46	0.260	4.34	2.53	1.81 0.30	1.84
γ Vir B	4826*	110380	2.706	3.836			1	0.36	0.343	5.96	4.83	1.13 0.53	1.41
18 Boo	5365	125451	2.676	3.824	0.2384	2	240	0.41	0.303	6.43	2.97	3.46 0.38	3.86
	5436	127821	2.671	3.821	0.2300	2	3	0.43	0.286	5.96	2.74	3.22 0.35	3.52
σ Boo	5447	128167	2.681	3.826	0.1896	2	3	0.40	0.312	5.21	3.22	1.99 0.37	2.27
	5583	132375	2.644	3.808	0.1483	2	3	0.49	0.232	3.39	2.44	0.95 0.27	0.92
45 Boo	5634	134083	2.664	3.818	0.2143	2	2	0.44	0.278	5.44	2.63	2.81 0.33	2.98
γ Ser	5933	142860	2.633	3.801	0.1579	2	2	0.52	0.203	3.37	2.34	1.03 0.26	0.93
	5975	143928	2.677	3.824	0.1816	1	1	0.41	0.303	4.89	3.02	1.87 0.35	2.10
	7126	175317	2.671	3.821	0.1776	1	1	0.43	0.286	4.60	2.74	1.86 0.32	2.03
	7354	182101	2.645	3.808	0.2107	2	350	0.49	0.232	4.82	2.45	2.37 0.30	2.30

Table 4 (Continued) Observed Parameters for Stars with Ca II Relative Surface Fluxes

Name	HR	HD	β	$\log T$		S Ref.	#	$B-V_c$	$\log C_{cf}$	R_{HK}	R_{phot}	R'_{HK}	F'_{HK}
(1)	(2)	(3)	(4)	(5)	(6)	(7)	(8)	(9)	(10)	(11)	(12)	(13)	(14)
θ Cyg A	7469A	185395	2.689	3.829	0.2160	1	1	0.39	0.320	6.05	3.66	2.39±0.43	2.81
17 Cyg A	7534A	187013	2.646	3.809	0.1492	2	366	0.49	0.232	3.41	2.46	0.95 0.27	0.93
	7697	191195	2.679	3.825	0.1973	1	1	0.41	0.303	5.32	3.12	2.20 0.37	2.49
	7729	192486	2.687	3.828	0.1330	1	1	0.39	0.320	3.72	3.55	< 0.55	< 0.65
	7793	194012	2.626	3.796	0.1939	2	351	0.54	0.182	3.95	2.28	1.67 0.27	1.44
	7925	197373	2.667	3.820	0.2100	2	2	0.43	0.286	5.44	2.66	2.78 0.33	2.99
ψ Cap	7936	197692	2.670	3.821	0.2196	1	1	0.43	0.286	5.69	2.69	3.00 0.34	3.27
	8013	199260	2.636	3.803	0.2722	1	1	0.50	0.222	6.09	2.36	3.73 0.32	3.44
	8031	199684	2.688	3.829	0.1915	1	1	0.39	0.320	5.36	3.61	1.75 0.41	2.05
ξ Peg	8665	215648	2.626	3.796	0.1420	2	3	0.54	0.182	2.90	2.28	0.62 0.25	0.54
5 And	8805	218470	2.672	3.822	0.1796	1	1	0.43	0.286	4.65	2.78	1.87 0.32	2.05
ι Psc	8969	222368	2.622	3.792	0.1543	2	3	0.55	0.172	3.07	2.24	0.83 0.25	0.69
	9074	212487	2.630	3.799	0.2240	2	1	0.53	0.193	4.68	2.31	2.37 0.25	2.13
Hz II 25		23061	2.662	3.817	0.2241	2	2	0.44	0.278	5.69	2.61	3.08 0.33	3.24
Hz II 164		23158	2.652	3.812	0.3272	2	2	0.47	0.251	7.81	2.51	5.30 0.38	5.33
Hz II 233		23195	2.663	3.818	0.1913	2	2	0.44	0.278	4.86	2.62	2.24 0.32	2.37
Hz II 405		23269	2.628	3.797	0.3132	2	3	0.53	0.193	6.54	2.29	4.25 0.33	3.72
Hz II 530		23326	2.691	3.830	0.2002	2	1	0.39	0.320	5.60	3.79	1.81 0.43	2.14
Hz II 605		23351	2.695	3.832	0.2599	2	1	0.38	0.328	7.41	4.04	3.37 0.48	4.05
Hz II 727			2.637	3.804	0.3569	2	3	0.50	0.222	7.98	2.37	5.61 0.37	5.21
Hz II 745			2.685	3.827	0.2773	2	1	0.40	0.312	7.62	3.43	4.19 0.44	4.85
Hz II 1122		23511	2.675	3.823	0.2811	2	1	0.41	0.303	7.58	2.92	4.66 0.40	5.18
Hz II 1139		23513	2.673	3.822	0.2240	2	1	0.43	0.286	5.81	2.83	2.98 0.35	3.29
Hz II 1309		23584	2.662	3.817	0.3592	2	1	0.44	0.278	9.12	2.61	6.51 0.42	6.85
Hz II 1613		282973	2.644	3.808	0.3077	2	1	0.49	0.232	7.03	2.44	4.59 0.35	4.44
Hz II 1726		23713	2.652	3.812	0.2844	2	2	0.47	0.251	6.79	2.51	4.28 0.35	4.30
Hz II 1766		23732	2.690	3.830	0.3597	2	2	0.39	0.320	10.10	3.72	6.38 0.52	7.52
Hz II 1797			2.625	3.795	0.3467	2	1	0.54	0.182	7.07	2.27	4.80 0.34	4.11
Hz II 1856		282971	2.628	3.797	0.3202	2	1	0.53	0.193	6.69	2.29	4.40 0.33	3.86
Hz II 2345		23912	2.671	3.821	0.3276	2	1	0.43	0.286	8.49	2.74	5.75 0.41	6.29

Table 4 (Continued) Observed Parameters for Stars with Ca II Relative Surface Fluxes

Name	HR	HD	β	$\log T$		S Ref.	#	$B-V_c$	$\log C_{cf}$	R_{HK}	R_{phot}	R'_{HK}	F'_{HK}
(1)	(2)	(3)	(4)	(5)	(6)	(7)	(8)	(9)	(10)	(11)	(12)	(13)	(14)
T 53		107067	2.625	3.795	0.2303	2	1	0.54	0.182	4.70	2.27	2.43±0.28	2.08
T 58		107132	2.626	3.796	0.2903	2	1	0.54	0.182	5.92	2.28	3.64 0.31	3.14
T 65		107214	2.605	3.774	0.3016	2	1	0.62	0.095	5.03	2.10	2.93 0.28	2.07
T 76		107399	2.613	3.783	0.2858	2	1	0.59	0.129	5.16	2.17	2.99 0.29	2.30
T 85		107583	2.596	3.763	0.2874	2	1	0.65	0.060	4.42	2.03	2.39 0.26	1.53
T 86		107611	2.652	3.812	0.2453	2	1	0.47	0.251	5.85	2.51	3.34 0.33	3.36
T 90		107685	2.636	3.803	0.2476	2	1	0.50	0.222	5.54	2.36	3.18 0.31	2.94
T 92		107701	2.632	3.800	0.3009	2	1	0.52	0.203	6.43	2.33	4.10 0.33	3.69
T 97		107793	2.617	3.787	0.2978	2	1	0.57	0.151	5.65	2.20	3.45 0.30	2.76
T 111		108102	2.612	3.782	0.4209	2	1	0.59	0.129	7.59	2.16	5.43 0.35	4.14
T 114		108154	2.651	3.812	0.2569	2	1	0.47	0.251	6.13	2.50	3.63 0.33	3.63
T 118		108226	2.657	3.815	0.2306	2	1	0.45	0.269	5.74	2.56	3.18 0.33	3.27
vB 29		27383	2.621	3.791	0.2650	3	179	0.56	0.162	5.15	2.23	2.92 0.29	2.42
vB 31		27406	2.623	3.793	0.2880	3	157	0.55	0.172	5.73	2.25	3.48 0.31	2.93
vB 35		27524	2.655	3.814	0.2400	3	123	0.46	0.260	5.85	2.54	3.31 0.33	3.38
vB 36		27534	2.671	3.821	0.2100	3	214	0.43	0.286	5.44	2.74	2.70 0.34	2.95
vB 37		27561	2.674	3.823	0.2470	3	146	0.43	0.286	6.40	2.87	3.53 0.37	3.91
vB 48		27808	2.626	3.796	0.2620	3	183	0.54	0.182	5.34	2.28	3.06 0.30	2.64
vB 49		27835	2.610	3.780	0.2930	3	12	0.60	0.118	5.15	2.14	3.01 0.28	2.24
vB 51		27548	2.659	3.816	0.1990	3	111	0.45	0.269	4.95	2.58	2.37 0.31	2.46
vB 52		27859	2.606	3.775	0.3150	3	101	0.61	0.107	5.40	2.11	3.29 0.29	2.35
vB 57		27991	2.644	3.808	0.2390	3	176	0.49	0.232	5.46	2.44	3.02 0.31	2.92
vB 59		28034	2.635	3.802	0.2780	3	60	0.50	0.222	6.22	2.36	3.86 0.33	3.54
vB 65		28205	2.620	3.790	0.2400	3	134	0.56	0.162	4.66	2.22	2.44 0.28	2.01
vB 77		28394	2.637	3.804	0.2620	3	97	0.50	0.222	5.86	2.37	3.49 0.32	3.24

Table 4 (Continued) Observed Parameters for Stars with Ca II Relative Surface Fluxes

Name	HR	HD	β	$\log T$		S		$B-V_c$	$\log C_{cf}$	R_{HK}	R_{phot}	R'_{HK}	F'_{HK}
						Ref.	#						
(1)	(2)	(3)	(4)	(5)	(6)	(7)	(8)	(9)	(10)	(11)	(12)	(13)	(14)
vB 78		28406	2.656	3.814	0.1960	3	163	0.46	0.260	4.78	2.55	2.23±0.31	2.28
vB 81		28483	2.654	3.813	0.2290	3	84	0.46	0.260	5.58	2.53	3.05 0.32	3.10
vB 85		28568	2.680	3.825	0.2360	3	116	0.41	0.303	6.36	3.17	3.19 0.39	3.62
vB 88		28635	2.635	3.802	0.2500	3	33	0.50	0.222	5.59	2.36	3.23 0.31	2.97
vB 101		29225	2.681	3.826	0.2230	3	101	0.40	0.312	6.13	3.22	2.91 0.39	3.31
KW 16		73061	2.656	3.814						5.04	2.55	2.49 0.31	2.55
KW 127			2.606	3.775	0.2570	2	1	0.61	0.107	4.40	2.11	2.29 0.26	1.63
KW 162			2.613	3.783	0.3104	2	1	0.59	0.129	5.60	2.17	3.43 0.30	2.64
KW 217			2.631	3.800	0.2763	2	1	0.52	0.203	5.90	2.32	3.58 0.31	3.20
KW 227		73641	2.673	3.822						5.36	2.83	2.53 0.34	2.79
KW 238			2.640	3.806	0.3648	2	1	0.50	0.222	8.16	2.40	5.76 0.38	5.45
KW 250			2.656	3.814	0.2156	2	1	0.46	0.260	5.26	2.55	2.71 0.32	2.78
Sun			2.600	3.763	0.1710	4		0.65	0.060	2.70	2.06	0.64 0.23	0.41

NOTES.

* Ca II flux obtained from line profile by Kelch *et al.* 1979. See text.

Column (1): Cluster Star Identifications:
Hz II: Pleiades cluster, Hertzsprung (1947).
vB: Hyades cluster, van Bueren (1952).
T: Coma Bernices cluster, Trumpler (1938).
KW: Praesepe cluster, Klein Wassink (1927).

Column (4): Strögren β index from Hauck and Mermilliod (1980).

Column (5): Effective temperature obtained using β index.

Column (6): Ca II H and K line core flux relative to the nearby continuum, expressed in terms of the Mt. Wilson S index. (Vaughan, Preston, and Wilson 1978).

Column (7): Sources for S measurements:
1. This work.
2. Duncan (1983, 1985).
3. Duncan *et al.* (1984).
4. Noyes *et al.* (1984).

Column (8): Number of S measurements averaged for mean value given in Column 6.

Column (9): Estimate of $B - V$ color obtained from β using the calibration of Hauck and Magnenat (1975). These values were used to obtain the Ca II relative surface flux R_{HK} and the "photospheric correction" R_{phot}.

Column (11), (12), and (13): ($\times 10^{-5}$).
R_{HK} is the total flux in the H and K cores relative to the total flux of the star. R_{phot} is the portion due to the quiet, radiatively heated atmosphere of the star. R'_{HK} is the remainder due to chromospheric activity.

Column (14): Ca II chromospheric surface flux in units of 10^6 erg $cm^{-2}s^{-1}$.

to luminosities, compositions, and effective temperatures derived from Strömgren photometry. The method obtained satisfactory results for individual stars in a nearby open cluster (NGC 752) compared to main sequence fitting for the cluster as a whole. The luminosities obtained from the Strömgren indices were consistent with those obtained from good quality parallax data (those with $\sigma(M_V) < \pm 0.20$).

Comparison of T_{eff} and luminosity of field stars with models of the correct composition is the most direct method of age determination, as long as good temperatures and luminosities can be found. In Chapter II, effective temperatures were obtained from Strömgren $b-y$ colors using the calibration of Hauck and Magnenat (1975). As Twarog (1980) has indicated, Hβ colors are to be preferred for T_{eff} calibrations, since this removes a source of systematic errors in the δc_1 and δm_1 indices. In spite of this, $b-y$ was used in Chapter II because a comparison of Hβ, $b-y$, and $B-V$ colors indicated that the correlation between Hβ and T_{eff} breaks down for $\beta < 2.600$, as has been noted by Strömgren (1966). As all stars considered here have Hβ greater than 2.60 and $b-y$ less than 0.36, this problem does not appear. Hβ was used throughout the remainder of this dissertation as a measure of effective temperature. However, rather than the Hauck and Magnenat T_{eff} calibration, the more recent calibration of Böhm-Vitense (1981) was used. All Hβ values were converted to $B-V$ estimates using the Hauck and Magnenat relations and effective temperatures were then obtained using Böhm-Vitense's Table 3. Where two branches of the T_{eff}–$B-V$ calibration appear, the T_{eff} used was the average of the two. This calibration is the same as that used by Wolff, Boesgaard, and Simon (1986).

An additional benefit of using Hβ as the effective temperature indicator is the capabilty of dereddening the Strömgren indices. While all stars in this work

are relatively nearby, some show a small amount of reddening. The dereddening technique used is that of Crawford and Barnes (1970). This technique also allows age determinations to be made for more distant stars with larger amounts of reddening present.

The metallicity calibration adopted is that of Crawford and Perry (1976)

$$[\mathrm{Fe/H}] = 0.15 - 11\delta m_0(\beta) \qquad 14$$

The absolute magnitude calibration was done as in Twarog (1980). The empirical absolute magnitude calibration of Crawford (1975) gives

$$M_V = M_V(ZAMS,\beta) - f\delta c_0(\beta) \qquad 15a$$

with

$$f = 9 + 20(2.720 - \beta). \qquad 15b$$

In order to preserve the differences in composition between the empirical ZAMS and the particular star being observed, and to limit uncertainty in the magnitude estimate arising from the empirical ZAMS calibration, only the difference $\delta M_V = M_V - M_V(ZAMS)$ will be used. The final luminosity of each star is based on the sum of the theoretical ZAMS of the proper composition and the δM_V.

The model isochrones used were those of VandenBerg (1983), with $Y = 0.25$ and $\alpha = 1.6$. This is a change from the earlier work (see Chapter II) in which the Ciardullo and Demarque (1977) isochrones were used. The VandenBerg models include more recent opacities and improved physics and boundary conditions. The value of the mixing length ratio $\alpha = 1.6$ allows a consistent set of open and globular cluster isochrones to be used (VandenBerg 1983).

The lack of a set of isochrones for field stars with significantly higher [Fe/H] values than the Sun causes a problem in estimating ages and masses for these objects.

If stars with [Fe/H] > 0.10 are modeled using the solar metallicity ($Z = 0.0169$) isochrones, the masses obtained from the fits would differ systematically from the correct values. A comparison of zero-age main sequences for $Z = 0.020$ and $Z = 0.0169$ (VandenBerg and Bridges 1984) indicates that for stars in the temperature range of interest the mass difference is on the order of $0.10M_{\odot}$, significantly larger than the uncertainties from photometric errors alone. As indicated in section (2), these stars were omitted from the final field star sample.

The lack of isochrones for [Fe/H] > 0.10 has also made it impractical to interpolate between two metallicities (the upper and lower bounds of the error bar, as described in Chapter II. Instead, the position of each star on the theoritical HR diagram was determined only for the isochrone sequence appropriate for its metallicity as determined from the δm_0 index. Thus the uncertainty indicated in Table 5 for the age and mass of each star reflects only the uncertainties in T_{eff} and δM_{bol} as determined from the Strömgren photometry.

Duncan (1984) has estimated ages for a large number of field F stars which are members of binary systems, often using an A star in the system to improve age discrimination. The models used were those of Maeder (1976) with $X = 0.70$ and $Z = 0.03$ for all stars. In Figure 14 are compared his ages and age determined using the methods described here and in Chapter II, using stars with well-determined ages from both methods. If a single Z value is used in choosing the isochrones to compare with the temperature and luminosity of the stars, a good linear relation exists between the methods. It appears that best agreement occurs using the Ciardullo and Demarque isochrones with $Y = 0.30$ and $Z = 0.015$ (Figure 14a). If the VandenBerg (1983) isochrones are used (Figure 14b), an age scale difference is apparent, such that for $Y = 0.25$ and $Z = 0.0169$, the maximum age observed

Table 5

Age and Mass Estimates for Stars with Ca II Relative Surface Fluxes

Name	HD	Age	Mass	$\log T_{eff}$	$\log(L_*/L_\odot)$	[Fe/H]
(1)	(2)	(3)	(4)	(5)	(6)	(7)
HR 35	739	2.55±0.56	1.311±0.051	3.812	0.512	−0.106
HR 251	5156	2.11 0.25	1.415 0.065	3.822	0.656	−0.020
HR 313	6479	2.63 0.56	1.247 0.046	3.826	0.540	−0.142
HR 329	6706	2.07 0.24	1.424 0.067	3.823	0.668	0.094
HR 410	8673	2.61 0.36	1.343 0.062	3.812	0.568	0.033
HR 417	8799	1.87 0.86	1.344 0.040	3.822	0.532	−0.053
HR 494	10481	< 0.90	1.373 0.033	3.831	0.420	0.044
HR 777	16538	2.32 0.83	1.306 0.042	3.814	0.492	−0.053
HR 790	16765	1.69	1.243 0.070	3.809	0.200	−0.060
HR 799	16895	5.82 2.67	1.037 0.038	3.795	0.244	−0.188
HR 1101	22484	10.61 2.06	0.953 0.034	3.780	0.236	−0.152
HR 1249	25457	< 1.38	1.258 0.049	3.809	0.268	0.028
HR 2233	43318	2.73 0.96	1.348 0.068	3.809	0.580	−0.091
HR 2241	43386	1.57 1.37	1.304 0.046	3.818	0.448	−0.080
HR 2943	61421	2.16 0.24	1.411 0.065	3.821	0.652	0.080
HR 3079	64379	< 2.12	1.276 0.041	3.812	0.344	0.078
HR 3499	75332	3.35 2.45	1.173 0.046	3.796	0.288	0.035
HR 4054	89449	2.51 0.30	1.368 0.066	3.813	0.604	0.075
HR 4826	110380	< 0.71	1.267 0.047	3.836	0.348	−0.124
HR 5365	125451	1.82 0.80	1.355 0.041	3.824	0.548	0.043
HR 5436	127821	< 1.06	1.322 0.040	3.821	0.348	−0.076
HR 5447	128167	1.99 1.54	1.215 0.042	3.826	0.440	−0.289
HR 5583	132375	2.84 0.57	1.306 0.058	3.808	0.516	0.050
HR 5634	134083	1.92 1.29	1.315 0.054	3.818	0.488	0.053
HR 5933	142860	5.28 1.82	1.081 0.036	3.801	0.340	−0.256
HR 5975	143928	2.75 0.86	1.254 0.062	3.824	0.560	−0.171
HR 7126	175317	2.08 0.50	1.364 0.053	3.821	0.576	0.051
HR 7354	182101	3.83 1.50	1.144 0.036	3.808	0.400	−0.306

Table 5 (Continued) Age and Mass Estimates for Stars with CaII Relative Surface Fluxes

Name	HD	Age	Mass	$\log T_{eff}$	$\log(L_*/L_\odot)$	[Fe/H]
(1)	(2)	(3)	(4)	(5)	(6)	(7)
HR 7469A	185395	1.11±1.08	1.364±0.046	3.829	0.520	0.026
HR 7534A	187013	2.77 0.58	1.317 0.060	3.809	0.532	−0.096
HR 7697	191195	1.94 0.45	1.386 0.053	3.825	0.604	0.040
HR 7729	192486	1.41 1.06	1.368 0.051	3.828	0.544	−0.084
HR 7793	194012	< 3.97	1.062 0.064	3.796	0.096	−0.174
HR 7925	197373	2.38 1.80	1.180 0.042	3.820	0.396	−0.122
HR 7936	197692	2.11 0.46	1.365 0.054	3.821	0.580	−0.027
HR 8013	199260	< 1.82	1.225 0.049	3.803	0.228	−0.078
HR 8031	199684	1.79 0.45	1.405 0.053	3.829	0.624	−0.072
HR 8665	215648	6.77 1.35	1.057 0.036	3.796	0.380	−0.334
HR 8805	218470	2.10 0.36	1.383 0.058	3.822	0.608	−0.016
HR 8969	222368	7.44 1.50	1.032 0.035	3.792	0.340	−0.219
HR 9074	212487	< 2.55	1.196 0.046	3.799	0.208	0.034
Hz II 25	23061	0.08 0.01	1.323 0.020	3.817	0.382	0.050
Hz II 164	23158	0.08 0.01	1.300 0.020	3.812	0.346	0.050
Hz II 233	23195	0.08 0.01	1.325 0.020	3.818	0.385	0.050
Hz II 405	23269	0.08 0.01	1.219 0.020	3.797	0.208	0.050
Hz II 530	23326	0.08 0.01	1.383 0.020	3.830	0.475	0.050
Hz II 605	23351	0.08 0.01	1.391 0.020	3.832	0.488	0.050
Hz II 727		0.08 0.01	1.253 0.020	3.804	0.267	0.050
Hz II 745		0.08 0.01	1.371 0.020	3.827	0.457	0.050
Hz II 1122	23511	0.08 0.01	1.350 0.020	3.823	0.426	0.050
Hz II 1139	23513	0.08 0.01	1.346 0.020	3.822	0.419	0.050
Hz II 1309	23584	0.08 0.01	1.323 0.020	3.817	0.382	0.050
Hz II 1613	282973	0.08 0.01	1.276 0.020	3.808	0.306	0.050
Hz II 1726	23713	0.08 0.01	1.300 0.020	3.812	0.346	0.050
Hz II 1766	23732	0.08 0.01	1.381 0.020	3.830	0.472	0.050
Hz II 1797		0.08 0.01	1.206 0.020	3.795	0.185	0.050

Table 5 (Continued) Age and Mass Estimates for Stars with CaII Relative Surface Fluxes

Name	HD	Age	Mass	$\log T_{eff}$	$\log(L_*/L_\odot)$	[Fe/H]
(1)	(2)	(3)	(4)	(5)	(6)	(7)
Hz II 1856	282971	0.08 0.01	1.219 0.020	3.797	0.208	0.050
Hz II 2345	23912	0.08 0.01	1.342 0.020	3.821	0.412	0.050
T 53	107067	0.65±0.10	1.206±0.020	3.795	0.185	−0.030
T 58	107132	0.65 0.10	1.210 0.020	3.796	0.193	−0.030
T 65	107214	0.65 0.10	1.102 0.020	3.774	−0.008	−0.030
T 76	107399	0.65 0.10	1.147 0.020	3.783	0.078	−0.030
T 85	107583	0.65 0.10	1.058 0.020	3.763	−0.093	−0.030
T 86	107611	0.65 0.10	1.300 0.020	3.812	0.346	−0.030
T 90	107685	0.65 0.10	1.249 0.020	3.803	0.261	−0.030
T 92	107701	0.65 0.10	1.235 0.020	3.800	0.235	−0.030
T 97	107793	0.65 0.10	1.168 0.020	3.787	0.117	−0.030
T 111	108102	0.65 0.10	1.142 0.020	3.782	0.068	−0.030
T 114	108154	0.65 0.10	1.297 0.020	3.812	0.341	−0.030
T 118	108226	0.65 0.10	1.311 0.020	3.815	0.364	−0.030
vB 29	27383	0.70 0.10	1.307 0.020	3.791	0.247	0.130
vB 31	27406	0.70 0.10	1.316 0.020	3.793	0.261	0.130
vB 35	27524	0.70 0.10	1.419 0.020	3.814	0.420	0.130
vB 36	27534	0.70 0.10	1.454 0.020	3.821	0.470	0.130
vB 37	27561	0.70 0.10	1.461 0.020	3.823	0.479	0.130
vB 48	27808	0.70 0.10	1.329 0.020	3.796	0.281	0.130
vB 49	27835	0.70 0.10	1.248 0.020	3.780	0.147	0.130
vB 51	27548	0.70 0.10	1.428 0.020	3.816	0.433	0.130
vB 52	27859	0.70 0.10	1.224 0.020	3.775	0.105	0.130
vB 57	27991	0.70 0.10	1.392 0.020	3.808	0.379	0.130
vB 59	28034	0.70 0.10	1.363 0.020	3.802	0.335	0.130
vB 65	28205	0.70 0.10	1.303 0.020	3.790	0.239	0.130
vB 77	28394	0.70 0.10	1.370 0.020	3.804	0.345	0.130

Table 5 (Continued) Age and Mass Estimates for Stars with CaII Relative Surface Fluxes

Name	HD	Age	Mass	$\log T_{eff}$	$\log(L_*/L_\odot)$	[Fe/H]
(1)	(2)	(3)	(4)	(5)	(6)	(7)
vB 78	28406	0.70±0.10	1.422±0.020	3.814	0.423	0.130
vB 81	28483	0.70 0.10	1.417 0.020	3.813	0.416	0.130
vB 85	28568	0.70 0.10	1.473 0.020	3.825	0.497	0.130
vB 88	28635	0.70 0.10	1.363 0.020	3.802	0.335	0.130
vB 101	29225	0.70 0.10	1.475 0.020	3.826	0.500	0.130
KW 16	73061	0.90 0.10	1.309 0.020	3.814	0.360	0.090
KW 127		0.90 0.10	1.107 0.020	3.775	0.002	0.090
KW 162		0.90 0.10	1.147 0.020	3.783	0.078	0.090
KW 217		0.90 0.10	1.231 0.020	3.800	0.228	0.090
KW 227	73641	0.90 0.10	1.346 0.020	3.822	0.419	0.090
KW 238		0.90 0.10	1.263 0.020	3.806	0.284	0.090
KW 250		0.90 0.10	1.309 0.020	3.814	0.360	0.090

NOTES.

Column (3): Photometric age estimates using the stellar model isochrones of VandenBerg (1983).

Column (4): Photometric mass estimates using the VandenBerg isochrones.

Column (5): Effective temperatures from the Strömgren β index.

Column (6): Estimates of stellar luminosity. These combine the ZAMS theoretical luminosities with δM_V found from δc_0.

Column (7): Estimates of metallicity based on δm_0.

using the VandenBerg isochrones is ~12 Gyr, while the age obtained by Duncan for the same star is ~8 Gyr, using the Maeder (1976) isochrones with $X = 0.70$, $Z = 0.03$.

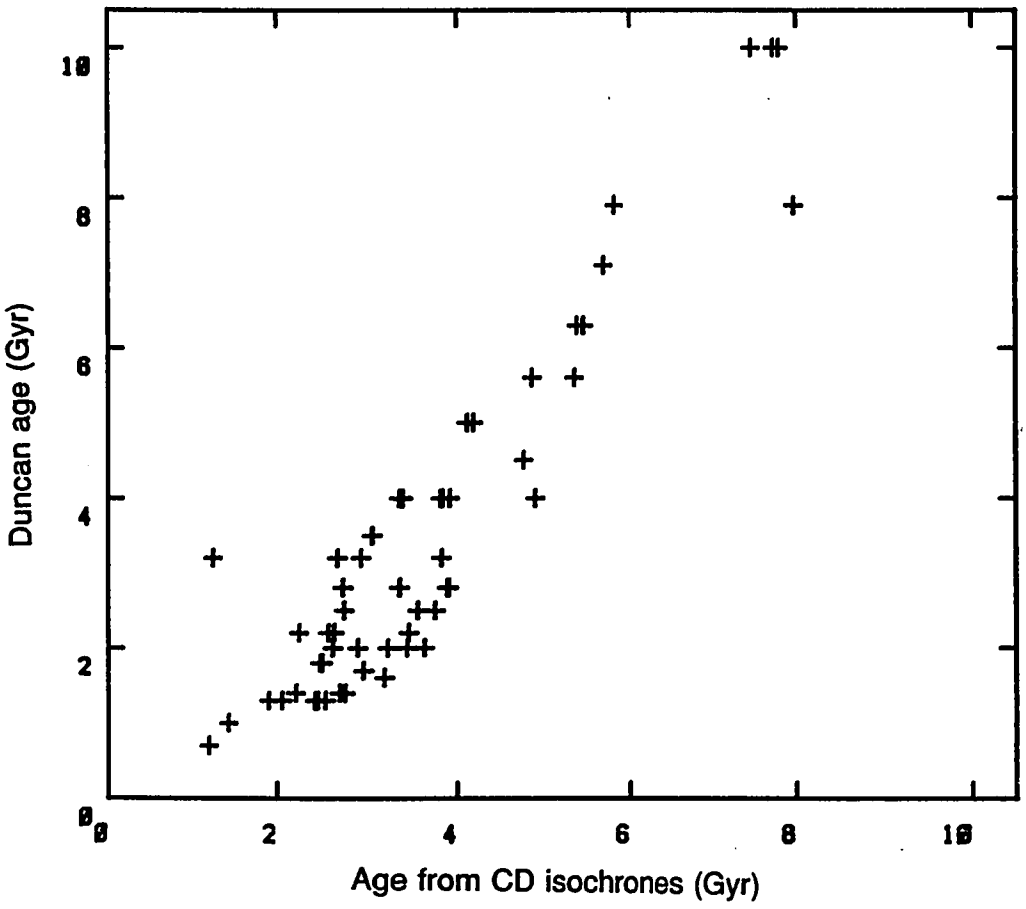

Figure 14a. Comparison of photometric ages found using the Ciardullo and Demarque isochrones for $Y = 0.30$ and $Z = 0.015$ and those of Duncan (1983).

In order to compare the cluster stars to the field stars, and group them into the field star mass bins, masses had to be estimated for the cluster stars. Because of recent work on very young active cluster members (LaBonte and Rose 1985) suggests a possible link between high activity levels and anomalous δc_1 index values,

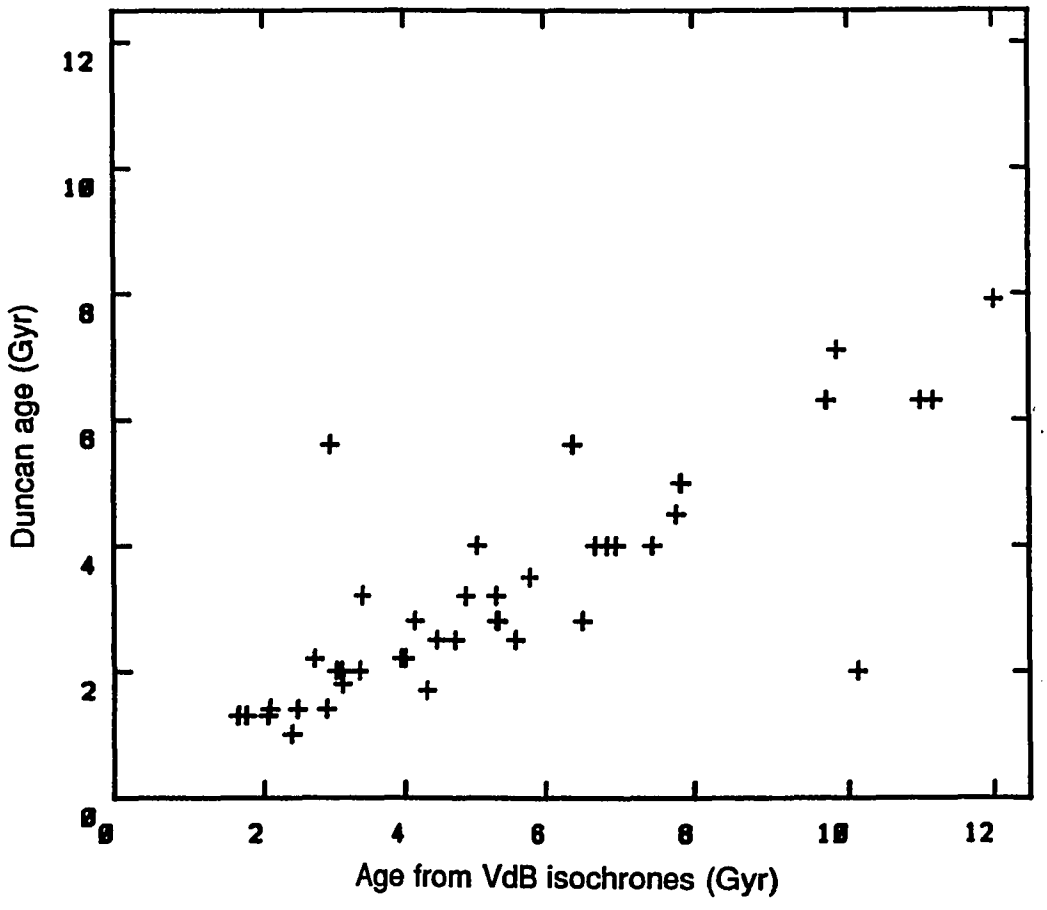

Figure 14b. Comparison of photometric ages found using the VandenBerg (1985) models with $Y = 0.25$ and $Z = 0.0169$ and the ages found by Duncan (1983). Different stellar interior models cause systematic age changes.

it was felt that using the Strömgren field star age estimate method might not yield consistent results. As all these clusters are quite young, the stars have not evolved far off the zero-age main sequence appropriate to their composition. Therefore, ages based on cluster main sequence fitting were used and masses were estimated from the stars' β indices alone, using the temperature calibration discussed above, using the zero-age main sequences of VandenBerg and Bridges (1984). A sequence at $Z = 0.026$ was interpolated from the $Z = 0.0169$ and $Z = 0.04$ sequences of VandenBerg and Bridges to allow the Hyades masses to be determined. In all

cases the $\log T_{eff}$ values of the VandenBerg and Bridges models were increased by 0.003 to compensate for the difference between the mixing length to scale height ratios of their models ($\alpha = 1.5$) and VandenBerg (1983) ($\alpha = 1.6$). This correction is consistent with the behavior of α in the VandenBerg models, and with the α corrections given by Ciardullo and Demarque (1979). Compositions for the cluster stars (based on Strömgren photometry) were taken from Nissen (1980), while the ages used were Pleiades, 0.08 Gyr (Duncan, 1981); Coma, 0.65 Gyr (van den Heuvel); Prsaesepe, 0.90 Gyr (VandenBerg and Bridges, 1984); and Hyades, 0.70 Gyr (Duncan, 1981).

This mass determination method for the young clusters also avoids most of the problems in using Strömgren photometry on the Hyades cluster stars. As was shown by Crawford (1969), the c_1 values for Hyades stars are anomalously large compared with the field and other clusters. The β index values, however, for the Hyades appear to show the same relationship to $B - V$ as do the other field and cluster stars (see Figure 15).

4. The Relative Chromospheric Ca II Surface Flux

Whatever measure of "chromospheric activity" we use ought to have some definite physical interpretation in terms of the relative importance of chromospheric activity in the total energy output of stars, independent of spectral type. As Duncan (1981) points out, this is a problem when using the Ca II line core emission since the emission observed is at the bottom of a strong line, which is itself strongly varying in strength with effective temperature, and is also in a region where the pseudo-continuum is strongly temperature-dependent. While the Mt. Wilson S

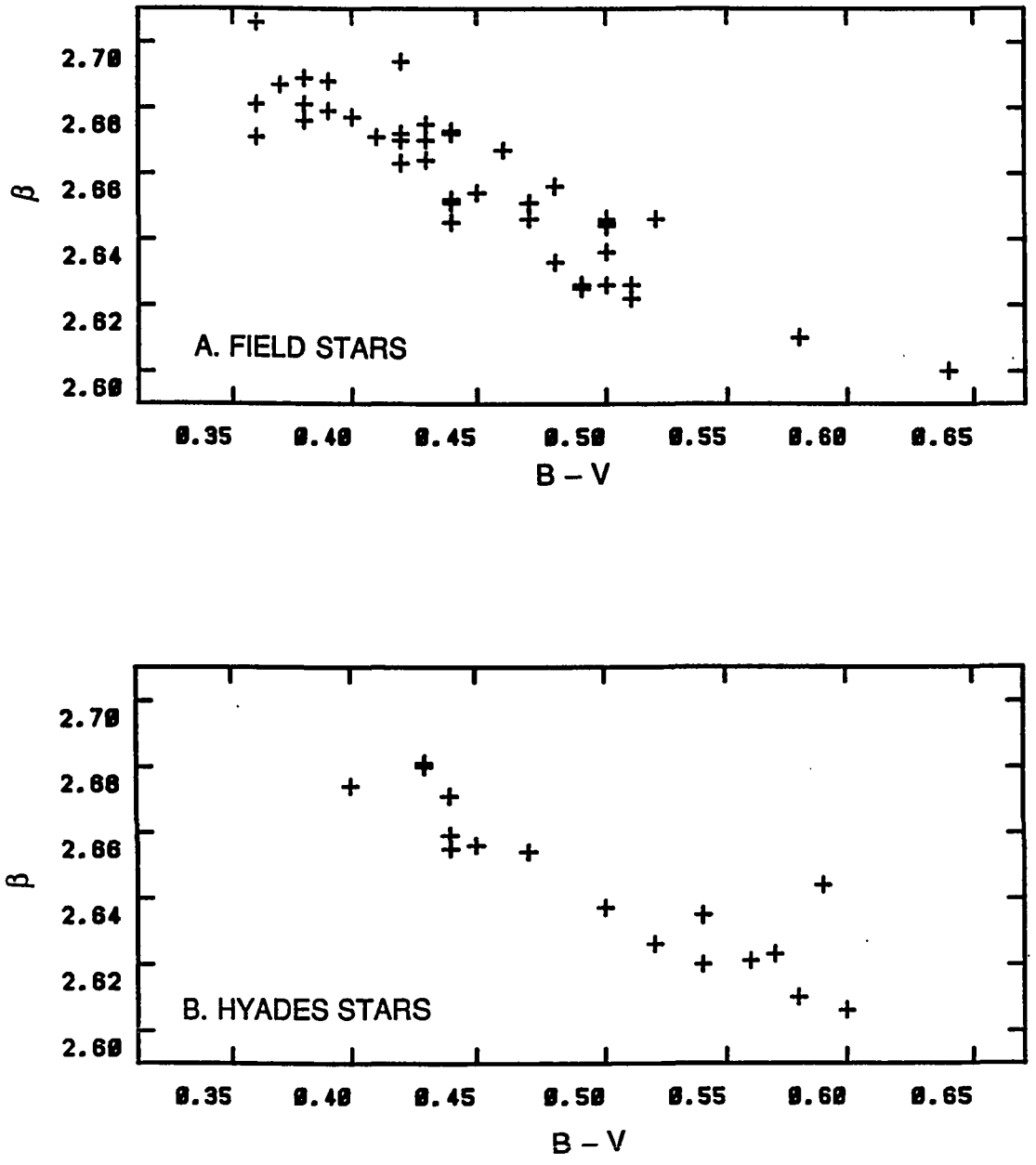

Figure 15. a) Field star β versus $B-V$ colors. b) Hyades β versus $B-V$ colors. No systematic difference is observed.

index is useful in comparing stars of similar spectral types, small decreases in temperature cause large increases in the S values, which then do not reflect the true significance of the chromospheric emission.

What Ca II flux indicator should then be used? Recent literature has emphasized two indices. One is the relative Ca II surface flux R_{HK} first used by Middelkoop (1982) and revised by Noyes *et al.* (1984). R_{HK} is the ratio of the surface flux observed in the core of the H and K lines to the total surface flux of the star. The great advantage of this approach is that, once allowance for the photospheric contribution to the H and K line cores is made (generating the Noyes *et al.* R'_{HK} index), a single relationship between chromospheric emission and Rossby number could be found for all late F, G, and K stars. The other approach has been to use F_{HK} directly (Rutten 1984) without dividing by the total surface flux. This allows relations to be found between F_{HK} and rotation to be found, but requires that the dependence of Ca II activity on rotation be color dependent Rutten 1985, Rutten and Schrijver 1985). Since the approach of Noyes *et al.* produces a final relation independent of color, I will extend their method to the early F stars and compare the results to those for later spectral types.

Noyes *et al.* have shown that the relative flux in the Ca II H and K line cores is given by $R_{HK} = 1.34 \times 10^{-4} C_{cf} S$, where C_{cf}, a function of $B-V$, corrects the HK continuum to a level corresponding to the bolometric surface flux of the star.

Noyes *et al.* (1984) have also adopted a correction for the contribution to the Ca II flux due to the photosphere. While I have adopted essentially the Noyes *et al.* calibration for R_{HK}, their photospheric correction is inadequate for early F stars. Noyes *et al.* assume that all emission in the Ca II K line core outside of the K_1 minima is photospheric, while all emission inside these boundaries is

chromospheric. This assumption is based on the close agreement between the chromospheric radiative loss in the solar K line and the flux emitted from between the K_1 minima (Noyes 1981). Linsky and Ayres (1978) have shown, however, that the Ca II line profile generated by a radiative equilibrium model atmosphere emits a non-negligible amount of flux between the K_1 minima. At least this much flux from the photosphere must be present in the H and K line cores whether magnetic activity is present or not. The results of Hartmann *et al.* (1984) indicate that $\log R_{photo} = \log R_{HK} - 0.12$ if the Linsky and Ayres photospheric correction is used. For the Sun the long-term mean S value is 0.171 (Noyes *et al.* 1984) and the $B-V$ and T_{eff} values adopted here are 0.64 and 5800 K (Böhm-Vitense, 1981). Hartmann *et al.* provide estimates of the flux outside the K_1 minima for stars as early as $B-V = 0.45$, but their correction for the photospheric flux between the K_1 minima (their "maximum correction") is based only on the Linsky and Ayres solar model. Use of the solar model for these mid-F stars ignores any changes in the photospheric Ca II emission due to the increase in T_{eff} in these stars.

In order to extend the method of Noyes *et al.* to earlier spectral types, two pieces of information are needed: values of C_{cf} and R_{phot} for main sequence stars with $0.3 \lesssim B-V \leq 0.45$. The C_{cf} parameter had already been adjusted by Noyes *et al.* (1984) for what they considered a non-physical maximum at $B-V = 0.43$. However, Noyes *et al.* only show spectrophotometric calibrations down to $B-V \approx 0.50$ in their Figure A1, while the stars considered in this chapter and Chapter V extend to $B-V = 0.36$. In order to be more certain of the correct C_{cf} for these bluer stars, $\log C_{cf}$ was recalculated using the spectrophotometry of O'Connell (1973) for stars with $0.16 < B-V < 0.82$ and the Barnes-Evans (1976) relation. The resulting correction factor was scaled to match the Middelkoop result for the G and K stars, and is shown in Figure 16. A least-squares fit yields the

following equation for C_{cf}:

$$\log C_{cf} = 0.520 - 0.223(B-V) - 0.746(B-V)^2 \qquad 16$$

For consistency with the stellar isochrone fitting, Hβ index values will be converted to B-V colors for use with the above calibration using a spline fit over the table of corresponding β and $B-V$ colors given by Hauck and Magnenat (1975). The quantity $R'_{HK} = 1.34 \times 10^{-4} C_{cf} S$ is then my best estimate of the relative surface flux observed in the Ca II H and K line cores.

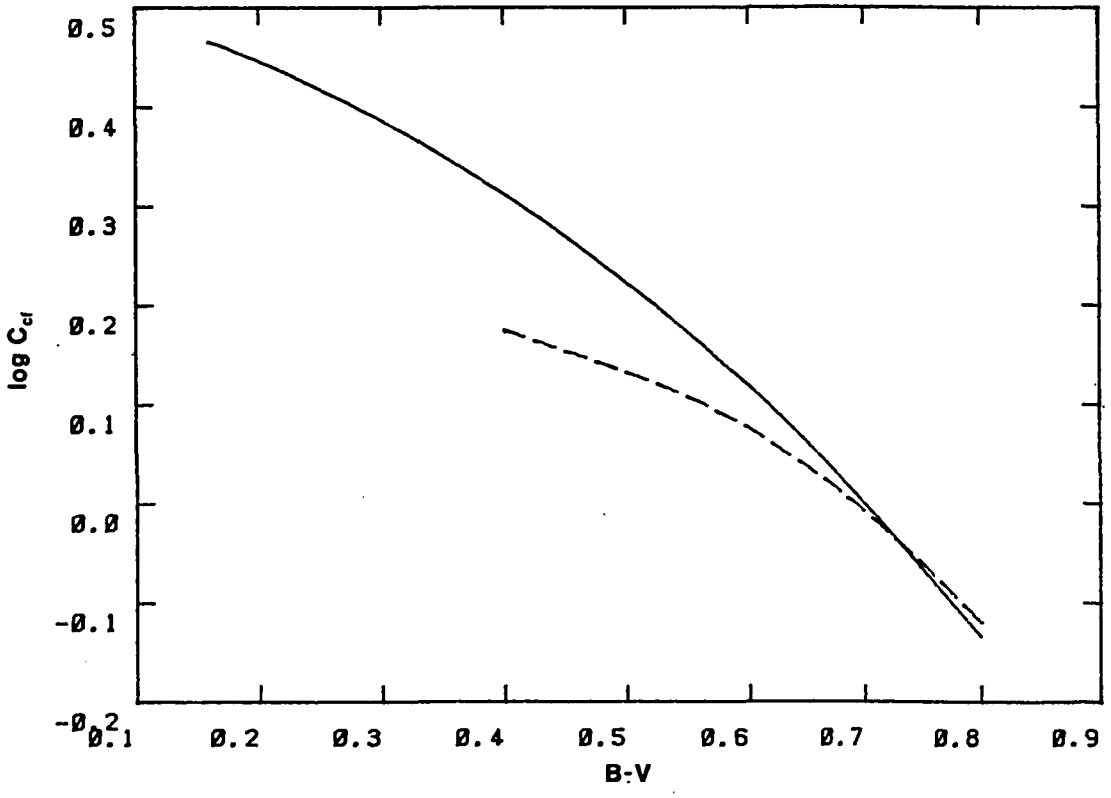

Figure 16. Calibration of the color correction factor C_cf with $B-V$. The calibration of Middelkoop (1982) is shown as a dashed line; the calibration used in this work (based on the spectrophotometry of O'Connell (1973) is shown as a solid line. The Ca II H and K relative surface flux is given by $R_{HK} = 1.34 \times 10^{-4} C_{cf} S$.

A major concern at this point then is the photospheric correction for stars bluer than $B-V = 0.45$. At some point the photospheric contribution in the core of the H and K lines will begin to increase substantially. Ideally the expected photospheric contribution could be estimated by using radiative equilibrium model atmospheres and calculating theoretical Ca II line profiles and then finding the flux emitted in the passband of the line index being used. This approach has been followed by Kelch *et al.* (1979) and Linsky *et al.* (1979). Since their passband is different from that used here, their photospheric contributions cannot simply be adopted. It is possible, however, to convert their results to the Mt. Wilson HK flux passband.

The star Procyon had available the observed flux between the K_1 minima and the photospheric contribution in the same band (Kelch *et al.* 1979), a RE model Ca II K line profile for the wings of the line (Ayres 1975), a flux calibrated observed profile of the K line core (Ayres, Linsky, and Shine 1974), and the profile of the entire line at high resolution (Griffin and Griffin 1979), so it appeared to be a good choice for use as a mid-F photospheric contribution reference point. The wings of the theoretical RE profile at 4 to 6 Å from line center are indistinguishable from the observed profile, and so these were used to match the theoretical profile to the Griffin atlas. In the region less than 1 Å from line center the RE profile was extrapolated linearly in flux to the line core. The extrapolated flux at the line core was 2.6×10^{-6}erg cm^{-1}s^{-1}Hz^{-1}. Integration between the K_1 minima showed that the K_1 flux index obtained from the extrapolated RE line profile was 49 % of the observed flux level, corresponding very closely to the 50% indicated by Kelch *et al.* The RE model Ca II flux in the Mt. Wilson passband (assuming that the total flux in H and K is equal to 1.91× the K line flux) is 0.548 of the total Ca II flux, or $R_{phot} = 2.69 \times 10^{-5}$.

The photospheric contribution in the core of the H and K lines becomes large in the early F dwarfs. The star γ Vir N was used to estimate the RE flux contribution in the core of the K line. Kelch *et al.* (1979) report that the RE contribution in the K line core (between the K_1 minima) is 80% of the observed flux. Unfortunately they don't say what the K_1 width is; therefore the spectrum given in Kelch *et al.* (1979) was digitized, and integrations were performed around the line center until the observed K_1 flux, $4.9 \times 10^6 \mathrm{erg\ cm^{-1}s^{-1}}$, was measured, yielding a K_1 width (distance between the K_1 minima) of 1.08 Å. Integrating the flux within the Mt. Wilson passband yielded a total R_{HK} of 5.96×10^{-5}, which is typical of other stars with β values similar to that for γ Vir B ($\beta = 2.706$). Note that here in passing from F_{HK} to $R_{HK} = F_{HK}/\sigma T^4$ a value of 6860 K was used for T_{eff}, corresponding to the Hβ index, and again the ratio of the K to H line fluxes was assumed to be 1.1.

In order to estimate the effect of the RE model over the Mt. Wilson passband, a linear correction function was constructed, and the observed profile was multiplied by it in order to approximate the RE model profile. The correction was such that the wings of the adjusted profile merged smoothly into the observed profile in the far wings (> 2 Å from line center) of the profile, while the line center inside the estimated K_1 minima at ± 0.54 Å had the correct integrated flux for the RE K line profile. Integrating the flux over the Mt. Wilson profile yielded a photospheric contribution $R_{phot} = 4.83 \times 10^{-5}$. This is 81% of the total observed relative flux in the Mt. Wilson passbands.

Over the temperature range considered here, the RE CaII flux contribution was considered to be a log-linear interpolation in Hβ of the above results:

$$\log R_{phot} = -4.686 + 1.657(\beta - 2.600) \qquad 17a$$

for $\beta < 2.670$ and

$$\log R_{phot} = -4.570 + 7.056(\beta - 2.670) \qquad 17b$$

for $\beta \geq 2.670$. The chromospheric relative Ca II flux will be designated R'_{HK}, where $R'_{HK} = R_{HK} - R_{phot}$. Values of R_{HK}, R_{phot}, and R'_{HK} are shown in Table 4.

An estimate of the uncertainty in the conversion from S to R_{HK} can be made based on the probable errors in the β index. The uncertainty of β values in the Hauck-Mermilliod catalog is roughly ± 0.007 (see Chapter II), which corresponds to an uncertainty in calculated $B - V$ of ± 0.015. Standard error propagation techniques yield an uncertainty $\sigma \log C_{cf} \approx 0.9\sigma(B - V)$. Then,

$$\left(\frac{\sigma(R_{HK})}{R_{HK}}\right)^2 = \left(\frac{\sigma(S)}{S}\right)^2 + \left(\ln 10 \sigma(\log C_{cf})\right)^2 \qquad 18$$

or,

$$\left(\frac{\sigma(R_{HK})}{R_{HK}}\right)^2 \approx \left(\frac{\sigma(S)}{S}\right)^2 + 4.2\sigma^2(B - V). \qquad 19$$

If $\sigma(B-V) = 0.015$ and the relative error in S is 1.9% (Vaughan, Preston, and Wilson 1978) for a single measurement, then $\sigma(R_{HK})/R_{HK} = 3.6\%$, approximately. Hartmann *et al.* (1984) suggest an uncertainty of 10% for their photospheric correction, while the corrections given above for the early F stars are comparable in uncertainty. Therefore it can be assumed that $\sigma(R_{phot})/R_{phot} \approx 10\%$, and the resulting uncertainty in R'_{HK}, listed in Table 4, is $\sigma^2(R'_{HK}) = (0.036R_{HK})^2 + (0.1R_{phot})^2$. One can immediately see the major problem of using Ca II flux as an activity indicator in F stars, the large uncertainty resulting from subtracting two quantities of almost equal magnitude. On the other hand, activity is clearly evident in all of the stars of the sample, and the uncertainties indicated are significantly smaller than the variations in activity seen in stars of similar masses. The

uncertainties quoted here also neglect any variation of activity due to activity cycles and other long-term variations. These variations appear to be at most ~30% for active late F stars, and are generally less (Wilson 1978, Baliunas and Vaughan 1985, Baliunas 1985)

In Figure 17 $\log R'_{HK}$ values are plotted against T_{eff} for the field and cluster F star sample. Features of these plots include:

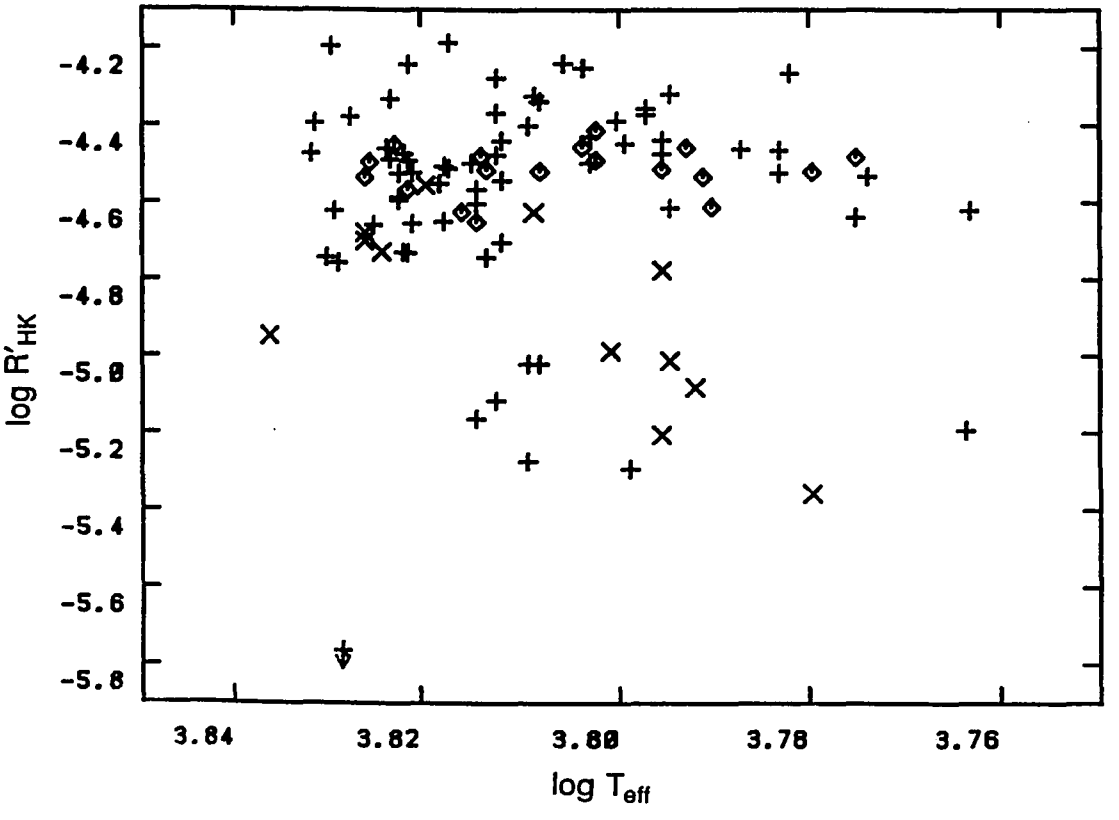

Figure 17. Plot of $\log R'_{HK}$ versus $\log T_{eff}$ for field and cluster stars. Note the apparent gap between high-activity and low-activity stars.

(1) The width of the $\log R'_{HK}$ distribution decreases from late to early F stars, but is still substantial at $\log T_{eff} = 3.82$ (= 6600K).

(2) The lower limit of R'_{HK} is nearly constant for all $\log T_{eff} < 3.82$. This limit is about 0.4×10^{-5}. For stars with $\log T_{eff} > 3.82$ the minimum value increases abruptly to $\sim 1.8 \times 10^{-5}$ and remains there in nearly all cases. The solar value is $R'_{HK} = 0.64 \times 10^{-5}$ at $\log T_{eff} \approx 3.763$ (based on the Böhm-Vitense value $B - V_o = 0.64$), while the least active stars at approximately solar temperature have $R'_{HK} = 0.14 \times 10^{-5}$ (calculated from Oranje, 1983). Such stars have β and δc_0 values too low to appear in this sample, however.

(3) The gap appearing at $\log T_{eff} = 3.82$ and continuing redward is the Vaughan-Preston gap (Vaughan and Preston, 1979) and is also seen in the R'_{HK} against $B - V$ plot of Soderblom (1985) (his Figure 3). The lower branch in Figure 17 does not merge into the upper branch; it just disappears.

5. Ca II and Age

a. *Activity–Age Dependence for the Sample as a Whole*

The chromospheric activity–age relation for solar- type stars has been the subject of much recent research. Skumanich (1972) suggested a $t^{-\frac{1}{2}}$ dependence of Ca II emission on age. A simple $t^{-\frac{1}{2}}$ dependence for Ca II activity was also suggested by Noyes (1981). More recent work has tended to modify this initial suggestion. Hartmann *et al.* (1984) performed an extensive program of statistical modeling of the dependence of Ca II activity with age for stars of $B - V = 0.45$ and later. They simulated the results of the Vaughan and Preston (1980) survey

assuming a constant star formation rate and several different possible forms of the chromospheric activity decay law. Best results for the entire sample were found with combination of an exponential decay in activity from zero age to 3 Gyr followed by a $t^{-\frac{1}{2}}$ decay, using their "minimum" photospheric correction (see section (3) above). It can be noted, however, that for the hotter stars in their sample ($0.45 < B-V \leq 0.68$) there appears to be little difference between the combination exponential and $t^{-\frac{1}{2}}$ decay and a pure exponential decay with the maximum photospheric correction (corresponding approximately to the RE correction proposed in section (3)). Hartmann *et al.* also provide evidence that the Vaughan-Preston "gap" (a decrease in the number of stars with intermediate activity levels observed in late F, G, and early K stars) (Vaughan and Preston 1980; Durney, Mihalas, and Robinson 1982; Middelkoop 1982) is the result of the existence of upper and lower limits on the chromospheric emission levels.

A recent study of chromospheric and transition region activity in solar-type stars (Simon, Herbig, and Boesgaard (1985), has also suggested a single exponential law for the activity–age dependence in stars slightly more massive than the Sun ($1.1M_{\odot}$), rather than a $t^{-\frac{1}{2}}$ dependence. This relation is of the form $R'_{HK} = 4.07 \times 10^{-5} e^{-0.355t}$ (here R'_{HK} refers to the relative Ca II HK surface flux using the photospheric correction of Noyes *et al.* 1984). Barry, Hege, and Cromwell (1984) suggest for solar-type stars a four-parameter model consisting of two exponential fits of the form $R_{HK} = 4.64 \times 10^{-5} e^{-0.122t} + 0.89 \times 10^{-5} e^{-17.9t}$, where no photospheric correction has been made. Here the second term is clearly only of significance for the youngest stars, and already at the age of the Pleiades the contribution of the second term is 5% of that of the first term.

The change from an overall power law dependence to an exponential law has been caused basically by the discovery that for solar-type stars the mean Ca II activity level in stars of the age of the Pleiades (0.08 Gyr) is only somewhat (roughly a factor of 1.3) higher than that in the Hyades (0.7 Gyr), rather than a factor of ~3 higher as would be required by a $t^{-\frac{1}{2}}$ relation. This plateau in Ca II flux is easily seen in the F star sample considered here as well. Figure 18 shows the overall distribution of relative Ca IIchromospheric surface flux as a function of age for the F star sample. Several points should be made concerning the distribution shown in this figure. First, the scatter of activity for stars of a given age appears to be quite large over the mass range considered here (~1.05 to 1.50 $M_{\odot}$), as is shown by the cluster members. Second, if only the cluster members are considered, the Pleiades stars show a larger range of activity than the Hyades, Coma, and Praesepe members. Third, there is a deficiency of field star age measurements between 1 and 2 Gyr. This is a selection effect due to uncertainty in the photometric indices and the isochrone fitting procedure, which make it difficult to obtain age measurements (rather than merely upper limits) for stars in this age range. Figure 18 also shows a least-squares fit (using uncertainty information on both axes) of $R'_{HK} = 4.59 \pm 0.06 \times 10^{-}5e^{-t/2.71\pm0.15}$ (with t measured in Gyr), The e-folding time, 2.71 Gyr, is consistent (within the uncertainties) with that reported by Simon, Herbig, and Boesgaard (1985), 2.82 Gyr for Ca II, but is much shorter than that given by the Barry *et al.* (1984) cluster data, 8.2 Gyr. An exponential law gives a better fit for the entire sample than a power-law fit. In this case, as in all of the fits reported in this work, stars with only upper limits in age or activity were not included in the least-squares calculations.

It has been suggested (Hartmann *et al.* 1984) that at high ages the main-sequence activity–age relation changes from an exponential to a power-law form.

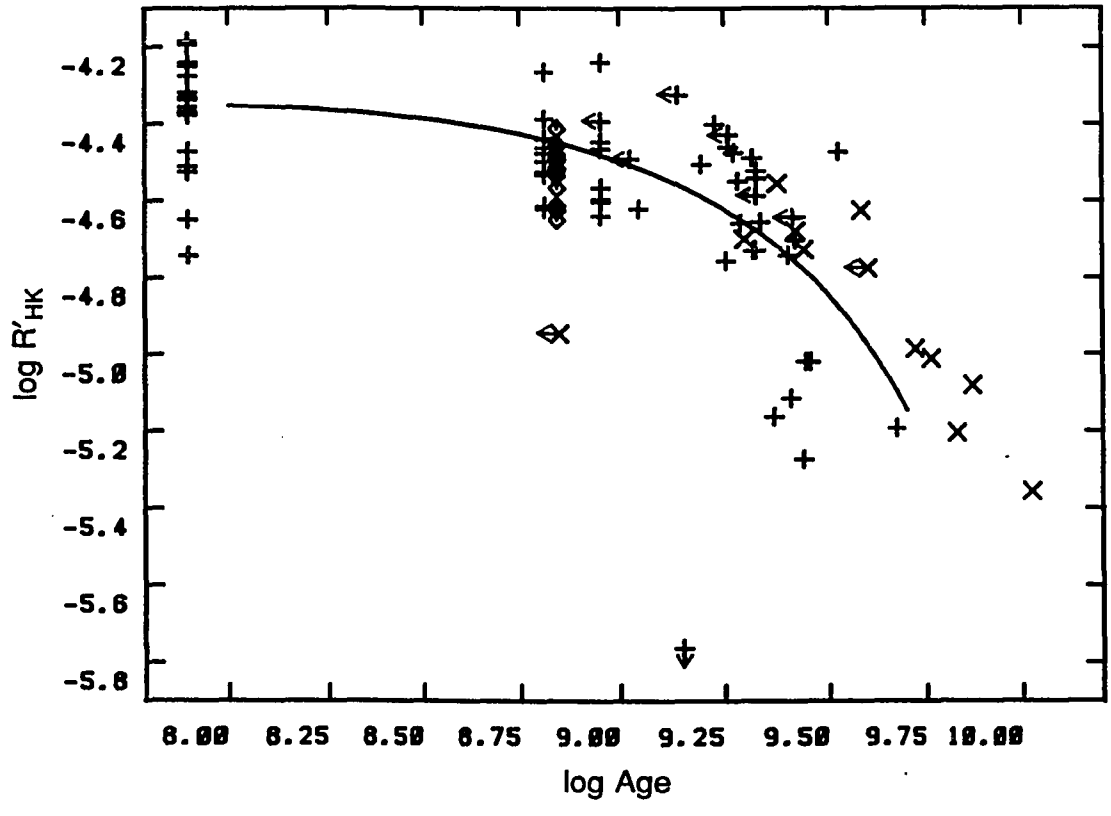

Figure 18. The relations between R'_{HK} and age for different compositions. Solar composition indicated by plus signs, "low-metallicity" stars ([Fe/H] ≤ -0.12) indicated by X's, and Hyades stars ([Fe/H] $= 0.13$) indicated by diamonds.

This idea is also suggested by recent theory (Gill and Roxburgh, 1984) as an explanation for the Vaughan-Preston gap. This possibility is discussed in a later section.

It is possible that differences in activity could result from causes other than stellar age. One possibility is differences in stellar composition. There are two possible ways in which changes in composition could affect the activity level observed in a star. First, the depth of the K and H line centers could be changed

to changes in the continuum level nearby (really a pseudocontinuum made up of closely spaced absorption lines), or due to changes in the amount of saturation of the K and H line profiles. Barry, Cromwell, Hege, and Schoolman (1981) suggest such effects are small. Second, the amount of activity in a star of differing metallicity but similar age and mass may vary with metallicity. Durney and Latour (1978) proposed a relation between the Ca II chromospheric surface flux and the Rossby number, an index of the amount of helicity in the motions of convection cells. The inverse Rossby number is equal to $\Omega\tau_C$, where τ_C is the convective turnover time in that part of the convection zone where the stellar dynamo is thought to be active, one-half pressure scale height above the base of the convective zone. Durney and Latour, in addition to proposing the dependence of activity on this number, also showed that the value of the Rossby number depends on the composition of the star. Durney and Latour found that the change in $\log \tau_C$ between $Z = 0.02$ and $Z = 0.03$ (corresponding roughly to the difference between solar and Hyades composition) in F stars is $\sim$ 0.3–0.4, depending on the mass of the star. The effect of composition on τ_C for stars with lower metallicity than the Sun is not yet known for stars only somewhat metal-poor. The effect for stars with 10 times lower than solar metallicity has been investigated (Ruciński and VandenBerg 1986); it was found that τ_C was higher for a given $B - V$ color for the reduced metallicity case, corresponding to a solar-composition star $\sim$ 0.05–0.06 redder than the observed value.

b. Effect of Differing Composition

When the early F stars are compared with the late F and solar-type stars, it is important to select the correct stars to compare them to. If effects such as

composition variations are significant then one must make sure to compare the early F stars with late F stars of similar composition.

As mentioned above, there is reason to believe that the convective turnover time for a given stellar mass depends on the composition of the star, and thus so will the activity for a given mass and rotation rate. The difference in activity between Coma and Praesepe stars (which are of solar composition) and Hyades stars (which have [Fe/H] = 0.13) is small. The Hyades stars are the only stars with greater than solar metallicity available (see section (3)), therefore it is not possible to come to any conclusions concerning the age dependence of activity in such stars.

The low-metallicity field stars (those with [Fe/H] ≤ -0.12) should show higher activity than solar composition stars of similar mass and age. The quantitative difference depends on stellar interior model calculations which are unfortunately not available. Figure 19 shows the relationship between Ca II activity and age for all of the low-metallicity stars. This relationship was best represented by an exponential law of the form $R'_{HK} = a_0 e^{a_1 t}$ where $a_0 = 3.68 \times 10^{-5} \pm 0.42 \times 10^{-5}$ and $a_1 = -0.212 \pm 0.058$.

c. Activity–Age Dependence for Differing Mass Ranges for Solar Composition

The early F stars in the current sample (except for the Hyades stars) are predominantly solar composition. A reasonable boundary between the early and late F stars terms of activity can be drawn at about $T_{eff} \approx 6600$ K, or for solar composition, $M_* = 1.325 M_\odot$. Figure 20 plots activity versus mass for the solar composition stars. It is readily seen that there is a difference in behavior between stars above and below $\sim 1.325 M_\odot$. Stars with $M_* > 1.325 M_\odot$ almost never have

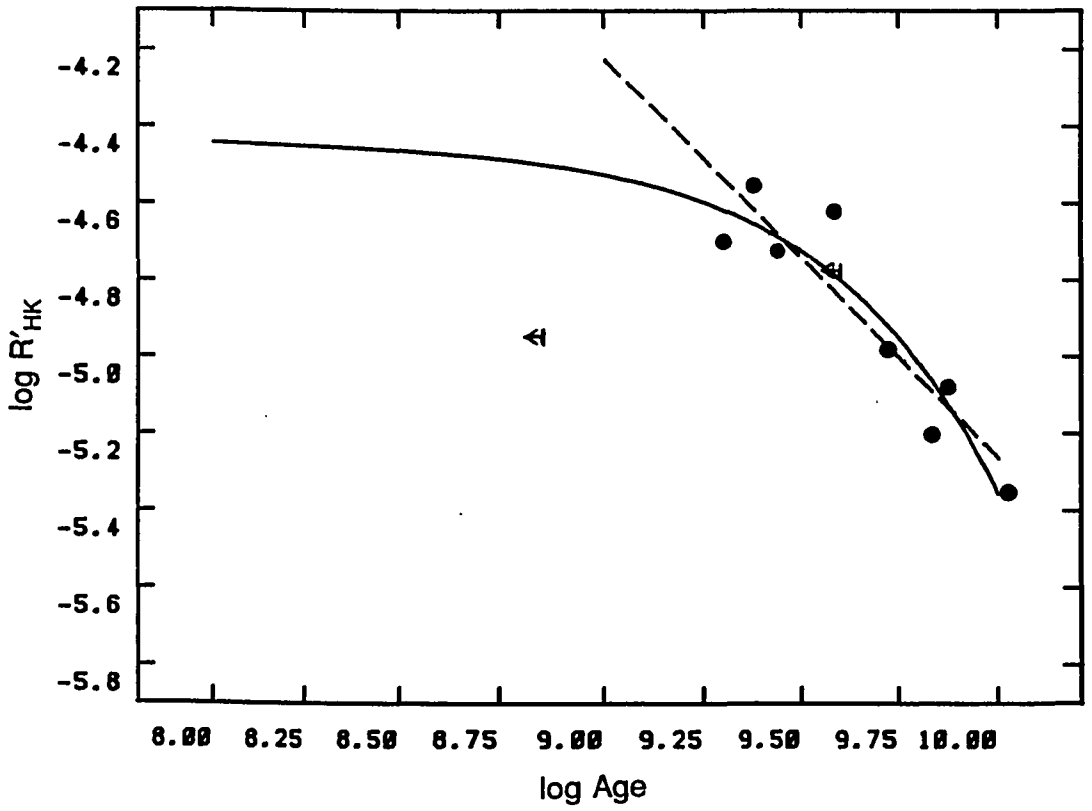

Figure 19. Log CaII relative surface flux versus log age (in Gyr) for the "low-metallicity" stars. Least-squares exponential (solid curve) and power law fits (dashed line), assuming uncertainties on both axes, are shown.

relative CaII flux $R'_{HK} < 1.8 \times 10^{-5}$, while stars with $M_* < 1.325 M_\odot$ often have much lower activity levels. It therefore seems reasonable to split the F star solar-composition sample into low and high mass groups.

The low mass solar composition F stars ($M_* < 1.325 M_\odot$) are shown in Figure 21. The overall best fit activity–age relation appears to be exponential in form (Table 6 gives comparisons between exponential and power-law fits and the resulting residuals in R'_{HK}). The best least-squares fit using error information from both

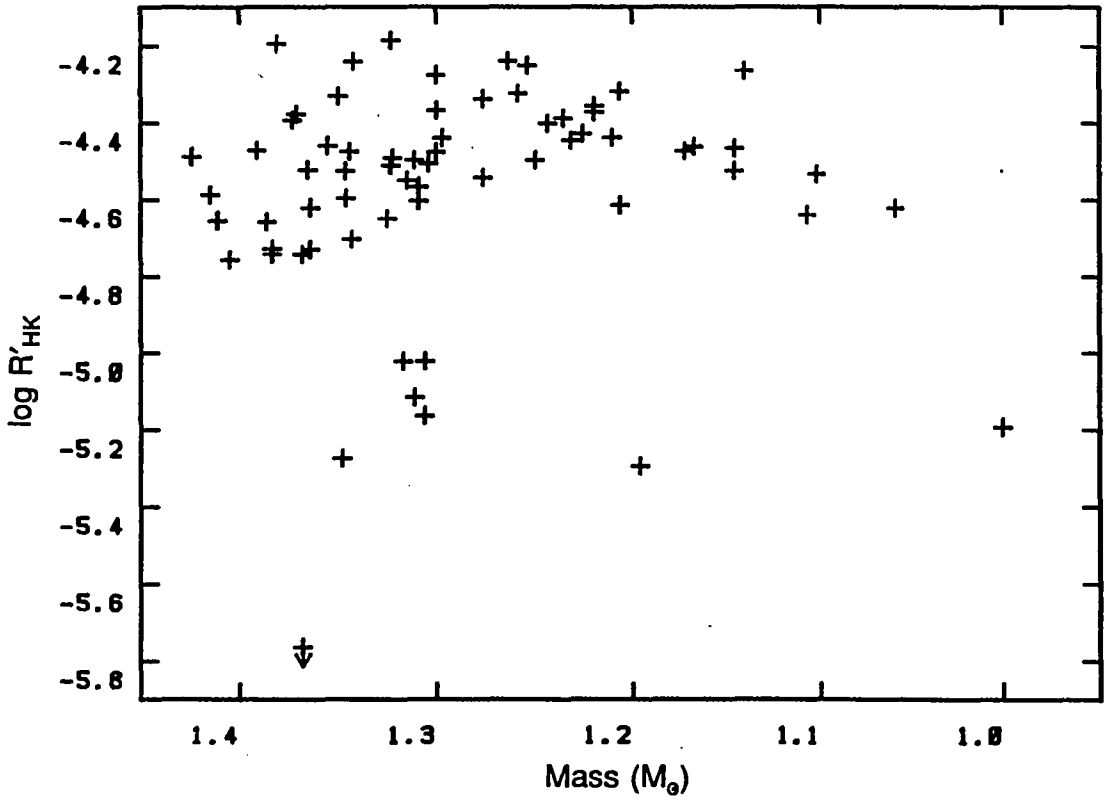

Figure 20. Plot of R'_{HK} versus mass for solar composition stars. The early F stars are much less likely to have low activity levels than the late F stars.

age and activity data was $R'_{HK} = a_0 e^{a_1 t}$ where $a_0 = 5.05 \times 10^{-5} \pm 0.09 \times 10^{-5}$ and $a_1 = -0.490 \pm 0.019$, resulting in an e-folding time of 2.04 ± 0.08 Gyr.

The high mass solar composition F stars ($M_* \geq 1.325 M_\odot$) are shown in Figure 22, and the least-squares relations found for them are shown in Table 6. The residuals from the fits are sufficiently similar that no objective conclusions can be made concerning the nature of the activity–age dependence. It does seem clear that a decline in activity with age does occur, and that an exponential decay law

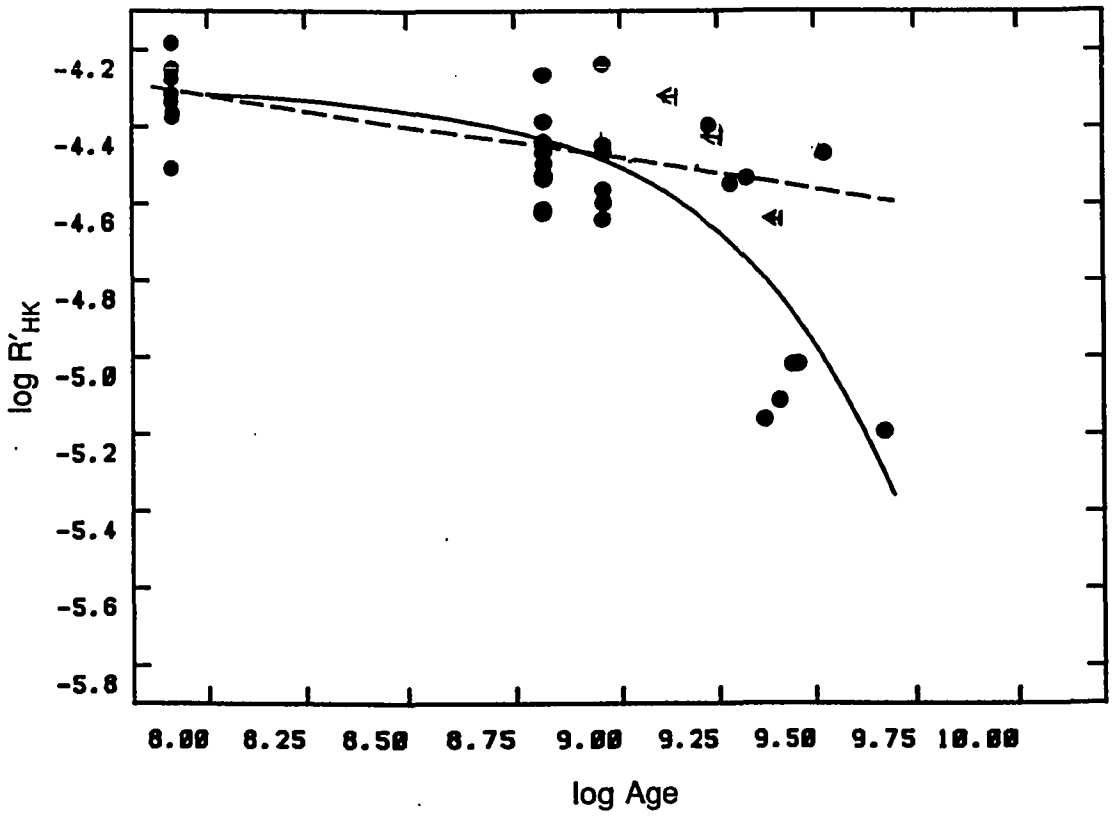

Figure 21. Plot of $\log R'_{HK}$ versus log age for solar composition sample with $M_* < 1.325 M_\odot$. Also shows exponential (solid curve) and power law (dashed line) fits.

is consistent with the observed data. The exponential fit results in an e-folding time of 3.12 ± 0.31 Gyr.

d. The Vaughan-Preston Gap

The preceding fits make no assumptions about the nature of the decay in activity. If one were to assume that something like the Gill and Roxburgh theory were correct, one would break the samples into stars above the Vaughan-Preston

Table 6

Ca II Activity–Age Relations

All Stars, All Masses

	Residual ($\times 10^{-6}$)	a_0 ($\times 10^{-5}$)		a_1	
$R'_{HK} = a_0 + a_1 t$	7.957	3.816	± 0.041	-7.164×10^{-6}	$\pm 0.039 \times 10^{-6}$
$R'_{HK} = a_0 e^{t/a_1}$	6.987	4.602	0.064	2.68	0.06
$R'_{HK} = a_0 t^{a_1}$	7.539	2.985	0.034	-0.197	0.010

Solar Composition, $M_* < 1.325 M_\odot$

	Residual ($\times 10^{-6}$)	a_0 ($\times 10^{-5}$)		a_1	
$R'_{HK} = a_0 + a_1 t$	8.031	4.147	± 0.060	-8.839×10^{-6}	$\pm 0.546 \times 10^{-6}$
$R'_{HK} = a_0 e^{t/a_1}$	7.426	5.047	0.093	2.04	0.08
$R'_{HK} = a_0 t^{a_1}$	8.505	3.281	0.053	-0.163	0.014

All Stars, $[Fe/H] \leq -0.12$

	Residual ($\times 10^{-6}$)	a_0 ($\times 10^{-5}$)		a_1	
$R'_{HK} = a_0 + a_1 t$	3.141	2.774	± 0.157	-2.617×10^{-6}	$\pm 0.627 \times 10^{-6}$
$R'_{HK} = a_0 e^{t/a_1}$	2.563	3.681	0.424	4.72	0.27
$R'_{HK} = a_0 t^{a_1}$	2.873	5.943	0.822	-1.037	0.287

Solar Composition, $M_* \geq 1.325 M_\odot$

	Residual ($\times 10^{-6}$)	a_0 ($\times 10^{-5}$)		a_1	
$R'_{HK} = a_0 + a_1 t$	8.227	3.683	± 0.089	-6.691×10^{-6}	$\pm 0.877 \times 10^{-6}$
$R'_{HK} = a_0 e^{t/a_1}$	8.773	4.592	0.138	3.12	0.10
$R'_{HK} = a_0 t^{a_1}$	8.898	2.838	0.080	-0.182	0.017

NOTE.

Here the residual is defined as: $(1/N) \sum |R'_{HK\ meas} - R'_{HK\ fit}|$.

gap (Vaughan and Preston 1980) and stars below the Vaughan-Preston gap, and investigate the dependence of activity on age in each group separately.

The Vaughan-Preston gap appears to be present in the current sample (see Figures 18 and 21) as a break in the run of R'_{HK} between 1.0 and 2.0×10^{-5} at ages between 2 and 3 Gyr. However, as has been seen above, it is important to make sure one is comparing truly similar objects, of similar masses and compositions,

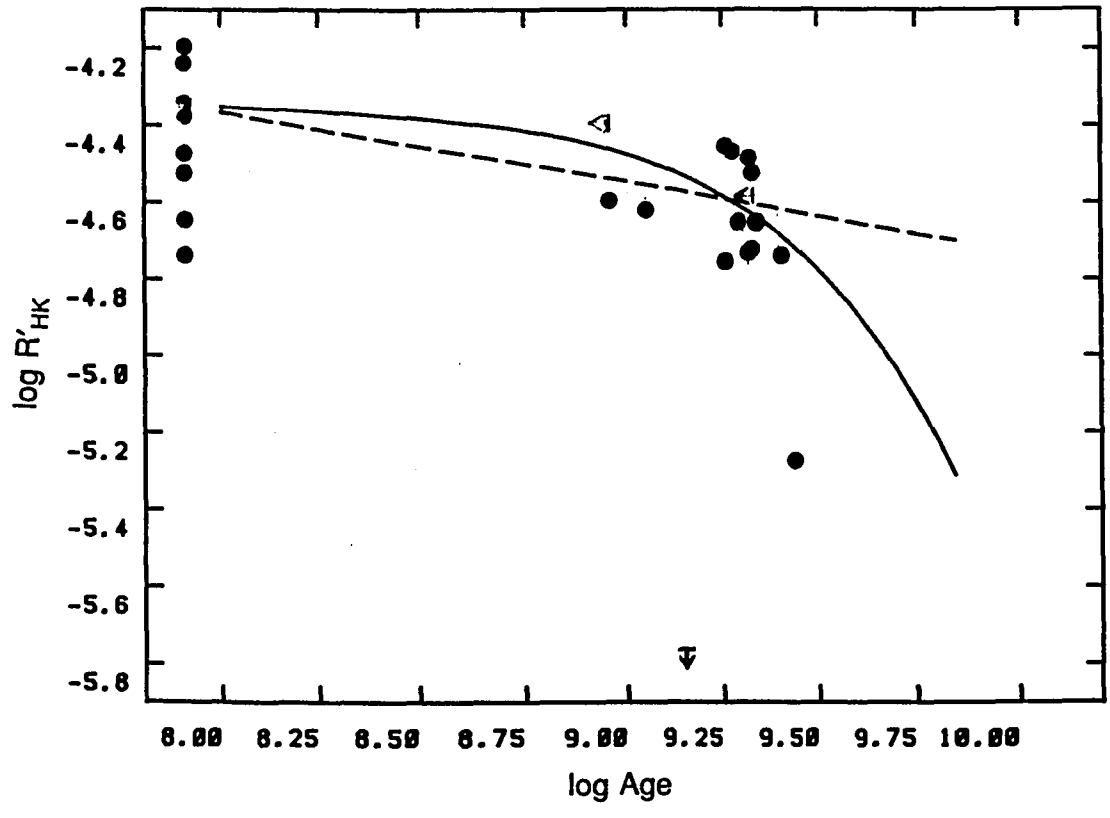

Figure 22. Plot of $\log R'_{HK}$ versus log age for solar composition stars with $M_* \geq 1.325 M_\odot$. Also shows exponential (solid) and power law (dashed) curves.

before making any conclusions about the activity–age relationship. The gap does appear in the low-mass solar-composition sample (see Figure 21) but is much less obvious than in the heterogeneous sample. Also, there appears to be little evidence from Figure 21 that the activity–age dependence for solar-composition stars is different for stars below the gap than it is for stars above the gap. Clearly more data on older late F stars is needed to confirm this conclusion. The Vaughan-Preston gap also appears to be present in the low-metallicity group (Figure 19)

and here it appears that a break in the activity–age relationship does occur at the gap.

If only low mass solar composition stars above the Vaughan-Preston gap (with $R'_{HK} > 1.8 \times 10^{-5}$) are considered, the exponential e-folding time becomes 2.56 ± 0.26 Gyr. In fact, the low mass and high mass solar composition fits for the activity–age relation become very similar, even though $V \sin i$ is generally higher for the same R'_{HK} in the high mass stars. This result will be discussed in Chapter V.

The low metallicity stars appear to have a different activity–age relation than the other late F stars (see Figure 19). The low-metallicity stars below the Vaughan-Preston gap are best modeled with a power law of the form $R'_{HK} = a_0 t^{a_1}$, with $a_0 = 6.8 \pm 1.5 \times 10^{-5}$ and $a_1 = -1.1 \pm 0.9$, but this is of little significance. The activity level for these stars is higher ($\sim 2\times$) than solar-metallicity stars of similar age. The low-metallicity stars are predominantly older than 2–3 Gyr and below the Vaughan-Preston gap. The power-law dependence of activity on age, while not highly statistically significant, suggests that older stars, below the VP gap differ in the activity–age relationship from that found for young stars. As indicated above the data in the current sample are insufficient to distinguish any difference in the activity-age relationship in solar-composition stars above and below the Vaughan-Preston gap.

It appears possible that given sufficient data, one could model the activity–age relationship for a given metallicity as an exponential, with magnitude and decay constant nearly independent of mass, followed by a power law. Much more data is required, however, to be certain of the power-law relation for older stars, however. The exponential form appears to be correct, however, and shows little variation

with mass. The basic conclusion for the solar-composition stars, then, is: Early F stars appear to behave similarly to young late F stars, stars which are above the Vaughan-Preston gap.

6. Discussion

Durney and Latour (1978) have made a simple prediction of the behavior of the decay of the magnetic activity in F stars as a function of mass. A simple estimate of the rate of loss of angular momentum in a solar-type star, assuming that the magnetic field corotates with the star out to the Alfven radius (determined by $B_A^2/(4\pi\rho_A u_A^2) = 1$) and is carried along by the stellar wind particles beyond that point yields

$$\frac{dJ}{dt} = \frac{2}{3}\Omega r_A^2 \frac{dM}{dt} \qquad 20$$

and if the magnetic flux is conserved between the surface and the Alfven radius and the magnetic field is purely radial (a monopole field), $B_0 R_0^2 = B_A R_A^2$, so that

$$\frac{dJ}{dt} = -\frac{2}{3}\frac{\Omega}{u_A}(B_0 R_0^2)^2 \qquad 21$$

where u_A is the stellar wind velocity at the Alfven radius. Durney and Latour (1978) then assume, based on simple dynamo theory, that $B_0 = B_n \Omega l/u_C$, where l is the mixing length and u_C is the velocity of convective cells at the base of the convection zone. This assumption does not agree with the observational results of Noyes *et al.* (1984), who find that $R'_{HK} = 6.0 \times 10^{-5} e^{-0.9P/\tau_C}$. The ratio l/u_C can be considered the convective turnover time (Gilman 1979). If it is then assumed that the stars are rotating as solid bodies, and that the effects of differing radius and moment of inertia can be neglected, the e-folding time t_e (defined as $-\Omega/(d\Omega/dt)$) for the angular momentum loss (and thus the rotation velocity loss

and the magnetic activity decline) assuming the stars all start with the same angular velocity, varies with mass so that

$$\frac{t_e(M_{*2})}{t_e(M_{*1})} = \left(\frac{\tau_C(M_{*1})}{\tau_C(M_{*2})}\right)^2 \qquad 22$$

Gilman (1979) gives plots showing the variation of τ_C with mass for differing values of the mixing length to pressure scale height ratio α. If values for $\alpha = 1.9$ (the τ_C value used by Noyes *et al.* (1984) for their relationship between activity and Rossby number) are interpolated from the data of Gilman, the ratio $t_{e\ 1.25}/t_{e\ 1.00} = 84$. This implies, if all stars begin their main sequence lifetimes with similar magnetic field strengths, that stars of mass greater than about $1.25M_\odot$ should show no loss of activity during their main-sequence lifetimes. The observed change in the *e*-folding times for magnetic activity is much smaller: $t_{eM_*\geq 1.325}/t_{eM_*1.325} \approx 1.5$. While the high mass stars ($M_* \geq 1.325M_\odot$) do show a smaller decline in activity with age than the lower mass stars, this decline is much smaller than predicted by the Durney-Latour theory.

The simple Durney and Latour theory, assuming a purely radial magnetic field also predicts that Ω (and thus B and R'_{HK}) $\propto t^{-\frac{1}{2}}$. While this result agrees with that found by Skumanich (1972), it does not agree with the exponential decay law seen here and elsewhere (Simon, Herbig, and Boesgaard 1985, Barry *et al.* 1984) in the F stars. The theory of Roxburgh and his collaborators (Gill and Roxburgh 1984, Roxburgh 1983, Rowse and Roxburgh 1981) offers alternatives. While in earlier theories the stellar magnetic field was considered to be purely radial, Roxburgh (1983) showed that in fact stellar angular momentum loss depends strongly on the form of the magnetic field. While for a radial field in a rigidly rotating star with $B \propto \Omega d(\Omega)/dt \propto \Omega^3$, and for a dipole field $d(\Omega)/dt \propto \Omega^{5/3}$, for a quadrupole field $d(\Omega)/dt \propto \Omega$ and the *e*-folding time is independent of B.

Of these possible field configurations the quadrupole field seems best applicable to F stars. The resulting rotational velocity–age dependence is exponential, and thus (if $B \propto \Omega$ and $R'_{HK} \propto B$) so is the R'_{HK} age dependence, in agreement with observation. According to Gill and Roxburgh (1984) the rotation–age relationship is

$$\Omega = \Omega_0 e^{-Kht/I}, \qquad 23$$

where $K = 8\pi/3\rho_0 V_S R^4$ and $h = 0.1$ for a wide range of B.

Roxburgh proposed (Roxburgh 1983) that the Vaughan-Preston activity gap seen in late F, G, and K stars is the result of a transition from a quadrupole field in young main-sequence stars to a dipole field, accompanied by an abrupt increase in the decay rate of angular momentum. If the Vaughan-Preston gap is real, two comments on this suggestion can be made: it appears that the F star sample of solar composition considered here is nearly completely dominated by the upper branch of the activity distribution, and no difference between the activity–age behavior above and below the gap can be seen. However, the behavior of the low metallicity stars below the gap (suggesting a power law dependence of activity on age) indicates that future work may be able to indicate such a change. It appears, however, that for solar composition, if the Roxburgh theory is correct, F stars generally have a quadrupole field geometry.

If it is assumed that $B = B_n \Omega \tau_C$, then the e-folding time for R'_{HK} in a quadrupole configuration (assumed to be proportional to B) is $t_e = I/Kh$. In other words, if the effects of changing moment of inertia and radius are neglected as above, the e-folding time should be nearly constant as a function of mass. This result is much closer to the observed e-folding times than the Durney-Latour theory.

As mentioned above, the Gill and Roxburgh (1984) theory attempts to explain the Vaughan-Preston gap as a result of the change from a quadrupole to a dipole field. As was shown above, nearly all the solar-composition F stars in the current sample lie either above this gap or at a T_{eff} value where the gap no longer exists. The low metallicity stars ([Fe/H] ≤ -0.12) on the other hand are all old and generally lie below the gap. As was shown in section (4), the best fit for the low metallicity stars below the Vaughan-Preston gap was found to be a power law with a slope of -1.28, unlike the exponential curves found for the solar mass stars. Gill and Roxburgh (1984), on the other hand, find that stars with a dipole field geometry should have an angular velocity given by

$$\frac{d(I\Omega)}{dt} = -F\Omega h \left(\frac{B}{B_c}\right)^{2/3} K \qquad 24$$

where B_c is the B value at the transition from quadrupole to dipole, or

$$B \propto \left(\frac{1}{\Omega_0} e^{2Kht_c/3I} + \frac{2FKh}{3I}(t - t_c)\right)^{-3/2} \qquad 25$$

If $t \gg t_c$ and $R'_{HK} \propto \Omega$, $R'_{HK} \propto t^{-1.5}$, while for a radial field, $R' \propto t^{-0.5}$. It appears that a change to a power law does occur in the low metallicity stars, but it is not clear which model best reproduces the data.

All of the above analysis assumes that the nature of the dependence of chromospheric activity on rotation is the same as is seen in solar type stars. The data used by Noyes *et al.* in establishing their dependence of activity on inverse Rossby number (Noyes *et al.* 1984) used only a very small number of early and mid-F stars compared to the number of G and K stars in their sample. Radick *et al.* (1982, 1983*a*, 1983*b*) and Lockwood *et al.* (1984) have shown that stars later than F7 show photospheric continuum variability apparently due to rotational modulation, just as Vaughan *et al.* (1981) and Baliunas *et al.* (1983) have demonstrated clear rotational variations in the chromospheric Ca II flux. On the

other hand, other researchers have found substantial differences in the relation between activity and rotation between stars earlier and later than $B-V \approx 0.42$. Stars earlier than this color show substantial differences from solar-like activity, in photospheric, chromospheric and coronal activity indicators.

When other activity indicators are considered, it becomes much more apparent that a significant difference in activity mechanisms exists between the low mass F stars and the higher mass objects. Walter (1983) has shown that while there exists a definite relation between rotation velocity and X-ray flux for G and K stars, this relation ceases at about spectral type F5. Stars earlier than this show clear X-ray emission, but no relationship with stellar rotation is apparent. Wolff, Heasley, and Varsik (1985) show that while the equivalent width of the He I 5876 Å line (which has been shown to be a stellar activity indicator for late type stars, see also Danks and Lambert (1985)) is correlated with stellar rotation for late-F, G, and K dwarfs, this correlation also ceases in the same region, at $B-V = 0.46$. Stars earlier than $B-V = 0.46$ show no correlation of the D_3 line with rotation. Walter (1985) has found similar results, but with a limit for correlation with rotation of $B-V = 0.42$, for the transition region C II and C IV lines in the ultraviolet. The typical equivalent width of D_3 and the C II and C IV surface flux increase or remain constant throughout the F stars.

Wolff, Boesgaard, and Simon (1986) have observed a sample of F stars in He I λ5876 and C IV λ1549, and report that while the solar type relationship between Rossby number and activity as measured by the He I and C IV lines is also observed in late F stars, stars hotter than 6600 K (corresponding to $B-V \approx 0.42$). It will be shown (Chapter V) that while the dependence of Ca II emission on Rossby number is much less steep among stars with $T_{eff} > 6600$ K than it is among cooler

stars, it does not appear to vanish for the stars in this sample. This boundary corresponds with that proposed by Walter (1985) for transition region flux. The authors suggest that the chromospheric flux seen in these hot stars may be due to acoustic flux rather than magnetic activity. If acoustic flux is significant in these stars there should be very little dependence of Ca II flux on age, since acoustic flux is determined only by the effective temperature and surface gravity of a star (Renzini *et al.* 1977). Therefore any acoustic flux heating will be nearly constant for all main sequence stars of a given mass.

De Loore (1970) showed that acoustic flux in main sequence stars should peak near F0. While it is clear that the contribution of purely acoustic flux to the heating of the outer atmospheres of solar-type and later stars is small (Vaiana *et al.* 1981), it is possible that in the early F stars it could be comparable to that of the magnetic field.

Figure 23 shows log C IV relative surface flux plotted against $\log T_{eff}$ for the Wolff, Simon, and Boesgaard sample, while Figure 24 shows $\log F'_{HK<}$ against $\log T_{eff}$ for the current sample, where F'_{HK} is the absolute Ca II surface flux. The behavior of the chromospheric flux is remarkably similar in both wavelengths: above $\log T_{eff} = 3.82$ the range of activity is much smaller than below this temperature. In Ca II the Pleiades stars are consistently more active than older cluster and field stars, however.

According to Stein (1981), the mechanical (acoustic) flux at the top of the convective zone has been analytically estimated to be $F_m \propto g^{-1}T_{eff}^{11}$. The amplitude of the acoustic flux is not well determined, however. Numerical calculations (Schmitz and Ulmschneider 1980) for several stars, including the Sun and

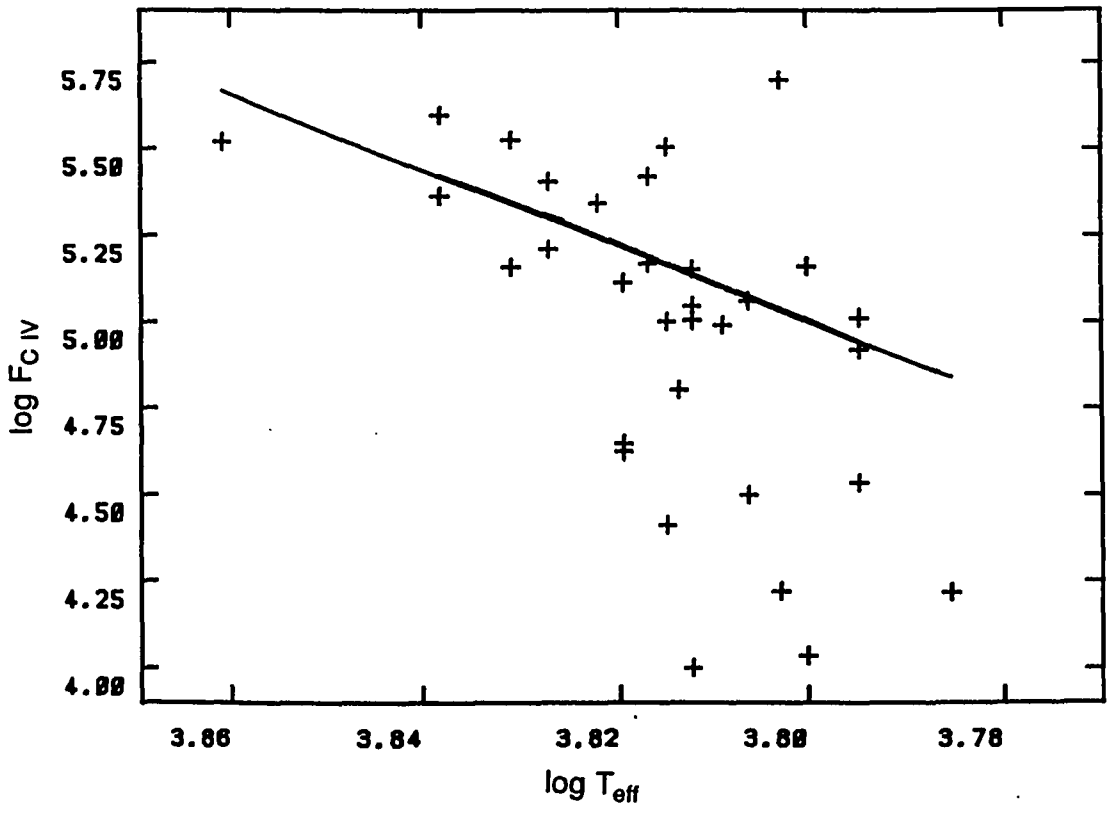

Figure 23. C IV surface flux versus $\log T_{eff}$ from Wolff *et al.* (1986). A line with a slope corresponding to T^{11} (the dependence expected for pure acoustic heating) is also shown. Note that many late F stars have C IV surface fluxes less than that expected if the surface flux in *early* F stars is dominated by acoustic heating.

Procyon, confirm Stein's basic result:

$$F_m = 9.1 \left(\frac{g}{1000}\right)^{-0.959} \left(\frac{T}{1000}\right)^{10.6} . \qquad 26$$

For a main sequence star of $\log g = 4.4$ and $T_{eff} = 6700$ K, $F_m/\sigma T^4 = 0.054$ while for the Sun $F_m/\sigma T^4 = 0.012$. It has been known for a long time (Ulmschneider 1971) that the great majority (~90%) of the energy in short period acoustic waves is lost to radiative dissipation in the photosphere, so that F_A, the actual acoustic

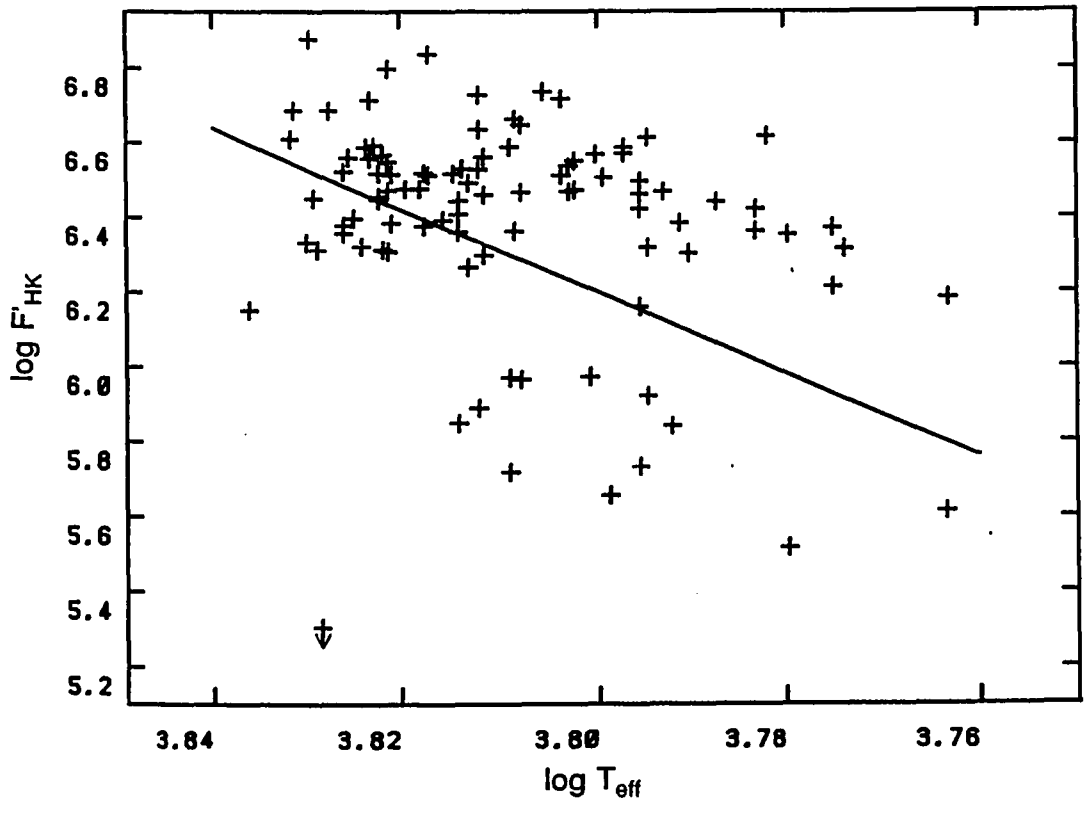

Figure 24. CaII surface flux versus $\log T_{eff}$ for sample used in Chapter III. Also includes a line corresponding to the expected temperature dependence of acoustic heating. As is seen in C IV as well, dominant pure acoustic heating in early F stars leads to too much heating in late F stars.

flux available to heat the chromosphere is only a small fraction (~10 % or less) of F_m.

This theoretical result must be compared to the total radiative loss from the chromosphere. Avrett (1981) has computed radiative loss estimates for three differing activity levels in the solar atmosphere, corresponding to a dark supergranule cell center, the average quiet Sun, and a bright network element. The contribution of the CaII H and K lines to the total radiative loss from the chromosphere in

these models ranges from 28% to 20% of the total. If the emission from Ca II in the early F stars is a similar fraction of the total chromospheric flux (~25%), then the total relative chromospheric flux is $\sim 8 \times 10^{-5}$, and the chromospheric surface flux for early F stars is 9×10^{6}erg cm^{-1}s^{-1}.

The amount of acoustic flux expected from the numerical models of Schmitz and Ulmschneider is then much larger than the amount emitted by stars, scaling from the semi-empirical models of Avrett for the Sun. Schmitz and Ulmschneider (1980) suggest that the radiative loss in the chromosphere from H^- is much larger than indicated by Avrett, and in fact is the major radiative loss mechanism in stellar chromospheres. According to their models for Procyon (T_{eff} from β = 6620 K) the chromospheric flux from Ca II H and K is 3.8×10^{6}erg cm^{-1}s^{-1}, while that from H^- is 2.4×10^{7}erg cm^{-1}s^{-1}. Even in this case the acoustic flux from the numerical model for Procyon is much larger than the chromospheric loss. The point of this exercise is that while there is disagreement concerning the amount of acoustic flux generated in stars, and the amount which can reach the chromosphere, under some assumptions it can be shown that there could be enough acoustic flux available to heat stellar chromospheres.

Since the temperature dependence of acoustic heating is well determined, it can be compared with observations. Figure 23 and 24 also show the temperature dependence of acoustic heating, where the flux is scaled to yield the above mean value for $T_{eff} = 6700$K and $\log g = 4.4$. The dependence of acoustic heating on temperature can be expected to be roughly valid as long as convection is efficient and the major source of opacity in the photosphere is H^-. These assumptions break down for stars earlier than F0, but should be valid for all stars considered here. It appears evident that if the chromospheric heating in the early F stars were

due to acoustic heating, then the late F stars would have much more chromospheric emission than what is observed. Figure 23 shows that the emission observed by Wolff, Boesgaard, and Simon (1986) in C IV plotted against T_{eff} shows a similar dependence on T_{eff} to the Ca II data presented here. Athay (1985) shows that acoustic heating cannot be a major contributor in the upper chromosphere, where C IV is emitted in the Sun. It therefore seems evident that pure acoustic heating is not a major contributor to chromospheric flux in early F stars.

On the other hand, the true photospheric contribution (the emission which would be present in the absence of a chromosphere, *i.e.* that generated by a RE model) is also increasing in this region. Uncertainties in the "photospheric" contribution could produce an apparent increase in chromospheric indicators, without actually requiring any acoustic flux to be present. While this problem would be most significant in chromospheric Ca II flux measurements, it is also a problem in other chromospheric activity indicators in early F stars (*e.g.* Mg II, see Böhm-Vitense and Dettman 1980). However, the results of Wolff, Simon, and Boesgaard suggest that chromospheric emission is indeed still substantial in the early F stars. A substantial increase in the minimum C IV relative flux level in stars hotter than 6450 K as compared to those cooler than 6450 K is observed, which cannot be simply explained by increased photospheric emission. This result suggests that the increase seen in Ca II is probably real.

Clearly there are other effects that may be important. The stellar interior models used do not include rotation effects. Very rapid rotation ($V \sin i \approx 100$ km s^{-1}) will have an effect on the age and mass determinations, although there are few such rapid rotators in this sample. The effects of rotation on the ages, and the

rotation–activity relationships for the different masses will be considered in Chapter V.

Another possible effect on the age and mass determinations would be a possible activity-caused change in the Strömgren indices (LaBonte and Rose 1985). This is one possible explanation of the "Hyades anomaly" (Crawford and Barnes 1969). However, it can be noted that the activity levels in Coma and the Hyades are quite similar, as are their ages (as determined by the main sequence turnoff (Nissen 1980)), but Coma does not show any anomalous δc_1 indices. The Pleiades stars, when individually dereddened using the method of Crawford and Barnes (1970) show δc_0 indices that are, if anything, ~0.01 mag. below the Crawford (1975) standard field star ZAMS. Since the Pleiades are somewhat more active than the Hyades, δc_0 should be increased by an amount larger than the 0.04 mag. predicted for the Hyades by LaBonte and Rose. If this were true, the corrected c_0 values for Pleiades stars would be ~0.05 mag. lower than the Crawford ZAMS relation, which seems unlikely. Ignoring this effect still leaves the origin of the Hyades anomaly an open question.

7. Conclusions

A large sample of field F dwarfs have been observed in order to investigate the dependence of chromospheric activity as measured in the Ca II H and K lines on age for stars of different masses. Ages and masses for the field stars were estimated using Strömgren photometric indices and model isochrones, using the method of Chapter II. Ca II relative fluxes were found both from observations using the University of Hawaii 2.2m telescope and from the Mt. Wilson survey

(Duncan 1983, 1985). The behavior of this sample of F dwarfs is consistent with the angular momentum decay theory of Gill and Roxburgh (1984) assuming a quadrupole geometry for the stellar magnetic field. The observed decay of activity with age is consistent with an exponential law, with the *e*-folding time increasing slowly with increasing mass.

The behavior of Ca II surface activity in early F dwarfs is consistent with a decline in activity with age similar to that observed in late F stars and solar-type stars. For young objects ($< \sim$ 2–3 Gyr) this decline is most likely exponential in form.

Other indicators of stellar activity show definite differences from solar behavior in the early to mid-F stars. That is, both coronal (X-ray flux, Walter 1983) and transition region features (C II and C IV surface fluxes, Walter 1985, C IV and He I fluxes Wolff, Simon, and Boesgaard 1986, Wolff, Heasley, and Varsik 1985) show no relation between stellar rotation rate and mean activity levels for F stars with $B - V < 0.42$. Thus stellar activity in these objects appears to be nearly independent of age and rotation rate. It has been suggested on the basis of the lack of relationship between activity and rotation for early F stars that their chromospheric activity is due to acoustic flux (Wolff, Simon, and Boesgaard 1986). The lack of a significant activity–age relationship for these stars is in agreement with this idea. The relation between Ca II activity, age and rotation will be discussed further in Chapter V.

CHAPTER IV
STELLAR ROTATION VELOCITIES MEASURED USING AUTOCORRELATION

1. Background

This chapter describes a method of measuring stellar projected rotational velocities using the autocorrelation of a section of the spectrum of a star which can contain one or many lines, and provides some of the $V \sin i$ values used in Chapter V of this dissertation.

Methods of measuring the Doppler broadening of stellar spectral lines are of three types: direct, Fourier transform, and correlation. The direct method involves matching a computed line profile with the observed line profile, or matching the spectral line profile of a star to that of another star with known rotation. The best-known example of this method using photographic spectra for late-type stars is the work of Kraft (1965, 1967). This method does not work well with slowly-rotating stars due to the effects of other sources of line broadening and the difficulty of obtaining high photometric accuracy with photographic spectra.

Gray (1973) and Smith (1976) have demonstrated the method of resolving rotational velocities from other broadening mechanisms using the Fourier transform of the line profile. The possibility of using Fourier analysis to obtain $V \sin i$ measurements has been known for a long time (Carroll 1933), but only recently has the combination of powerful computers and electronic detectors with high photometric precision allowed it to be applied to a relatively large number of stars (*e.g.*, Soderblom 1983). This method allows other broadening mechanisms such as turbulence and instrumental effects to be taken explicitly into account.

The purpose of this chapter is to obtain $V \sin i$ values for some of the stars used in Chapter V of this dissertation. In order to obtain significant results in such a study, a large number of stars must be measured. While the Fourier transform method allows precise $V \sin i$ determinations for slowly-rotating stars, it requires careful modeling of the various broadening contributors and must be done one line at a time. The typical stellar spectrum contains many lines, each line containing the same rotational broadening information. It would be useful to have a method of measuring $V \sin i$ which is simple, can be applied to a large sample of stars, and uses the rotational information from all the lines in the spectrum.

Benz and Mayor (1981) have described a method of measuring $V \sin i$ for large numbers of stars using the width of the cross-correlation of the stellar spectrum with a mask based on the positions of the lines in the star Arcturus. Their method has been successful in measuring $V \sin i$ in a large number of late-type stars (Benz, Mayor, and Mermilliod 1985). The spectrum of the target stars from 3600 Å to 5200 Å is physically cross-correlated with a mask based on the spectrum of Arcturus using the CORAVEL instrument (Baranne, Mayor, and Poncet 1979). Use of this wide spectral range allows the $V \sin i$ information from many lines to be combined into a single measurement.

Because they use a large spectral range (3600 Å to 5200 Å), Benz and Mayor can assume that the broadening of a typical spectral line can be expressed as a Gaussian, due to the statistical effect of blends. This effect will also reduce the significance of the difference between the spectral type of the star upon which the cross-correlation mask is based and the target stars. If the number of lines in the wavelength region is small, then the difference between the mask and the target stars should be considered more carefully.

Stauffer *et al.* (1984) and Stauffer and Hartmann (1986) have used a similar cross-correlation technique, based on the work of Tonry and Davis (1979) on galaxy redshifts, for measuring rotational velocities in late-type stars. This method uses a spectrum from a star with well-determined $V \sin i$ as a mask for cross-correlation during data reduction, rather than a physical mask in the spectrograph. There are two problems with the use of the cross-correlation mask technique. First, in order to measure rotational velocities one must build the mask and the spectrograph. Second, the effectiveness of the mask decreases greatly as the difference in spectral type between the target stars and the star used to construct the mask increases.

One way to address this problem is to use the target star as its own mask, that is, to use an autocorrelation instead of a cross-correlation. This assures that the mask is the same spectral type as the target star, and allows any spectrograph to be used.

2. Autocorrelation Width for Weak Lines in a Rotating Star

Gray (1976) has shown that if the center to limb variation of the line profile in a non-rotating star is small, the profile of a spectral line can be considered a convolution of the non-rotating profile and the "rotation profile" G_λ, where

$$G(\Delta\lambda) = c_1 \left[1 - \left(\frac{\Delta\lambda}{\Delta\lambda_L}\right)^2\right]^{\frac{1}{2}} + c_2 \left[1 - \left(\frac{\Delta\lambda}{\Delta\lambda_L}\right)^2\right] \qquad 27$$

(see Carroll, 1933). This assumes the limb darkening law is of the form $I = I_0((1-\epsilon) + \epsilon\cos\theta)$ and $\Delta\lambda_L = (\lambda v \sin i)/c$.

If the observed line profile can then be described as a convolution of a non-rotating line profile and the above rotation profile, the observed line profile can be described as:

$$\frac{F_\lambda}{F_c} = H_\lambda * N_\lambda * \Theta_\lambda * G_\lambda * D_\lambda, \qquad 28$$

where F_λ/F_c is the ratio of flux in the line to continuum flux, H_λ is the intrinsic non-rotating line profile for the star, N_λ is the microturbulence profile, Θ_λ is the macroturbulence profile, G_λ is the rotation profile, and D_λ is the instrumental broadening function. For weak lines on the linear part of the curve of growth, H_λ is a Gaussian. D_λ will be considered Gaussian as well, as will the macroturbulence.

The utility of the autocorrelation is based on the assumption that all sources of broadening other than rotation (turbulence, the intrinsic profiles, instrumental broadening) are the same for the reference star as for the stars to be measured. The validity of these assumptions is examined below.

The widths of the intrinsic profiles of weak absorption lines in dwarf stars, excluding the effects of turbulence and rotation, are nearly entirely due to thermal Doppler broadening. The Maxwellian mean speed for the absorbing atoms is

$$v_0 = \sqrt{\frac{2kT}{m}} \qquad 29$$

where m is the mass of the atom. If the selected region of the spectrum is populated by lines from high mass atoms, the effect of thermal broadening will be small and relatively uniform for all lines present.

For stars observed from the same observing run, the instrumental broadening profiles are identical (if the instrumental settings are not changed), and so the reference star and the star being measured will have the same instrumental broadening profile convolved with the intrinsic spectrum.

There are two sources of turbulence generally considered in computing line profiles for main sequence stars: macro- and microturbulence. These sources of turbulence dominate the spectral line profiles in slowly rotating stars, hence they must be considered carefully in any method for obtaining $V \sin i$.

The use of a convolution to represent the macroturbulence profile deserves some discussion. Gray (1976) points out that the macroturbulent velocities, rather than having a simple isotropic distribution, may be better described by separate radial and tangential distributions. The problem with this approach is, like the full treatment of rotational velocities, the resulting line profile cannot be accurately described as a convolution of a non-turbulent line profile and a position-independent turbulence profile. However, for weak lines (as used in this chapter), the approximation of the effect of macroturbulence by a Gaussian turbulence profile is reasonable. As Gray (1976) states, this makes it impossible to use weak lines to distinguish macro- from microturbulence.

Recent papers by different authors give substantially different observational results for the dependence of stellar turbulence on stellar parameters such as effective temperature. Gray (1981) on a suggestion by Smith (1981) indicates that at least one component of the macroturbulence caused by non-radial oscillations is proportional to $T^3 g^{-0.25}$. An additional source of broadening due to the Zeeman effect has been observed in late G and K stars by Robinson, Worden, and Harvey (1980), Marcy (1982), and Gray (1984*a*). Gray (1984*b*) has examined this effect in late G and K stars, and found an empirical relation for the mean width $\zeta(\Theta) \approx (3.95/1000) T_{eff} - 19.25$. Over the range from $\sim$ 6000 to $\sim$ 6500 K, the variation amounts to or a change of $\sim$ 2.0 km s^{-1} from 4.5 km s^{-1} to

6.5 km s^{-1} . The microturbulence depends on the lines observed, but is typically 0 to 2 km s^{-1} .

On the other hand, Soderblom (1983) obtained satisfactory results for a large number of stellar rotation measurements using constant values of 1.0 km s^{-1} for microturbulence and 3 km s^{-1} for macroturbulence, using a radial-tangential form for the macroturbulence. These values were taken to be independent of age and spectral type.

It is unclear which approach is to be preferred; I have chosen to assume macro- and microturbulence constant over the spectral range observed in this chapter. If Gray is correct, this may introduce a systematic error of roughly 1.0 km s^{-1} in $V \sin i$, depending on the ratio of the temperature of the reference star to that of the observed star. Since all stars I observed are near the main sequence, any effect due to gravity should be small.

If it can be assumed that over the relevant spectral region the broadening due to turbulence is constant, then the line profile is of the form

$$\frac{F_\lambda}{F_c} = A_\lambda * G_\lambda * H_\lambda \qquad 30$$

where A_λ, the total turbulence profile, is assumed to be constant for stars of similar spectral type. If the thermal profile varies little with temperature, the entire non-rotational part of the line profile can be replaced by a nearly Gaussian profile H'_λ, so that the observed profile is just

$$\frac{F_\lambda}{F_c} = H'_\lambda * G(\lambda, v) \qquad 31$$

For the purposes of this dissertation, only symmetrical lines will be considered. Then in the case of single isolated lines, autocorrelation is equivalent to self-convolution. Then the autocorrelation of the line profile is

$$\frac{F_\lambda}{F_c} \star \frac{F_\lambda}{F_c} = (H' \star H') * (G \star G) \qquad 32$$

The autocorrelation of the rotation profile $G(\lambda, v)$ is difficult to compute analytically, however, numerical analysis indicates that at least for the range of velocities of interest here, it can be very well approximated by a Gaussian of the form

$$G(\Delta\lambda') \star G(\Delta\lambda') \approx \frac{a}{v} e^{-((b\Delta\lambda')/v)^2)} \qquad 33$$

such that the area under the autocorrelation remains constant as v is varied.

Let $H'_\lambda = 1 - c \exp(-(\lambda/d)^2)$. Then, setting the continuum level equal to zero, $R'_\lambda = c \exp(-(\Delta l/d)^2)$, and the normalized autocorrelation $(R'_\lambda \star R'_\lambda) = \exp(-(\Delta\lambda'/d)^2/2)$. Then

$$\frac{F_\lambda}{F_c} \star \frac{F_\lambda}{F_c} = (R' \star R') * (G \star G) = C e^{-\frac{\Delta\lambda^2}{2([v/b]^2+d^2)}}, \qquad 34a$$

where

$$C = \frac{b}{v} d \frac{\sqrt{2\pi}}{\sqrt{[v/b]^2 + d^2}} \frac{a}{v} \qquad 34b$$

Therefore, the $1/e$ halfwidth of the autocorrelation is just $E = \sqrt{2([v/b]^2 + d^2}$, and does not depend on the strength of the line, but only on the broadening terms discussed above.

Now consider the case where the wavelength region used for the autocorrelation contains many lines. This is essentially similar to the case for the cross-correlation technique of Benz and Mayor (1981) or Tonry and Davis (1979). Due to the

statistical effects of the blending of many lines, the autocorrelation function is again Gaussian, and it is clear that the $1/e$ halfwidth versus rotation velocity is similar to that shown above.

For the case where only a few lines are present in the spectrum, the relationship is not as clean. Consider two spectral lines of different strengths, and let each one have a Gaussian profile. Then the residual flux in each line is:

$$A_1 = A_{0\ 1} e^{-\left(\frac{\lambda-\lambda_1}{\sigma_1}\right)^2} \qquad 35a$$

$$A_2 = A_{0\ 2} e^{-\left(\frac{\lambda-\lambda_2}{\sigma_2}\right)^2} \qquad 35b$$

and the sum is $R = A_1 + A_2$. The transform of the autocorrelation is then $\overline{R * R} = |\bar{R}|^2 = |\bar{A}_1 + \bar{A}_2|^2$. Let $a = \lambda_2 - \lambda_1$. Then the Fourier transforms of the profiles separately are:

$$\bar{A}_1 = A_{0\ 1}\sqrt{\pi}\sigma_1 e^{-\pi^2 s^2 \sigma_1^2} \qquad 36a$$

and

$$\bar{A}_2 = A_{0\ 2}\sqrt{\pi}\sigma_2 e^{-\pi^2 s^2 \sigma_2^2} \qquad 36b$$

Let

$$A_2' = A_{0\ 2} e^{-\left(\frac{\lambda-\lambda_1}{\sigma_2}\right)^2} \qquad 37$$

Then

$$\bar{A}_1 + \bar{A}_2 = \bar{A}_1 + \bar{A}_2' e^{-2\pi i(\lambda_2-\lambda_1)s} \qquad 38$$

using the shift theorem. The transform of the autocorrelation function is given by

$$\begin{aligned} |\bar{R}|^2 = {} & A_{0\ 1}^2 \pi\sigma_1^2 e^{-2\pi^2 s^2 \sigma_1^2} + A_{0\ 2}^2 \pi\sigma_2^2 e^{-2\pi^2 s^2 \sigma_2^2} \\ & + 2A_{0\ 1}A_{0\ 2}\pi\sigma_1\sigma_2 \cos(2\pi a s) e^{-\pi^2 s^2(\sigma_1^2+\sigma_2^2)} \end{aligned} \qquad 39$$

It can be easily shown that the autocorrelation of the spectrum is then

$$R * R = A_{0\,1}^2 \sqrt{\pi}\sigma_1 e^{\frac{-\omega^2}{2\sigma_1^2}} + A_{0\,2}^2 \sqrt{\pi}\sigma_2 e^{\frac{-\omega^2}{2\sigma_2^2}}$$

$$+ A_{0\,1} A_{0\,2} \frac{\sigma_1\sigma_2\sqrt{\pi}}{2\sqrt{\sigma_1^2+\sigma_2^2}} \left[e^{\frac{-(a-\omega)^2}{\sigma_1^2+\sigma_2^2}} + e^{\frac{-(a+\omega)^2}{\sigma_1^2+\sigma_2^2}} \right] \qquad 40$$

If a is large (that is, the lines are widely spaced) the autocorrelation function is the sum of the autocorrelations of the individual lines. If a is small relative to the widths of the individual lines, then the cross term becomes similar in magnitude to the other two, and will affect the autocorrelation width–$V \sin i$ calibration.

A similar result can be expected for more than two lines, and suggests that the calibration one can expect for each wavelength for a given range of spectral types will be different. Therefore in order to use the autocorrelation method for a particular wavelength region and spectral type, a calibration curve must be constructed using stars with well-determined rotational velocities.

3. Calibration

The autocorrelation width–$V \sin i$ calibration curve must be established for each instrumental resolution and wavelength region used. To do this most simply, a reference star with a well-determined rotational velocity was chosen for each observing run. For consistency, the $V \sin i$ values for the reference stars were taken from Soderblom (1983). All reference stars were chosen to have as low a measured value for $V \sin i$ as possible.

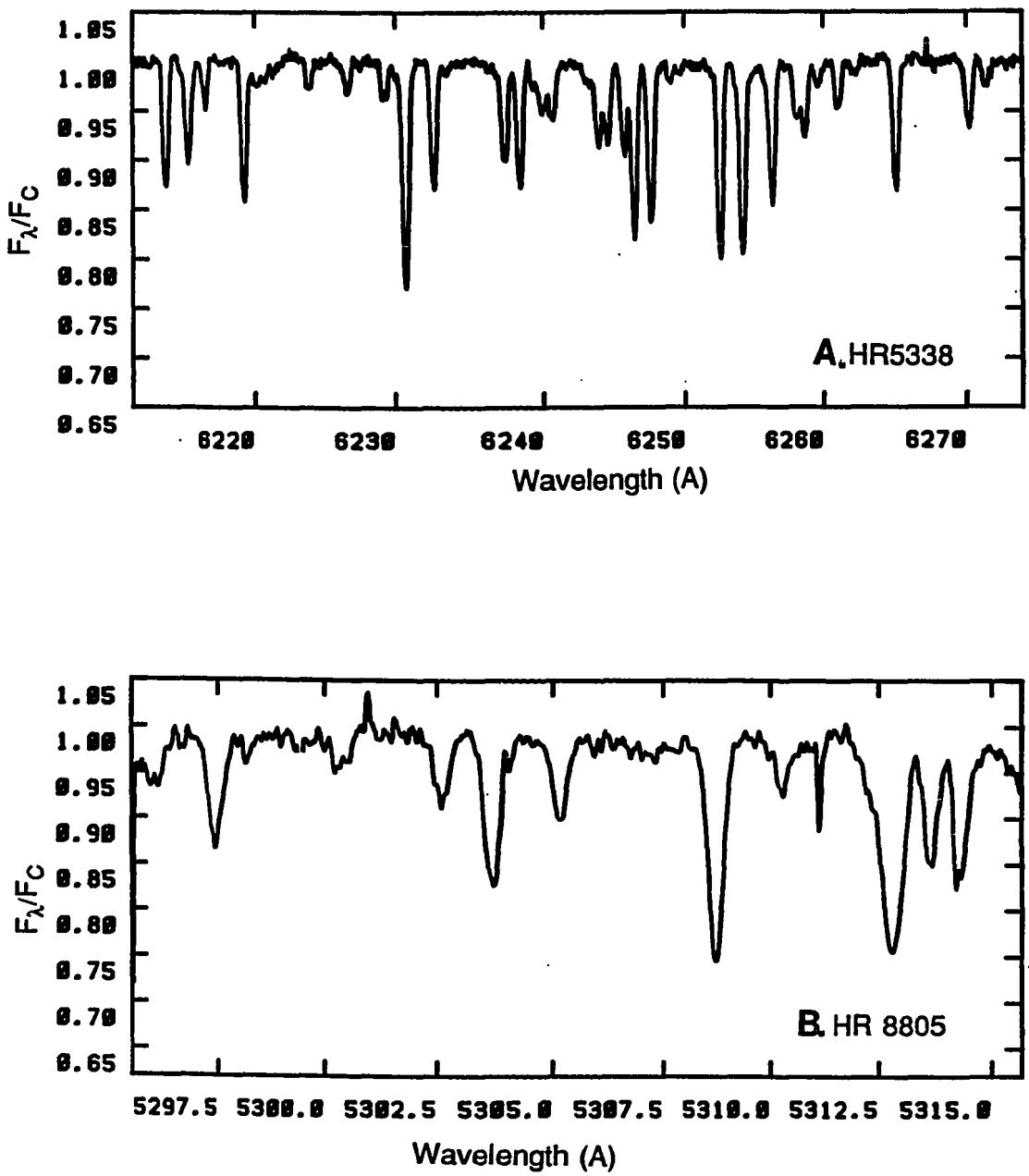

Figure 25. Examples of typical spectra obtained using a) the 1872 element Reticon at the Canada-France-Hawaii telescope (HR 5338) and b) the 800 × 800 CCD at the UH 2.2 m telescope (HR 8805).

The spectrum of the reference star was deconvolved with the rotational profile appropriate to its measured velocity, after removing the effect of noise on the Fourier transform with a cosine-bell filter (Brault and White 1971). This yields essentially the spectrum the reference star would have if it did not rotate. Then to compare the other stars in the sample to the reference star, the reference star is convolved with a rotation profile for a range of $V \sin i$ values. The resulting spectra are then autocorrelated and the $1/e$ half-width of the autocorrelation peaks are measured. This allows the construction of a curve for an observing run, relating $V \sin i$ to the $1/e$ half-width of the autocorrelation peak.

An example of the computation of the synthetic autocorrelation half-width – $V \sin i$ relation for a single isolated line, is illustrated by the following. First consider the rotation profile *alone*. If this profile and its autocorrelation is computed assuming a line center wavelength of 5306 Å, a linear relationship between the $1/e$ half-width of the autocorrelation broadening and $V \sin i$ is obtained, as expected from section (2). See Figure 26. Clearly if the rotational broadening function dominates the line profile, for a single stellar line a similar relationship should be observed. As an example, the 5305.9 Å line of Cr II in HR 7469 was chosen. This star has a well-observed $V \sin i$ value of 5.3 km s^{-1} (Soderblom 1983). The rotation profile for this velocity was deconvolved from the line profile, and various rotation profiles were reconvolved. The resulting autocorrelation $1/e$ half-width values are also plotted in Figure 26. Note that the linear relation is preserved for high velocities, but at low velocities the intrinsic broadening of the non-rotating profile dominates, as expected. Other single lines show similar results.

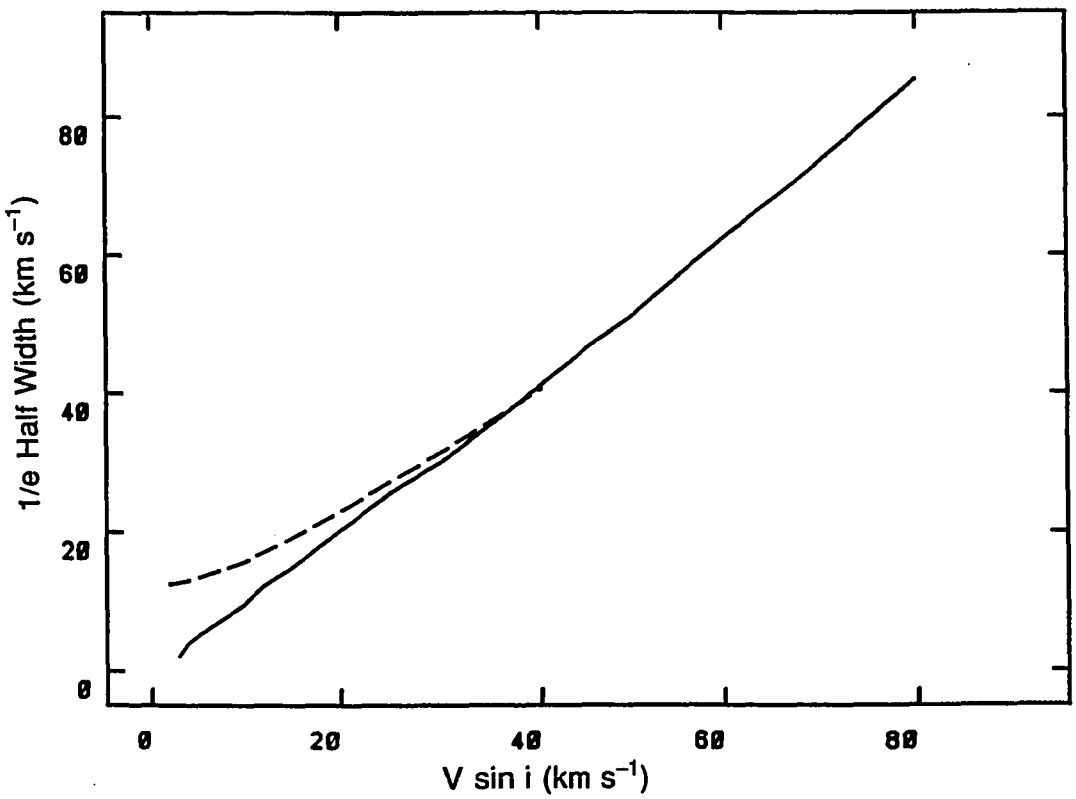

Figure 26. The solid line shows the $V \sin i$–autocorrelation width calibration curve using only the rotation profile calculated for 5309Å. The dashed line shows the calibration curve for a single line using using the 5305.9Å Cr II line of HR 7469 (actual $V \sin i = 4.0$ km s^{-1} [Soderblom 1983]).

The lines used for measurement of $V \sin i$ should be intermediate to weak in strength. Lines which are intermediate in strength ($\sim$ 100 mÅ) are best for determining stellar velocity fields (Gray 1978). Somewhat weaker lines, while more sensitive to continuum level selection and noise, may be better for rotation determinations since microturbulence has a more Gaussian behavior (Gray 1976), which implies that the line profile may be more legitimately considered a convolution of the intrinsic, turbulence, and rotation profiles.

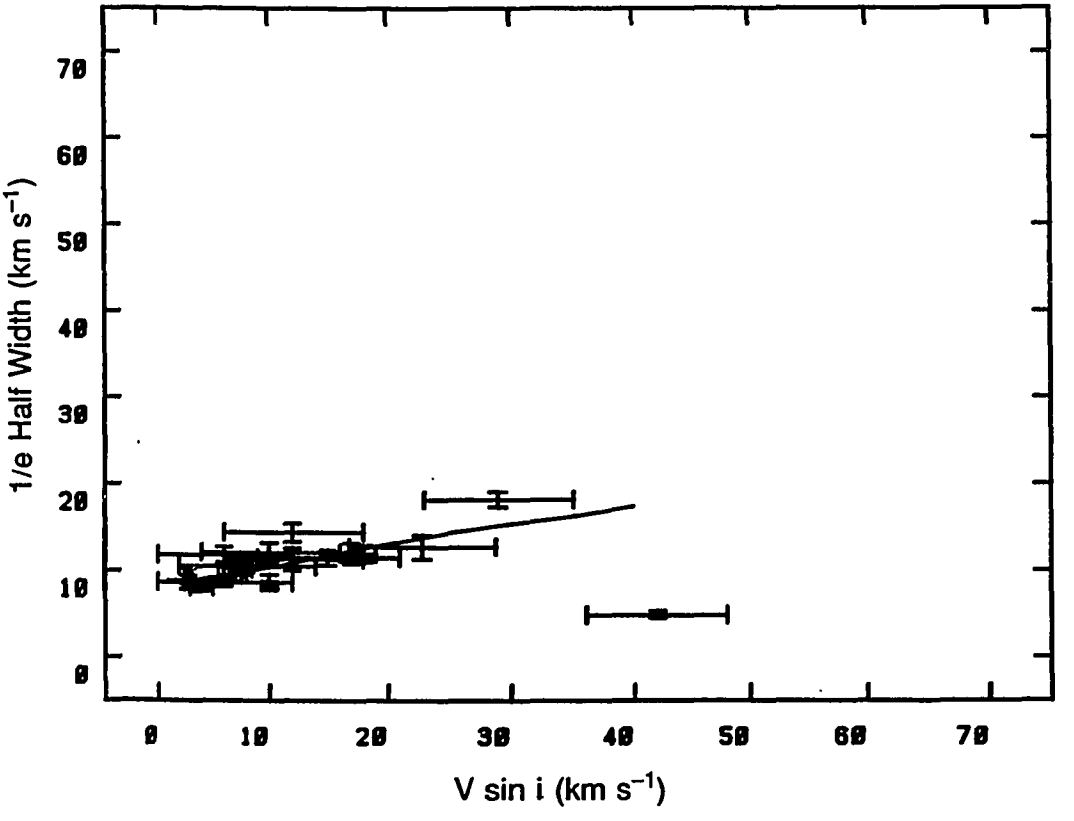

Figure 27a. Autocorrelation calibration curve for 2-3 February 1984 observations using the UH 2.2 meter telescope and the 500 × 500 CCD. The reference star (HR 4533) is marked by an asterisk.

4. Observations and Results

Determinations of stellar rotation were made based on data from three observing runs. The first run was on the University of Hawaii 2.2m telescope using the IFA/Galileo 500 × 500 CCD detector at the coudé spectrograph on February 23 and 24, 1984 (UT). The second run was again on the Canada-France-Hawaii telescope using the Reticon at coudé on June 8, 1984 (UT). The final set of data

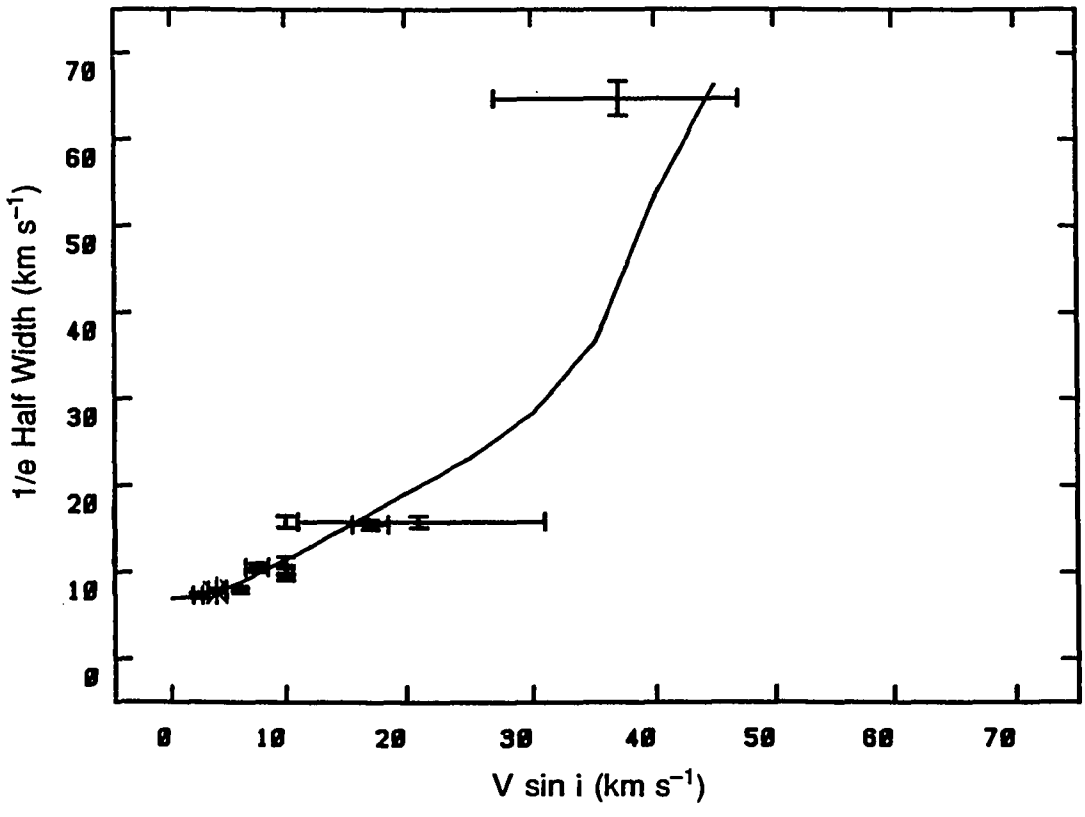

Figure 27b. Autocorrelation calibration curve for 8 June 1984 observations using the 3.6 meter Canada-France-Hawaii telescope and the 1872 element Reticon. The reference star (HR 4540) is marked by an asterisk.

was collected September 2 through 6, 1984 at the UH 2.2m telescope. The wavelength regions and lines used are shown in Table 7. For each run, a star with a known, well-determined rotation rate was used as a reference star as described in section (3) above. Figure 28 shows for each data set the calibration curve of $1/e$ half-width versus $V \sin i$ for the reference star after deconvolution with its known $V \sin i$ and then convolved with rotation profiles for a range of $V \sin i$ values. Also plotted are other stars in each data set with known $V \sin i$ values. The scatter

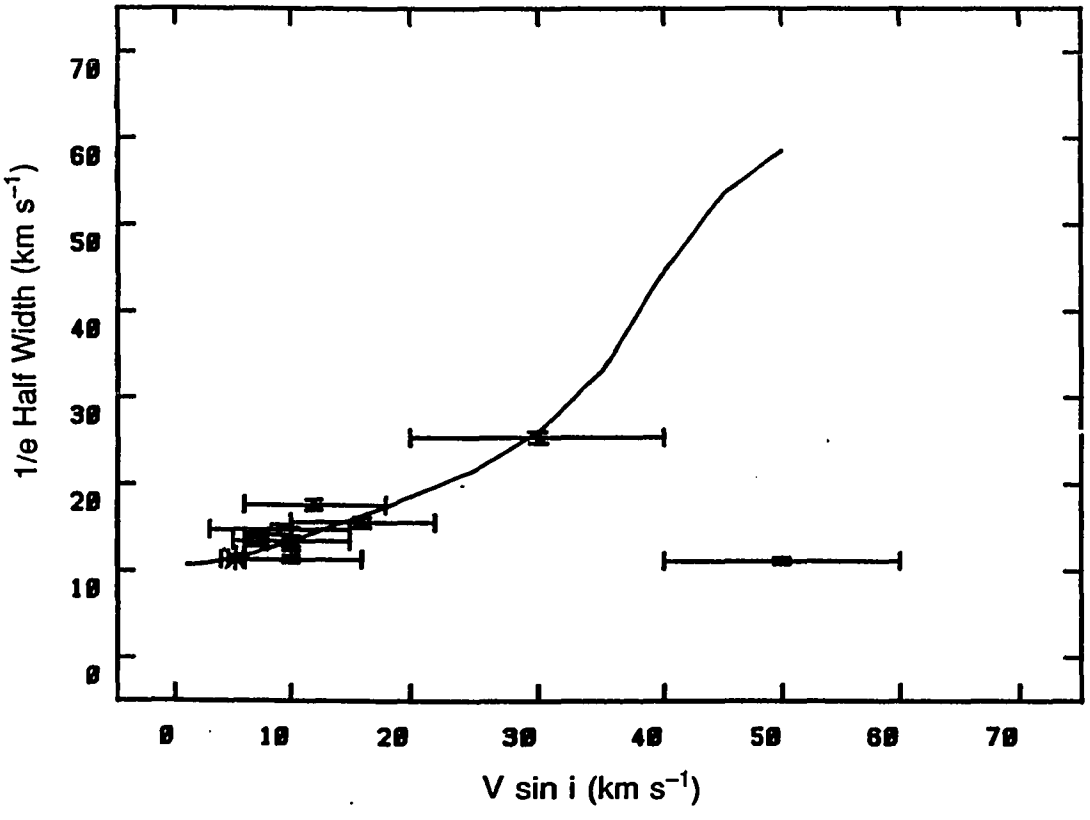

Figure 27c. Autocorrelation calibration curve for 2-6 September 1984 observations using the UH 2.2 meter telescope and the 800 × 800 CCD. The reference star (HR 7469) is marked by an asterisk.

shown gives an indication of the uncertainty associated with the autocorrelation technique. The resulting $V \sin i$ measurements are listed in Table 8.

The uncertainties shown include that in the fit of a Gaussian to the observed autocorrelations and the external uncertainty based on comparison of the autocorrelation values and the values based on Fourier analysis by Soderblom (1983). The uncertainties in the autocorrelation results are clearly higher than in the Fourier analysis of Soderblom (1983) or Smith (1979), but they appear satisfactory for

Table 7

Wavelength Regions Observed for $V \sin i$ Measurements

Date* (1984)	Tel.	Detector	Dispersion (Å / pixel)	Instr. Profile (1/e HW, Å)	Lines Used
2/23 2/24	2.2m	500 × 500 CCD (3 phase)	0.032	0.172	Cr II 5305.87 Å Fe I 5307.37 Å
6/8	3.6m	1872 Reticon	0.034	0.054	Region between approx. 6205 Å and 6260 Å, depending on stellar radial velocity.
9/2 9/3 9/4 9/6	2.2m	800 × 800 CCD (virtual phase)	0.025	0.086	Fe I 5302.31 Å Cr II 5305.87 Å Fe I 5307.37 Å Cr II 5308.43 Å

NOTE.

* All dates are UT.

survey work. Given the results of Benz, Mayor, and Mermilliod (1985) using the cross-correlation technique in the Pleiades, Hyades, Praesepe, and Coma clusters, it appears that increasing the wavelength coverage and reducing the resolution somewhat would likely decrease the uncertainty to $\sim$1 km s^{-1} , even for faint objects. The internal precision is best for the CFH data set, which is not surprising as it has the widest wavelength coverage and largest number of spectral lines. However, even using a small wavelength region and only five lines, as in the September 2.2 m data, can yield usable results.

Table 8a

$V \sin i$ Results for February 1984
500 × 500 Three Phase CCD—2.2 m Telescope

DATE	HR	HD	1/e HW* (km s^{-1})		$V \sin i$ (km s^{-1})		Other $V \sin i$	Ref.	Remarks
2/23	2943	61421	9.3±0.9		< 9.2		2.8	9	
	2220	43042	8.8	0.7	< 6.5		<10	5	
	3176	67228	8.2	0.5	< 1		<10	5	
	3954	87141	12.1	1.1	16.0±4.0		10	2	
	4251	94388	9.7	0.8	7.3	3.7			
	4533	102634	9.5	0.8	6.5	4.3	6.5	1	Reference
	4856	111199	11.4	1.2	13.7	4.4			
	4934	113337	9.7	0.9	7.3	4.4	<6	3	
	5128	118646	11.0	1.2	12.4	4.4			
	5185	120136	12.0	1.2	15.6	4.4	17.0	1	
	5258	122106	14.4	1.1	25.0	4.9	12	2	
	5365	125451	4.8	0.4	~0		42	2	
	5542	131117	9.1	0.7	<7.6				
2/24	2943	61421	8.6	0.8	<6.0		2.8	9	
	1536	30562	9.2	0.6	<7.6				
	1257	25621	12.3	0.9	16.8	3.4			
	1278	25996	12.7	1.4	18.4	5.2	22.8	2	
	2122	40832	11.3	1.3	13.4	4.8	12	2	
	3759	81997	18.2	0.9	42.6	2.4	29	2	
	2483	48682	8.6	0.5	<4.6		<6	3	
	4149	91706	10.9	0.9	12.0	3.3			
	4054	89449	11.9	1.0	15.3	3.6	18.0	1	
	3299	71030	9.4	0.9	<9.6				
	4067	89744	10.5	0.8	10.4	3.0	8.0	2	
	4130	91280	11.3	1.1	13.4	4.0			
	4455	100563	11.5	0.9	14.0	3.2	15.0	2	
	4540	102870	8.0	0.5	~0		4.0	1	
	4677	106975	11.5	0.9	14.0	3.2			
	5447	128167	10.1	0.7	8.8	2.8	7.5	1	
	5581	132254	11.8	0.9	15.0	3.2	6	2	
	6012	145100	8.3	0.8	<4.6				
	6310	153363	14.6	1.0	25.9	4.6			

NOTE.

External error from Soderblom points is ±2.3 km s^{-1} for this set of observations.

Table 8b

$V \sin i$ Results for June 1984
1872 Element Reticon—3.6 m CFH Telescope

DATE	HR	HD	1/e HW* (km s^{-1})		$V \sin i$ (km s^{-1})		Other $V \sin i$	Ref.	Remarks
6/8	4540	102870	7.8	±0.3	4.0	±0.8	4.0	1	Reference
	5340	124897	8.6	0.3	5.6	0.6			
	4708	107705	10.0	0.4	7.9	0.6	<10	5	
	5322	124553	7.7	0.3	3.7	0.9			
	5338	124850	15.5	0.6	15.3	0.8	17.0	1	
	5447	128167	10.5	0.5	8.6	0.7	7.5	1	
	5694	136202	8.0	0.3	4.5	0.7	<6	3	
	5868	141004	7.2	0.3	2.0	1.0	2.3	9	
	5933	142860	11.8	0.5	10.4	0.8			
	6202	150453	11.3	0.5	9.7	0.7			
	6496	157968	13.1	0.6	12.3	0.8			
	6541	159332	11.2	0.5	9.6	0.7	<10	5	
	7126	175317	16.8	0.8	17.0	1.0			
	7496	186185	15.8	0.7	15.7	0.9	21	10	
	7560	187691	7.8	0.3	4.0	0.8	<6	3	
	7697	191195	9.4	0.4	7.0	0.6	<10	5	
	7727	192455	15.8	0.7	15.7	0.9	<10	5	
	7936	197692	64.7	1.9	44.1	1.5	45	8	
	8472	210855	12.6	0.5	11.6	0.7			
	8131	202447	7.7	0.3	3.7	0.9			

NOTE.

External error from Soderblom points is ±1.2 km s^{-1} for this series of observations.

5. Conclusions

The autocorrelation method allows $V \sin i$ measurements to be made using all the rotational broadening information available in a typical spectrogram with a number of lines present, and does not require a special cross-correlation mask to be constructed. The reduction process is much simpler than the Fourier transform method.

The method described here cannot be used for fundamental $V \sin i$ measurements, as the measurements given here are limited by the accuracy of the $V \sin i$

Table 8c

$V \sin i$ Results for September 1984
800 x 800 Virtual Phase CCD—2.2 m Telescope

DATE	HR	HD	1/e HW* (km s^{-1})	$V \sin i$ (km s^{-1})	Other $V \sin i$	Ref.	Remarks
9/2	6212	150680	11.3±0.4	4.5±1.5	10	4	
	35	739	11.1 0.4	3.6 1.6	50	8	
	329	6706	58.2 0.4	49.5 0.5			
	869	18256	15.6 0.6	14.4 1.2	16	2	
9/3	8457	210464	13.0 0.6	9.0 1.5			
	8536	212487	12.9 0.6	8.7 1.5	<10	3	
	8805	218470	14.7 0.6	12.6 1.2	9	2	
	297	6210	55.6 0.8	46.7 0.8			
9/4	7061	173667	17.6 0.6	18.4 1.0	12	2	
	7925	197373	25.4 0.7	29.5 0.8	30	4	
	7469	185395	11.4 0.4	5.0 1.5	5.3	1	Reference
	8732	217096	11.9 0.5	6.5 1.8			
	66	1343	12.0 0.5	6.7 1.2			
	251	5156	15.4 0.6	14.0 1.2			
	635	13421	14.4 0.6	12.0 1.2	<10	5	
	772	16417	11.4 0.4	5.0 1.5			
9/6	6948	170773	62.2 0.4	55.1 0.6			
	7729	192486	10.9 0.4	< 4.5			
	8548	212754	13.3 0.5	9.8 1.2	7.0	2	
	88	1835	13.9 0.5	11.1 1.0	7.0	1	
	790	16765	34.2 0.8	35.6 0.4			
	870	18262	13.4 0.6	10.0 1.3	<10	5	

NOTES.

External error from Soderblom points is ±2.9 km s^{-1} for this series of observations.

* Half width of the autocorrelation function peak at $1/e$ times its peak value.

** References for other $V \sin i$ data:

1. Soderblom (1983).
2. Kraft (1967).
3. Kraft (1967) upper limit.
4. Wilson (1966).
5. Wilson (1966) upper limit.
8. Huang (1953).
9. Gray (1982, 1984).
10. Danziger and Faber (1972).

measurements of the reference stars. In addition, the method depends critically on the assumptions used about the behavior of stellar turbulence. In the autocorrelation method, it is assumed that turbulence in all measured stars behaves identically to the reference star. There is evidence (see above) that this may not be the case. The macroturbulence in F–G dwarfs may vary proportional to T_{eff}^3, which may result in a variation of $\sim$1.5 km s^{-1} over the temperature range considered here. Microturbulence measurements (Gray 1982) appear to range between 1 and $\sim$2 km s^{-1} for F dwarfs. If this scatter is real it will increase the uncertainty quoted above.

Problems also arise due to using a reference star of different spectral type from the object. Since the lines in the reference star have somewhat different strengths from the lines in the star to be measured, the effect of blends at high $V \sin i$ will differ somewhat in the two stars. The importance of this effect decreases if the wavelength range of the spectrum used increases.

6. Summary

A new method of obtaining $V \sin i$ for late-type stars is described. This method compares the autocorrelation half-width for a star to be measured with that of a star with known $V \sin i$ which has been convolved with a rotation profile for a given velocity. It is shown that $V \sin i$ can be measured for F stars with an internal precision of $\sim$ 1.2 km s^{-1} , provided that assumptions are made about the behavior of turbulence in these objects. Rotational velocity data from this technique are presented for 71 stars.

CHAPTER V
STELLAR ACTIVITY IN F STARS II. THE DEPENDENCE OF CHROMOSPHERIC ACTIVITY ON ROTATION

1. Background

This chapter is the continuation of a study of the relationship between chromospheric activity, age, and rotation velocity in a sample of F dwarfs in the field and in the Pleiades, Hyades, Praesepe, and Coma clusters. The F stars, particularly the early F stars, are of interest to the study of stellar activity because of their thin convective zones. Durney and Latour (1978) have predicted that the time required for significant angular momentum loss in F stars should increase by a large amount with increasing mass. This prediction is based on the assumption that the magnetic field in these stars is predominantly radial, that the magnetic field strength is proportional to the angular velocity, and that in general the chromospheric activity in F dwarfs is essentially similar to that observed in solar-type stars.

It is already clear that this last assumption is not valid. Observed differences between the activity observed in early to mid-F stars from that observed in solar-type stars include the lack of a $V \sin i$–X-ray flux relationship (Walter 1983), the lack of a He I D_3–$V \sin i$ relationship for early and mid-F dwarfs (Wolff, Heasley, and Varsik 1985), and the lack of observed Ca II flux rotational modulation (Baliunas *et al.* 1983).

Previous parts of this study estimated stellar ages by fitting stellar model isochrones to effective temperatures and luminosities obtained from Strömgren

photometry. Chapter III used these age estimates to measure the effect of age on chromospheric activity as determined from the relative surface flux observed in the cores of Ca II H and K. The basic conclusions of that study were:

(1) The dependence of the age–activity relationship on mass is much smaller than expected from the Durney-Latour theory.

(2) The dependence of activity on mass actually observed for stars of solar composition is much closer to that expected from the theory of Gill and Roxburgh (1984), assuming a quadrupole magnetic field geometry.

(3) There appears to be an additional non-magnetic source of activity which becomes dominant at $T_{eff} \geq 6450$ K, or $M_* = 1.32 M_\odot$ for solar composition. The results of the activity-age relations are not consistent with the proposal of Wolff, Simon, and Boesgaard (1986) that this non-magnetic activity is due to acoustic heating of the chromosphere.

2. Data and the *Vsini* Correction

a. *Strömgren Photometry and Age Estimates*

The sample of field and cluster stars used here is basically the same as that used in Chapter III. Field stars with homogenized Strömgren photometry from the catalog of Hauck and Mermilliod (1979) with $2.590 \leq \beta < 2.720$ were used so that the metallicity calibration of Crawford and Perry (1976) could be used. The the temperature calibration used (Hauck and Magnenat 1979) declines in effectiveness for stars with $\beta < 2.600$, when compared with other temperature indicators (see

Strömgren 1969 for a discussion of this effect) meant that all such stars were discarded. Only stars classed as luminosity class V, III-IV, and IV in the Yale Bright Star Catalog (3rd edition, Hoffleit 1964) were included. This preliminary list was examined, and short-period spectroscopic binaries, close visual binaries with periods either less than 10 years or of unknown length, and close binaries with a small magnitude difference between the components (less than about 3 mag. in V) were removed from the sample.

Ages and masses for the field stars were determined using Strömgren photometric indices for effective temperature and luminosity, and stellar isochrones to convert from these parameters to mass and age. This procedure is based on the method of Twarog (1980) and is more fully described in earlier chapters of this work. The β index was used to obtain effective temperatures using the calibration given by Böhm-Vitense (1981), using the calibration of β in terms of $B-V$ developed by Hauck and Magnenat (1975). The metallicity of the stars was determined from the $\delta m_0(\beta)$ parameter using the calibration of Crawford and Perry (1976). A constant value was assumed for the helium abundance ($Y = 0.25$) and the mixing-length to pressure scale height ratio α ($\alpha = 1.6$).

As in Chapter III, the field star age estimates were made by using the Strömgren β and δc_0 indices to find the effective temperature and the difference in luminosity between the star and the zero-age main sequence (ΔL). The luminosity of the star was found by adding ΔL to the theoretical ZAMS luminosity of the model sequence with the correct composition corresponding to the temperature obtained from β. The resulting H-R diagram position was compared to the isochrone tracks of VandenBerg (1983).

Mass estimates for the cluster stars were found using a somewhat different procedure. Ages and compositions based on main-sequence fitting (for ages) and mean cluster δm_1 values (see Chapter III) were determined for all members of each cluster. Masses were found by interpolating along the ZAMS values of VandenBerg and Bridges (1984) using only the Strömgren β index as a temperature indicator. The δc_0 values for the cluster stars were not used, thus avoiding the complications of the Hyades anomaly (Crawford and Barnes 1969). An additional ZAMS with [Fe/H] = 0.20 was interpolated between the [Fe/H] = 0.40 and 0.00 sequences of VandenBerg and Bridges and was used for the Hyades stars. The zero-age isochrones were increased in $\log T_{eff}$ by 0.003 to compensate for the difference in the mixing length to scale height ratios between VandenBerg and Bridges (1984) ($\alpha = 1.5$) and VandenBerg (1983) ($\alpha = 1.6$). This change is consistent with the dependence of $\log T_{eff}$ on α shown in VandenBerg (1983) and in Ciardullo and Demarque (1979).

One would like to be able to compare the masses derived here with independently obtained stellar mass estimates. The only truly reliable stellar masses come from measurements of binary systems, which were deliberately selected against in this sample in order to avoid possible effects of close companions on stellar activity. Only two systems in the sample have known masses based on binary orbits. The first, Procyon (α CMi) has a period of 41 years and rotates with $P/\sin i = 29.4$ days, so it can be expected that the presence of the white dwarf Procyon B has a negligible effect on the activity of Procyon A. However, the mass obtained for Procyon A from its orbit is $1.77 \pm 0.2 M_\odot$ (Popper 1981), while the photometric estimate obtained here is 1.41 $M_\odot$. Also, the luminosity estimate ($\log L_*/L_\odot = 0.65$) is low compared to the known value of $\log L_*/L_\odot = 0.82$. According to the δm_1

index Procyon is near the upper limit of what I have considered here solar composition, and a higher metallicity model would lead to a higher mass for the star.

The other binary system with known mass is γ Vir (HR 4825/6), with an orbital period of 170 years and rotation rates of 25 (HR 4825) and 33 (HR 4826) km s^{-1} , respectively. Once again, there should be no difference between the activity levels of the components and those of single stars. Both components have masses of $1.08 \pm 0.35 M_{\odot}$ according to their orbits (Popper 1981). This value is consistent with the photometric estimates: $1.38 \pm 0.05 M_{\odot}$ for HR 4825 and $1.27 \pm 0.05 M_{\odot}$ for HR 4826. As in the case of Procyon, this system is at a boundary between two metallicity groups, the solar-composition group and a group in which a lower-metallicity model with [Fe/H] = -0.23 was used. Slight differences in the photometric indices placed one member of the pair (HR 4825) in the solar composition group and the other in the low metallicity group, leading to a difference in the estimated mass. Such changes would not affect any of the results concerning activity and rotation obtained in this dissertation, so I have left the photometric estimates in the text. This results do not affect the calibration of the R'_{HK} index.

Stars beyond the main-sequence turnoff point for their isochrones (subgiants) were also omitted. The final field star sample contains 40 field stars, 58 cluster stars, and the Sun.

b. Ca II Relative Surface Fluxes

Chromospheric activity levels were determined for individual stars using data obtained from the Mt. Wilson Ca II survey (Duncan 1983, 1985 private communication) and Ca II H and K fluxes obtained from spectroscopic measurements made using the University of Hawaii 2.2 m telescope (see Chapter III). For the Hyades, Mt. Wilson S values were also obtained from Duncan *et al.* (1984). All data were converted into chromospheric Ca II surface fluxes relative to the total stellar flux using an estimate of the photospheric contribution to the core Ca II flux, as described in Chapter III. This "photospheric contribution" was based on the flux in the Mt. Wilson passband calculated from radiative-equilibrium model atmospheres for γ Vir, Procyon, and the Sun (Kelch *et al.* 1979, Ayres 1975, Linsky *et al.* 1979). The objective of the analysis was to obtain a mean flux value for each star. While many field stars and some cluster stars have hundreds of measurements available (due to the Mt. Wilson synoptic monitoring program) many of the field and cluster stars have only a few or one measurement available. For these stars I must assume that the measured value is typical. The Mt. Wilson survey does not include many early F stars, and for many of them the Mauna Kea values are the first Ca II flux measurements available.

c. Rotational Velocities

Rotational velocities for the field and cluster sample are expressed in terms of $V \sin i$. While Ca II surface flux variations have been used (Vaughan *et al.* 1983, Baliunas *et al.* 1984, Noyes *et al.* 1985) to obtain rotation periods for late F, G, and K stars, no periodicity has been observed in the Ca II flux variations for early and mid-F stars (Baliunas *et al.* 1985) which could be attributed to

rotational modulation. Therefore all rotational velocities used here are estimated from Doppler broadening. Most of the $V \sin i$ values are from Kraft (1965, 1967), Wilson (1966), Soderblom (1983), Huang (1953), Gray (1984). The remainder have been derived using an autocorrelation technique from coudé spectra obtained with the University of Hawaii 2.2 m telescope (see Chapter IV). The observational lower limit for detected $V \sin i$ values of $\sim$3–6 km s^{-1} , depending on the observer, with only a few lower rotation velocities detected. Only stars with observed $V \sin i$ values or upper limits are included in the current sample. The observational data, including $V \sin i$ measurements, are listed in Table 9.

There is a well-known effect on the luminosity and effective temperature of stars due to rotation. In the Strömgren photometric system for A and F stars this effect makes itself felt as a movement to the red in the $b - y$ or β color, and an increase in the c_0 index. This results from the expansion of the envelope of the star in the equatorial regions, and a corresponding reduction in the overall surface temperature and gravity. Discussions of this effect can be found in Wolff (1983, pp. 158-160) and in Twarog (1983). The magnitude of this effect is such that it can alter the mass and age estimated from Strömgren photometry for rapidly rotating stars. The magnitude of this effect is investigated here. Several models of rotating A and F stars (Collins and Sonneborn 1977, Maeder and Peytremann 1972) have been calculated, but these models have not been entirely satisfactory. It seems clear, however, that the effect of rotation is primarily a decrease in the surface temperature and an increase in luminosity over a non-rotating star of the same temperature. Thus a zero-age main sequence of rotating stars lies above and to the right of an equivalent non-rotating sequence. The amount of change in T_{eff} and L_* varies with the inclination as well.

Table 9

Observed Parameters for Stars with $V \sin i$ Measurements

Name	HR	HD	β	$V \sin i$ (km s^{-1})		Ref.	R'_{HK} ($\times 10^{-5}$)	$\log T_{eff}$	$R_*/R_\odot$	$P/\sin i$ (days)	$\Omega \sin i$ ($\times 10^{-5}$)	$\log(C\tau_C)$	$\Omega\tau_C C$
(1)	(2)	(3)	(4)	(5)		(6)	(7)	(8)	(9)	(10)	(11)	(12)	(13)
θ Scl	35	739	2.652	3.6	±3.5	1	0.77	3.812	1.44	20.2	0.36	5.86	2.6
	251	5156	2.673	14.0	3.6	1	2.58	3.822	1.63	5.9	1.23	5.62	5.1
78 Psc	327	6680	2.677	125	19	7		3.824	1.58	0.6	11.4	5.57	42.2
	410	8673	2.651	32	6	4	1.98	3.812	1.55	2.4	2.97	5.87	21.9
ω And	417	8799	2.672	65	10	5	3.35	3.822	1.43	1.1	6.53	5.63	27.8
84 Cet	790	16765	2.646	35.6	3.4	3	3.96	3.809	1.03	1.5	4.94	5.92	41.6
θ Per	799	16895	2.625	8.8	0.6	3	0.97	3.795	1.15	6.6	1.10	6.18	16.6
10 Tau	1101	22484	2.610	4.5	1.0	3	0.44	3.780	1.22	13.7	0.53	6.37	12.5
71 Ori	2220	43042	2.661	< 6.5		1		3.817					
	2233	43318	2.646	< 6		4	0.53	3.809					
74 Ori	2241	43386	2.663	17	6	4	3.12	3.818	1.31	3.9	1.86	5.73	10.1
α CMi	2943	61421	2.670	2.8	0.3	2	2.21	3.821	1.63	29.4	0.25	5.65	1.1
	3499	75332	2.626	11	6	4	3.36	3.796	1.20	5.5	1.32	6.17	19.3
40 Leo	4054	89449	2.654	18.0	1.0	3	1.81	3.813	1.59	4.5	1.62	5.84	11.1
	4677	106975	2.692	14.0	3.9	1		3.830	1.27	4.6	1.59	5.39	3.9
γ Vir A	4825	110379	2.694	25	5	5		3.831	1.37	2.8	2.62	5.36	6.1
γ Vir B	4826	110380	2.706	33	5	5	1.13	3.836	1.07	1.6	4.42	5.21	7.2
39 Com	4946	113848	2.675	30	10	5		3.823	1.68	2.8	2.57	5.59	10.1
	5128	118646	2.681	12.4	5.0	1		3.826	1.82	7.4	0.98	5.52	3.3
18 Boo	5365	125451	2.676	42	10	5	3.46	3.824	1.43	1.7	4.21	5.58	16.2
	5436	127821	2.671	50	10	5	3.22	3.821	1.16	1.2	6.20	5.64	27.1
σ Boo	5447	128167	2.681	7.5	1.0	3	1.99	3.826	1.25	8.4	0.86	5.52	2.9
	5583	132375	2.644	8	6	4	0.95	3.808	1.48	9.3	0.78	5.95	6.9
45 Boo	5634	134083	2.664	46	10	5	2.81	3.818	1.37	1.5	4.83	5.72	25.4
γ Ser	5933	142860	2.633	7	6	4	1.03	3.801	1.24	9.0	0.81	6.08	9.7
	6012	145100	2.682	< 4.6		1		3.826					
26 Oph	6310	153363	2.685	25.9	5.1	1		3.827	1.37	2.7	2.72	5.48	8.1

Table 9 (Continued) Observed Parameters for Stars with $V \sin i$ Measurements

Name	HR	HD	β	$V \sin i$ (km s^{-1})		Ref.	R'_{HK} ($\times 10^{-5}$)	$\log T_{eff}$	$R_*/R_\odot$	$P/\sin i$ (days)	$\Omega \sin i$ ($\times 10^{-5}$)	$\log(C\tau_C)$	$\Omega\tau_C C$
(1)	(2)	(3)	(4)	(5)		(6)	(7)	(8)	(9)	(10)	(11)	(12)	(13)
	7126	175317	2.671	17.0	±1.6	1	1.86	3.821	1.49	4.4	1.64	5.64	7.2
	7354	182101	2.645	13	6	4	2.37	3.808	1.29	5.0	1.45	5.94	12.5
θ Cyg A	7469A	185395	2.689	5.3	0.7	3	2.39	3.829	1.34	12.8	0.57	5.43	1.5
17 Cyg A	7534A	187013	2.646	9	6	4	0.95	3.809	1.50	8.4	0.86	5.92	7.3
	7697	191195	2.679	7.0	1.3	1	2.20	3.825	1.51	10.9	0.67	5.55	2.4
	7729	192486	2.687	< 4.5		1	< 0.55	3.828					
	7793	194012	2.626	6	6	4	1.67	3.796	0.96	8.1	0.90	6.17	13.1
	7925	197373	2.667	29.5	3.0	1	2.78	3.820	1.36	2.3	3.11	5.69	15.1
ψ Cap	7936	197692	2.670	44.1	1.9	1	3.00	3.821	1.50	1.7	4.21	5.65	18.9
ξ Peg	8665	215648	2.626	8.9	0.7	3	0.62	3.796	1.34	7.6	0.96	6.17	14.0
5 And	8805	218470	2.672	9	6	4	1.87	3.822	1.54	8.7	0.84	5.63	3.6
ι Psc	8969	222368	2.622	5.7	0.7	3	0.83	3.792	1.30	11.6	0.63	6.22	10.4
	9074	224635	2.630	7	6	4	2.37	3.799	1.08	7.8	0.93	6.11	12.1
Hz II 25		23061	2.662	40	12	4	3.08	3.817	1.23	1.6	4.68	5.74	25.9
Hz II 164		23158	2.652	30	12	4	5.30	3.812	1.20	2.0	3.60	5.86	25.9
Hz II 233		23195	2.663	< 20		4	2.24	3.818					
Hz II 405		23269	2.628	15	12	4	4.25	3.797	1.09	3.7	1.98	6.14	27.2
Hz II 530		23326	2.691	< 12		4	1.81	3.830					
Hz II 727			2.637	45	12	4	5.61	3.804	1.16	1.3	5.59	6.03	59.7
Hz II 745			2.685	65	12	4	4.19	3.827	1.31	1.0	7.15	5.47	21.3
Hz II 1122		23511	2.675	28	12	4	4.66	3.823	1.25	2.2	3.23	5.59	12.6
Hz II 1139		23513	2.673	30	12	4	2.98	3.822	1.25	2.1	3.46	5.62	14.3
Hz II 1309		23584	2.662	85	12	4	6.51	3.817	1.28	0.8	9.51	5.74	52.8
Hz II 1613		282973	2.644	18	12	4	4.59	3.808	1.16	3.3	2.22	5.95	19.7
Hz II 1726		23713	2.652	< 12		4	4.28	3.812					
Hz II 1766		23732	2.690	20	12	4	6.38	3.830	1.28	3.2	2.25	5.41	5.9

Table 9 (Continued) Observed Parameters for Stars with $V \sin i$ Measurements

Name	HR	HD	β	$V \sin i$ (km s^{-1})		Ref.	R'_{HK} ($\times 10^{-5}$)	$\log T_{eff}$	$R_*/R_\odot$	$P/\sin i$ (days)	$\Omega \sin i$ ($\times 10^{-5}$)	$\log(C\tau_C)$	$\Omega\tau_C C$
(1)	(2)	(3)	(4)	(5)		(6)	(7)	(8)	(9)	(10)	(11)	(12)	(13)
Hz II 1797			2.625	15	±12	4	4.80	3.795	1.07	3.6	2.01	6.18	30.2
Hz II 1856		282971	2.628	12	12	4	4.40	3.797	1.09	4.6	1.58	6.14	21.8
Hz II 2345		23912	2.671	130	12	4	5.75	3.821	1.40	0.5	13.4	5.64	58.5
T 53		107067	2.625	< 12		4	2.43	3.795					
T 58		107132	2.626	12	6	4	3.64	3.796	1.08	4.6	1.60	6.17	23.4
T 86		107611	2.652	15	6	4	3.34	3.812	1.19	4.0	1.81	5.86	13.0
T 90		107685	2.636	< 12		4	3.18	3.803					
T 92		107701	2.632	15	12	4	4.10	3.800	1.11	3.8	1.94	6.09	23.9
T 111		108102	2.612	35	6	4	5.43	3.782	1.01	1.5	4.96	6.35	110.1
T 114		108154	2.651	< 12		4	3.63	3.812					
T 118		108226	2.657	< 12		4	3.18	3.815					
vB 29		27383	2.621	8.5	1.3	3	2.92	3.791	1.17	7.0	1.04	6.23	17.7
vB 31		27406	2.623	12.0	1.0	3	3.48	3.793	1.18	5.0	1.46	6.20	23.3
vB 35		27524	2.655	90	6	4	3.31	3.814	1.36	0.8	9.48	5.82	63.0
vB 36		27534	2.671	40	6	4	2.70	3.821	1.33	1.7	4.32	5.64	18.9
vB 37		27561	2.674	12	6	4	3.53	3.823	1.32	5.6	1.30	5.61	5.2
vB 48		27808	2.626	< 12		4	3.06	3.796					
vB 51		27548	2.659	30	6	4	2.37	3.816	1.30	2.2	3.31	5.78	19.9
vB 52		27859	2.606	8.0	0.7	3	3.29	3.775	1.07	6.8	1.07	6.42	28.1
vB 57		27991	2.644	15	6	4	3.02	3.808	1.26	4.3	1.71	5.95	15.1
vB 59		28034	2.635	< 6		4	3.86	3.802					
vB 65		28205	2.620	9	6	4	2.44	3.790	1.16	6.6	1.11	6.24	19.4
vB 77		28394	2.637	25	6	4	3.49	3.804	1.24	2.5	2.89	6.03	30.9
vB 78		28406	2.656	20	6	4	2.23	3.814	1.29	3.3	2.22	5.81	14.4
vB 81		28483	2.654	18	6	4	3.05	3.813	1.29	3.6	2.01	5.83	13.7
vB 85		28568	2.680	55	6	4	3.19	3.825	1.36	1.2	5.80	5.53	19.9
vB 101		29225	2.681	40	6	4	2.91	3.826	1.35	1.7	4.26	5.52	14.2

Table 9 (Continued) Observed Parameters for Stars with $V \sin i$ Measurements

Name	HR	HD	β	$V \sin i$ (km s^{-1})		Ref.	R'_{HK} ($\times 10^{-5}$)	$\log T_{eff}$	$R_*/R_\odot$	$P/\sin i$ (days)	$\Omega \sin i$ ($\times 10^{-5}$)	$\log(C\tau_C)$	$\Omega\tau_C C$
(1)	(2)	(3)	(4)	(5)		(6)	(7)	(8)	(9)	(10)	(11)	(12)	(13)
KW 16		73081	2.656	40	±10	6		3.814	1.21	1.5	4.73	5.81	30.7
KW 146		73429	2.680	75	10	6		3.825	1.31	0.9	8.23	5.53	28.2
KW 155			2.682	30	10	6		3.826	1.26	2.1	3.41	5.51	11.1
KW 218		73597	2.694	45	20	6		3.831	1.30	1.5	4.97	5.36	11.5
KW 227		73641	2.673	15	10	6		3.822	1.24	4.2	1.74	5.62	7.2
KW 232		73617	2.692	120	20	6		3.830	1.41	0.6	12.2	5.39	30.0
KW 239		73640	2.666	32	10	6		3.819	1.23	2.0	3.73	5.70	18.7
KW 268			2.651	20	10	6		3.812	1.19	3.0	2.41	5.87	17.8
KW 275			2.612	< 20		6		3.782					
KW 332			2.688	35	10	6		3.829	1.28	1.8	3.93	5.44	10.8
KW 341			2.628	< 20		6		3.797					
KW 411		73937	2.677	35	20	6		3.824	1.26	1.8	4.00	5.57	14.9
KW 421			2.641	< 20		6		3.806					
KW 439		73994	2.696	15	10	6		3.832	1.29	4.3	1.68	5.34	3.7
KW 458			2.635	20	20	6		3.802	1.13	2.8	2.55	6.05	28.8
KW 459		74058	2.699	145	20	6		3.833	1.51	0.5	13.8	5.30	27.6
KW 496		74186	2.643	32	10	6		3.807	1.17	1.8	3.94	5.96	35.8
KW 536			2.653	20	20	6		3.813	1.20	3.0	2.40	5.85	16.9
Sun*			2.600	1.5	0.1	8	0.64	3.763	1.00	33.7	0.21	6.51	6.9

NOTES.

For the Sun, $V \sin i$ was replaced by $(\pi/4)V_{rot}$.

Column (1): Cluster Star Identifications:
vB: Hyades cluster, van Bueren (1952).
Hz II: Pleiades cluster, Hertzsprung (1947).
KW: Praesepe cluster, Klein Wassink (1927).
T: Coma Bernices cluster, Trumpler (1938).

Column (5): Stellar rotation velocity.

Column (6): References for $V \sin i$ values:
1. This dissertation.
2. Gray (1984).
3. Soderblom (1983).
4. Kraft (1967).
5. Wilson (1966).
6. McGee *et al.* (1967).
7. Danziger and Faber (1972).
8. Noyes *et al.* (1984).

Column (7): R'_{HK} listed here for convenience. See Chapter III.

Column (8): Effective temperature from β index.

Column (9): Stellar radii, estimated using temperature and luminosity obtained from the Strömgren indices.

Column (10), (11), and (12): Estimated from Strömgren indices.

Column (13): From Ruciński and VandenBerg (1986).

Column (14): From (11) and (12).

Crawford and Perry (1976) suggest that the lower envelope of the field star distribution in the c_0–β diagram is occupied by zero-age field stars with zero rotation. Therefore on the average the position of a non-rotating zero-age star in this diagram is given by the standard Crawford (1975) calibration, while a rotating star will be displaced by the effect noted above. If the rotation velocity and inclination of the star are known, it is possible to completely remove the effect of rotation on c_0 and β and thus obtain the effective temperature and luminosity the star would have if it did not rotate. The models of Collins and Sonneborn (1977) show that the effect of varying the inclination is primarily a change in the degree of reddening observed, rather than a change in the nature of the effect for small inclinations, as proposed by Maeder and Peytremann (1972).

A correction for the effect of $V \sin i$ on the observed β and c_0 indices was made for both the field and cluster stars. Due to the uncertainities in the theory, it seemed best to use an empirical correction corresponding to the effect of $V \sin i$ at intermediate inclinations. For the cluster stars, only a correction in β was used, since the c_0 index was not used in the cluster stars as a luminosity indicator (see Chapter III). The correction used was that observed by Golay (1968, quoted in Maeder and Peytremann 1972) for the $B-V$ color, $\Delta B-V = 0.2\times10^5/(V \sin i)^2$. Converting to β using the table given in Hauck and Magnenat (1975), this yields a correction $\beta_{non-rotating} = \beta_{obs} + 8.2 \times 10^{-7}/(V \sin i)^2$.

For the field stars a small correction was also made for rotation in the c_0 index. This correction was based on the observation of Golay of a shift of $0.24 \times 10^{-5}(V \sin i)^2$ in c_0. The results of the Collins and Sonneborn (1977) models indicate that the change in the photometric indices for zero-age stars is such that

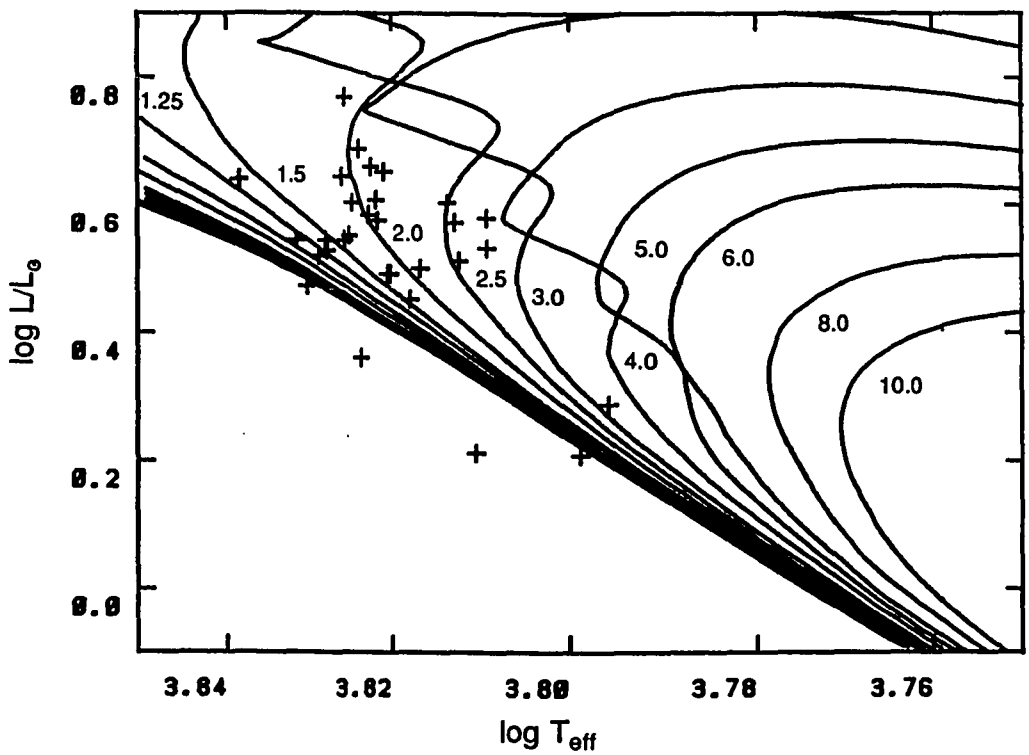

Figure 28. Solar composition effective temperature–luminosity diagram with isochrones from VandenBerg (1983) for $Y = 0.25$ and $Z = 0.0169$. Age of each isochrone indicated in Gyr.

the star moves nearly parallel to the non-rotating main sequence, basically independent of the inclination of the star, although the magnitude of the shift does depend on the inclination. As a simple empirical fit, I assume the above values for the observed shifts, and using the slope m of the observational ZAMS (see Figure 28) obtain a small correction for c_0:

$$\Delta c_0 = (8.2 \times 10^{-7} m \; - \; 2.4 \times 10^{-6})(V \sin i)^2 \qquad 41$$

The size of this correction is quite small, 0.0032 in c_0 for $V \sin i = 100$ km s^{-1} .

The largest effects of the $V \sin i$ correction for the photometric indices are seen in the young open cluster members, which make up the majority of the rapid rotators in the sample. Again, only the temperature correction is used in the calculation of the mass of these stars, while the ages are based on main-sequence fitting of the entire cluster (see Chapter III).

The only field stars where the rotation velocity correction is even marginally significant are those with $V \sin i \geq 60$ km s^{-1} (e.g., HR 2484 and HR 417). The maximum change seen in the age is 0.36 Gyr (for HR 417). Changes in the mass estimate are insignificant for all field stars. A maximum change of $0.01 M_{\odot}$ is seen in HR 2484.

The changes in estimated mass in the cluster stars due to the rotation correction are somewhat larger, due to the high rotation velocities present. The fastest rotators in the Pleiades, Hertzsprung (1947) numbers 2345, 1309, and 745, with $V \sin i$ of 130, 85, and 65 km s^{-1} respectively, show changes in mass of 0.01 $M_{\odot}$. It therefore appears that for normal F dwarfs the effect of rotation on the photometric age and mass estimates is, even for rapidly rotating young cluster stars, less than the intrinsic uncertainties in the photometry and calibration. Age and mass estimates including the rotation correction are found in Table 10.

3. Results

a. R'_{HK} and Age

As was shown in Chapter III, there is little apparent difference between Ca II activity in the late F stars and that in the early G stars as determined by other

Table 10

Age and Mass Estimates for Stars with $V \sin i$ Measurements

Name (1)	HD (2)	Age (3)		Mass (4)		[Fe/H] (5)
HR 35	739	2.55	±0.56	1.311	±0.051	−0.106
HR 251	5156	2.10	0.24	1.418	0.066	−0.020
HR 327	6680	1.35	0.69	1.433	0.043	−0.014
HR 410	8673	2.55	0.36	1.347	0.062	0.042
HR 417	8799	1.61	1.09	1.361	0.053	−0.047
HR 790	16765	< 0.86		1.250	0.070	−0.047
HR 799	16895	5.78	2.68	1.038	0.038	−0.187
HR 1101	22484	10.61	2.06	0.953	0.034	−0.152
HR 2220	43042	2.14	0.91	1.316	0.040	0.036
HR 2233	43318	2.72	0.95	1.348	0.068	−0.091
HR 2241	43386	1.58	1.36	1.306	0.046	−0.078
HR 2943	61421	2.15	0.24	1.411	0.065	0.080
HR 3499	75332	3.30	2.44	1.174	0.046	0.037
HR 4054	89449	2.50	0.30	1.369	0.066	0.078
HR 4677	106975	< 1.23		1.370	0.023	0.045
HR 4825	110379	1.12	1.01	1.379	0.048	−0.106
HR 4826	110380	< 0.61		1.273	0.047	−0.131
HR 4946	113848	2.04	0.22	1.438	0.069	−0.115
HR 5128	118646	1.92	0.19	1.499	0.072	0.058
HR 5365	125451	1.71	0.85	1.362	0.039	0.044
HR 5436	127821	< 0.91		1.335	0.040	−0.068
HR 5447	128167	1.98	1.54	1.215	0.064	−0.289
HR 5583	132375	2.83	0.57	1.306	0.058	0.050
HR 5634	134083	1.73	1.25	1.325	0.051	0.067
HR 5933	142860	5.27	1.82	1.081	0.036	−0.255
HR 6012	145100	1.94	0.31	1.412	0.060	0.057
HR 6310	153363	1.29	1.08	1.362	0.049	−0.001
HR 7126	175317	2.06	0.51	1.364	0.052	0.052
HR 7354	182101	3.81	1.49	1.144	0.035	−0.304
HR 7469A	185395	1.11	1.08	1.364	0.046	0.026
HR 7534A	187013	2.77	0.57	1.317	0.060	−0.095
HR 7697	191195	1.94	0.46	1.386	0.053	0.040
HR 7729	192486	1.41	1.08	1.368	0.051	−0.085
HR 7793	194012	< 3.93		1.063	0.064	−0.174
HR 7925	197373	1.71	1.24	1.325	0.051	−0.117
HR 7936	197692	2.02	0.50	1.370	0.052	−0.019
HR 8665	215648	6.74	1.35	1.057	0.036	−0.333
HR 8805	218470	2.10	0.36	1.383	0.058	−0.016
HR 8969	222368	7.43	1.48	1.033	0.035	−0.218
HR 9074	224635	< 2.52		1.196	0.046	0.034
Hz II 25	23061	0.08	0.01	1.330	0.020	0.050
Hz II 164	23158	0.08	0.01	1.304	0.020	0.050
Hz II 233	23195	0.08	0.01	1.327	0.020	0.050
Hz II 405	23269	0.08	0.01	1.221	0.020	0.050
Hz II 530	23326	0.08	0.01	1.383	0.020	0.050
Hz II 727		0.08	0.01	1.265	0.020	0.050

Table 10 (Continued)

Age and Mass Estimates for Stars with $V \sin i$ Measurements

Name (1)	HD (2)	Age (3)		Mass (4)		[Fe/H] (5)
Hz II 745		0.08	±0.01	1.391	±0.020	0.050
Hz II 1122	23511	0.08	0.01	1.354	0.020	0.050
Hz II 1139	23513	0.08	0.01	1.350	0.020	0.050
Hz II 1309	23584	0.08	0.01	1.354	0.020	0.050
Hz II 1613	282973	0.08	0.01	1.278	0.020	0.050
Hz II 1726	23713	0.08	0.01	1.301	0.020	0.050
Hz II 1766	23732	0.08	0.01	1.383	0.020	0.050
Hz II 1797		0.08	0.01	1.208	0.020	0.050
Hz II 1856	282971	0.08	0.01	1.220	0.020	0.050
Hz II 2345	23912	0.08	0.01	1.414	0.020	0.050
T 53	107067	0.65	0.10	1.207	0.020	−0.030
T 58	107132	0.65	0.10	1.211	0.020	−0.030
T 86	107611	0.65	0.10	1.301	0.020	−0.030
T 90	107685	0.65	0.10	1.251	0.020	−0.030
T 92	107701	0.65	0.10	1.236	0.020	−0.030
T 111	108102	0.65	0.10	1.152	0.020	−0.030
T 114	108154	0.65	0.10	1.298	0.020	−0.030
T 118	108226	0.65	0.10	1.312	0.020	−0.030
vB 29	27383	0.70	0.10	1.308	0.020	0.130
vB 31	27406	0.70	0.10	1.317	0.020	0.130
vB 35	27524	0.70	0.10	1.455	0.020	0.130
vB 36	27534	0.70	0.10	1.462	0.020	0.130
vB 37	27561	0.70	0.10	1.461	0.020	0.130
vB 48	27808	0.70	0.10	1.330	0.020	0.130
vB 51	27548	0.70	0.10	1.433	0.020	0.130
vB 52	27859	0.70	0.10	1.224	0.020	0.130
vB 57	27991	0.70	0.10	1.393	0.020	0.130
vB 59	28034	0.70	0.10	1.363	0.020	0.130
vB 65	28205	0.70	0.10	1.303	0.020	0.130
vB 77	28394	0.70	0.10	1.373	0.020	0.130
vB 78	28406	0.70	0.10	1.423	0.020	0.130
vB 81	28483	0.70	0.10	1.419	0.020	0.130
vB 85	28568	0.70	0.10	1.487	0.020	0.130
vB 101	29225	0.70	0.10	1.483	0.020	0.130
KW 16	73081	0.90	0.10	1.317	0.020	0.090
KW 146	73429	0.90	0.10	1.387	0.020	0.090
KW 155		0.90	0.10	1.369	0.020	0.090
KW 218	73597	0.90	0.10	1.399	0.020	0.090
KW 227	73641	0.90	0.10	1.347	0.020	0.090
KW 232	73617	0.90	0.10	1.446	0.020	0.090
KW 239	73640	0.90	0.10	1.336	0.020	0.090
KW 268		0.90	0.10	1.300	0.020	0.090
KW 275		0.90	0.10	1.145	0.020	0.090
KW 332		0.90	0.10	1.383	0.020	0.090
KW 341		0.90	0.10	1.222	0.020	0.090

Table 10 (Continued)

Age and Mass Estimates for Stars with $V \sin i$ Measurements

Name (1)	HD (2)	Age (3)	Mass (4)	[Fe/H] (5)
KW 411	73937	0.90±0.10	1.360±0.020	0.090
KW 421		0.90 0.10	1.269 0.020	0.090
KW 439	73994	0.90 0.10	1.394 0.020	0.090
KW 458		0.90 0.10	1.248 0.020	0.090
KW 459	74058	0.90 0.10	1.497 0.020	0.090
KW 496	74186	0.90 0.10	1.279 0.020	0.090
KW 536		0.90 0.10	1.304 0.020	0.090

NOTES.

Column (3): Photometric age estimate with $V \sin i$ correction, using VandenBerg (1983) isochrones.

Column (4): Photometric mass estimate with $V \sin i$ correction, using VandenBerg (1983) isochrones.

Column (5): Metallicity estimate based on δm_0.

authors (e.g. Simon, Herbig, and Boesgaard 1985). However, the early F stars, with $M_* > 1.325 M_\odot$, were found to behave somewhat differently.

The Ca II activity–age relation was discussed in Chapter III. The overall relation between activity and age for solar composition ($-0.12 < [\mathrm{Fe/H}] \leq 0.10$) stars with $M_* < 1.325 M_\odot$ is given by an exponential law with an e-folding time of 2.04 Gyr. Low mass F stars with low metallicity ($\sim -0.30 < [\mathrm{Fe/H}] \leq -0.10$) and age greater than 3 Gyr below the Vaughan-Preston gap follow a shallower decay law best described by a power law with an index of -1.1. The Vaughan-Preston gap is prominent in the low mass solar composition F star sample and is seen as a break in the run of R'_{HK} at roughly 2 to 3 Gyr.

The age dependence of activity in the high mass solar composition stars is similar to that for the low mass F stars, except that only two out of 25 stars are observed in Chapter III to have a Ca II relative flux value or upper limit below the gap seen in the low mass solar composition F stars. The R'_{HK} measurements are consistent with an exponential decay with e-folding time of 3.12 ± 0.31 Gyr. No stars with $[\mathrm{Fe/H}] \leq -0.10$ and $M_* > 1.325 M_\odot$ were observed.

The exponential form of the activity decay law suggests that alterations must be made in the model of stellar activity decay and spindown proposed by Durney and Latour (1978). Chapter III suggests that changing the magnetic field geometry inside the Alfven radius from purely radial to quadrupole (as suggested by Roxburgh 1982, and Gill and Roxburgh 1985) allows an exponential decay of activity to occur, while still allowing $B \propto \Omega$, which can be argued is consistent with theory (Roberts 1974). As will be shown here, such a linear dependence is consistent with observations for low values of R'_{HK} (and thus B) and Ω.

The relatively small range in activity observed in early F stars suggested to Wolff, Boesgaard, and Simon (1986) that chromospheric heating in these objects is dominated by pure acoustic waves rather than by a magnetic dynamo. The data in Chapter III suggest that while there does appear to be a minimum activity level in the early F stars higher than what would be expected from dynamo heating alone, the temperature dependence of this minimum level is not consistent with pure acoustic heating.

b. $V \sin i$ and Age

The $V \sin i$—age relation for stars earlier than F7 has not been discussed in earlier work. The relation for solar-type stars has been the focus of a great deal of interest, however. Kraft (1967) first proposed that the rotational velocity in stars with $M_* < 1.25 M_\odot$ declines with age, and that the rapidly rotating stars of such mass are generally also those with high chromospheric activity levels (as measured by Ca II emission). Skumanich (1972) proposed that the decay in rotation velocity in stars of solar type could be described by a law of the form $V \propto t^{-\frac{1}{2}}$, where t is the age of the star. This result was confirmed by the work of Soderblom (1983), who measured $V \sin i$ in nearby field stars and used the decline of surface Li abundance with age (Herbig 1965, Duncan 1981) to estimate their ages. The $t^{-\frac{1}{2}}$ relationship appeared to be confirmed for solar-type stars with ages greater than that of the Pleiades.

A recent study of rotational velocities in young clusters by Benz, Mayor, and Mermilliod (1984) may modify this conclusion somewhat. Using a cross-correlation technique, these authors were able to measure $V \sin i$ for a large sample of stars in the Pleiades, Hyades, Coma Bernices, and Praesepe clusters with uncertainties

of $\sim$1 km s^{-1} . The result of these measurements has been to somewhat lower the mean cluster $V \sin i$ for solar-type stars from values obtained using earlier methods. An example of the results of this change is shown in Figure 29. Here mean $V \sin i$ values are plotted using results from Benz, Mayor, and Mermilliod (1984) and from Soderblom (1983) for stars with $T_{eff} < 6000$ K. The difference in the resulting mean $V \sin i$ of the Pleiades, for which he used $V \sin i$ data from Kraft (1967), than for the Hyades and Ursa Major groups, for which Soderblom used high-precision Fourier transform-derived velocities. It appears that the decline of rotation rate with age for solar-type stars is shallower than $t^{-\frac{1}{2}}$ for stars younger than 1 Gyr. In the F stars considered here, which generally have higher rotational velocities than the G stars, such systematic errors should have a smaller effect on the $V \sin i$–age dependence.

Figures 30 and 31 show the dependence of $V \sin i$ on age for the mass bins described above. The differing symbols refer to stars of different composition. Stars with $M_* = 1.00 M_\odot$ and $Z = 0.010$ exceed 6000 K at approximately 1.5 Gyr, while objects with $Z = 0.0169$ and $M_* = 1.00 M_\odot$ never do. Therefore the lowest mass stars in this sample are generally slightly metal deficient ([Fe/H] ~ -0.20). These low mass stars show high $V \sin i$ values compared to what might be expected for stars of their age based on the solar value. Solar composition stars of the Sun's age are too cool to be included in the sample. While the composition does have an effect on the Rossby number (see the section below) it is not clear what that effect is for stars with $Z \approx 0.010$.

Field stars with [Fe/H] > 0.10 could not be included in the sample due to the lack of models of appropriate composition for comparison. The Hyades stars appear to have lower $V \sin i$ values than stars of similar mass from Coma and

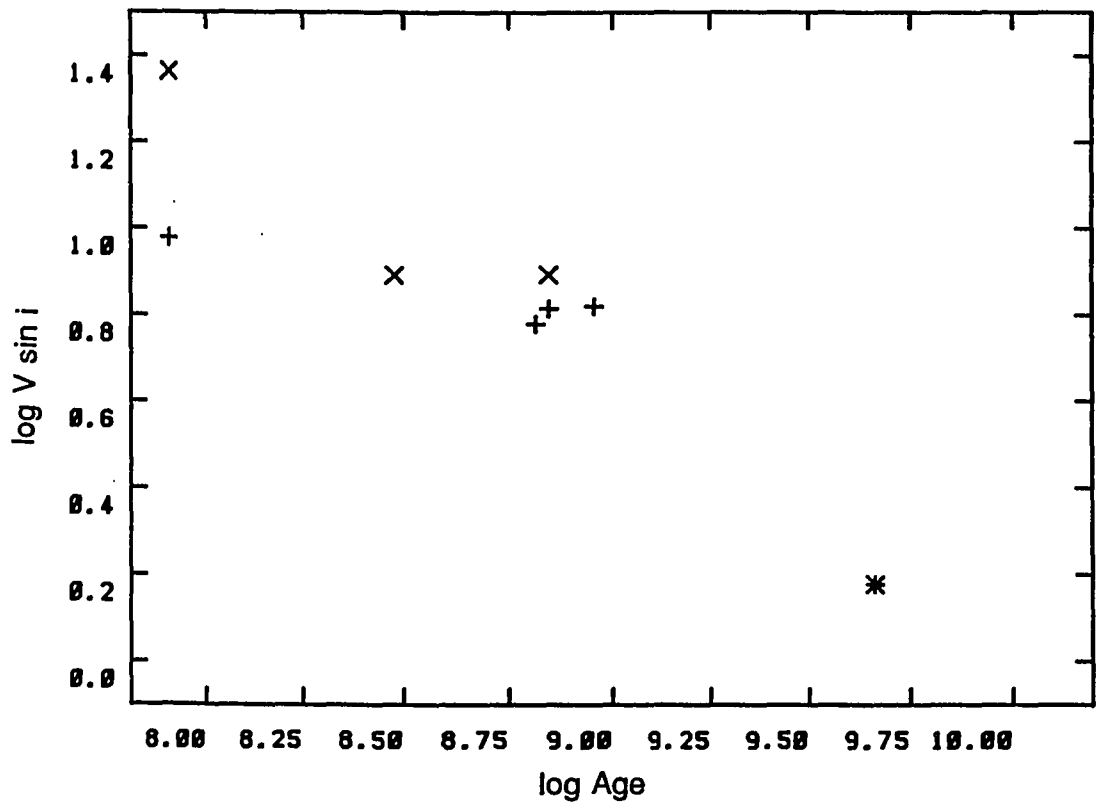

Figure 29. Comparison of mean cluster $V sini$ values from Soderblom (1983) and from Benz, Mayor, and Mermilliod (1984) for stars with $T_{eff} < 6000$K. Benz, Mayor, and Mermilliod data indicated by X's, Soderblom data indicated by +'s. Asterisk is the Sun (with $< V \sin i >_{\odot} = (\pi/4)V_{\odot}$).

Praesepe, clusters of similar age but lower (roughly solar) metallicity. The $V \sin i$–age dependence for the cluster stars (including the Pleiades) is similar to that for the G stars observed by Benz, Mayor, and Mermilliod.

As has been noted above, there appears to be a significant difference in the behavior of activity as a function of age for stars on either side of the $1.325 M_{\odot}$ boundary. It then seems most important to examine the $V \sin i$–age behavior seen on either side of this boundary, and check whether the relationship seen between

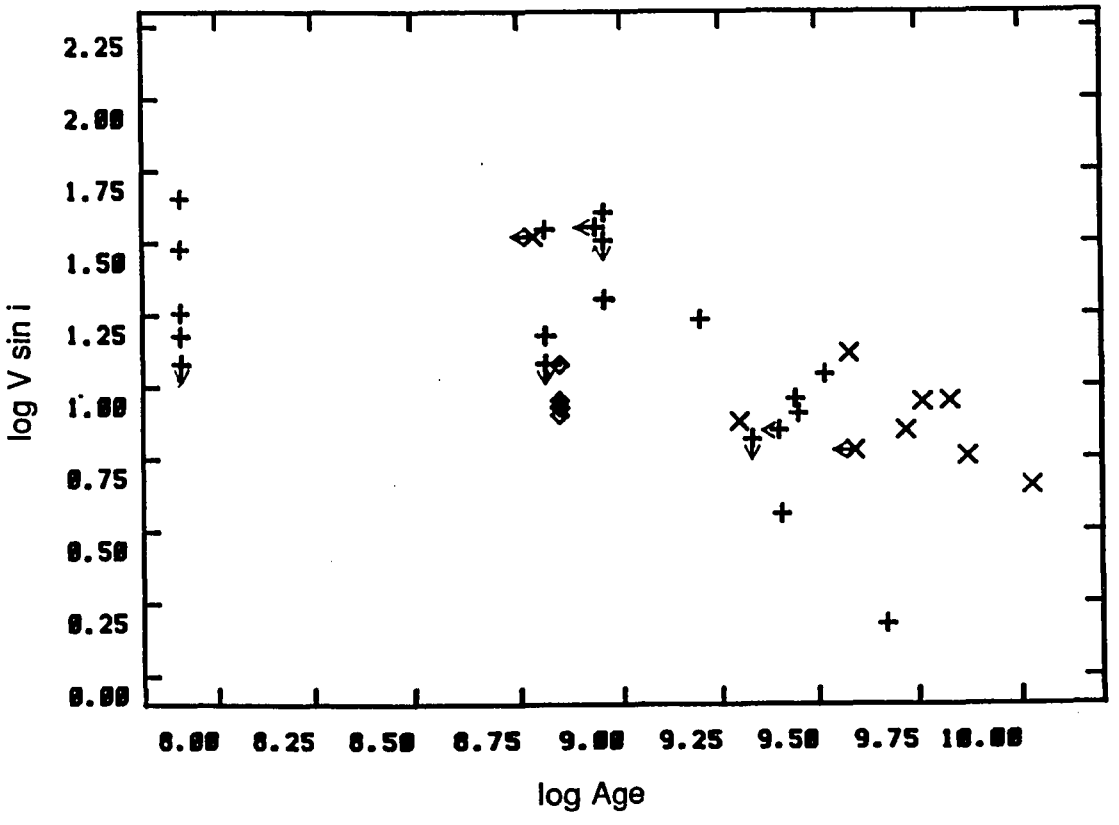

Figure 30. $V \sin i$–age relation for cluster and field stars with $M_* < 1.325 M_\odot$. Different symbols reflect different composition groups; solar composition stars are indicated by plus signs, low-metallicity stars are indicated by X's, and Hyades stars are indicated by diamonds.

rotation and activity observed for solar-type stars needs to be changed for early F stars.

Figures 32 and 33 show the age dependence of $V \sin i$ for each solar-composition mass bin. Stars with well-measured $V \sin i$ values (those with $\sigma(V \sin i)/V \sin i < 0.5$) are shown with solid symbols, while less well-measured values are indicated with open symbols. Shown on the plots are least-squares fits obtained based on the well measured data assuming both exponential and power-law decay. The

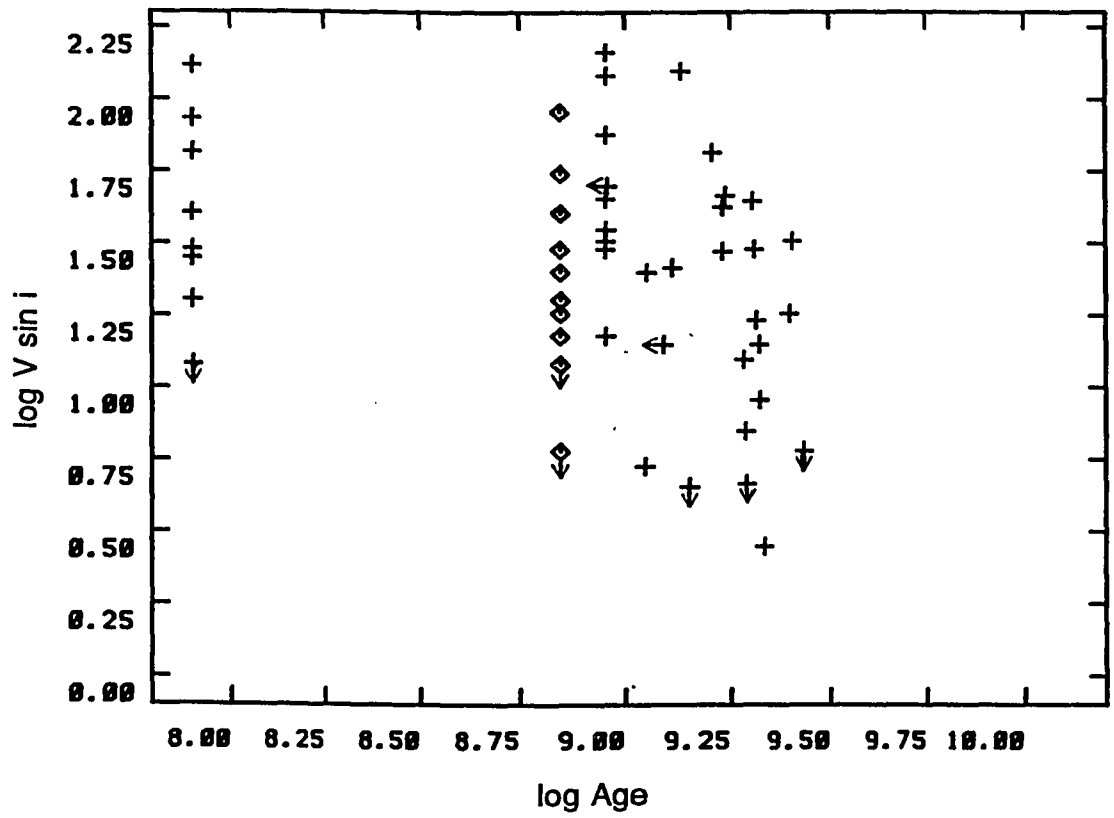

Figure 31. $V \sin i$–age relation for cluster and field stars with $M_* \geq 1.325 M_\odot$ Different symbols reflect different composition groups; solar composition stars are indicated by plus signs and Hyades stars are indicated by diamonds.

corresponding coefficients for the least-squares fits are shown in Table 11. The relatively flat $V \sin i$–age distribution seen in the young cluster stars appears to make a power law fit less acceptable than the exponential fit, and in fact the χ^2 values indicate that the exponential fit is objectively better for the low mass stars.

The $M_* < 1.325 M_\odot$ group shows a $V \sin i$–age behavior similar to that seen in the cluster $V \sin i$–age results of Benz *et al.* (1984) (see Figure 32). That is, there is a very slow decline in $V \sin i$ up to 1 Gyr, followed by a more rapid decline

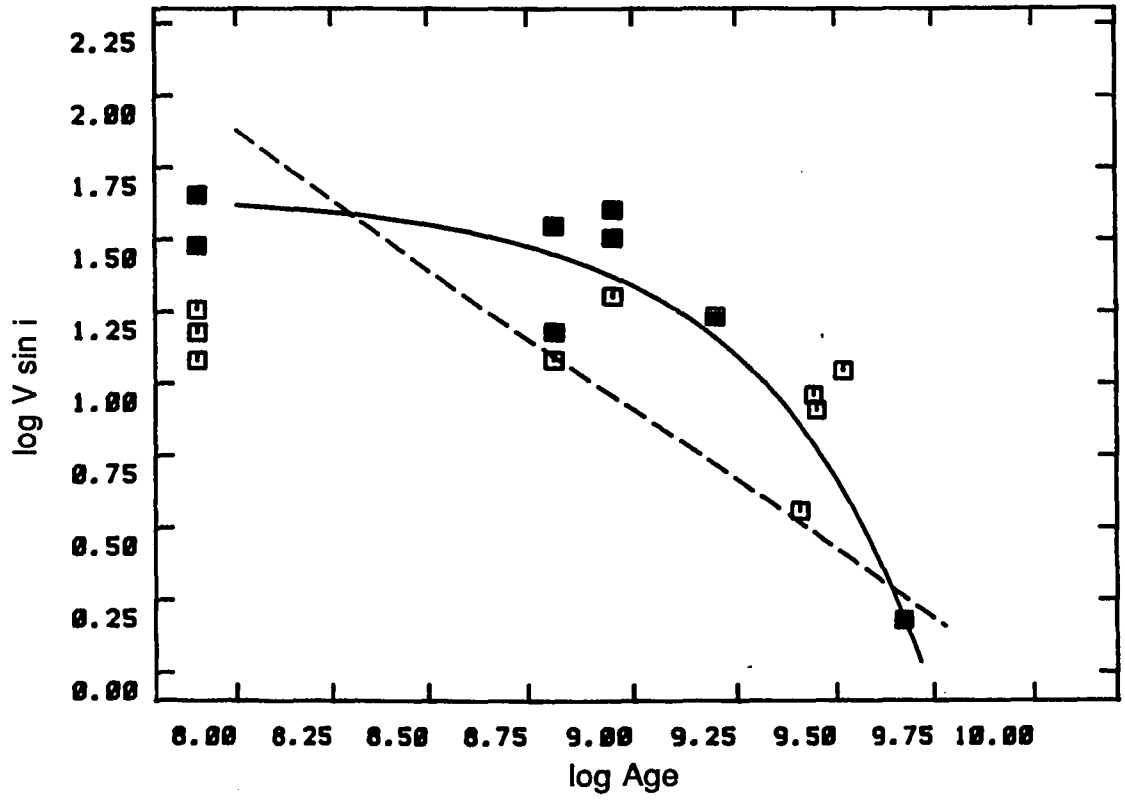

Figure 32. Plot of $\log V \sin i$ against log age for solar composition stars with $M_* < 1.325 M_\odot$ and measured rotation velocities and ages (no upper limits are shown). Well measured rotation velocities ($\sigma(V \sin i)/V \sin i < 0.5$) shown with solid symbols. Solid curve is an exponential fit (using uncertainties from both axes). Dashed line is a power law fit.

to near the solar value. The exponential fit is preferred with an e-folding time of 1.40 ± 0.06 Gyr.

For solar composition early F stars the overall fits using a power law or an exponential are essentially the same in terms of the size of the residuals. However, the exponential appears more consistent with the envelope of the scatter in $V \sin i$. This exponential fit has an e-folding time of 1.16 ± 0.08 Gyr.

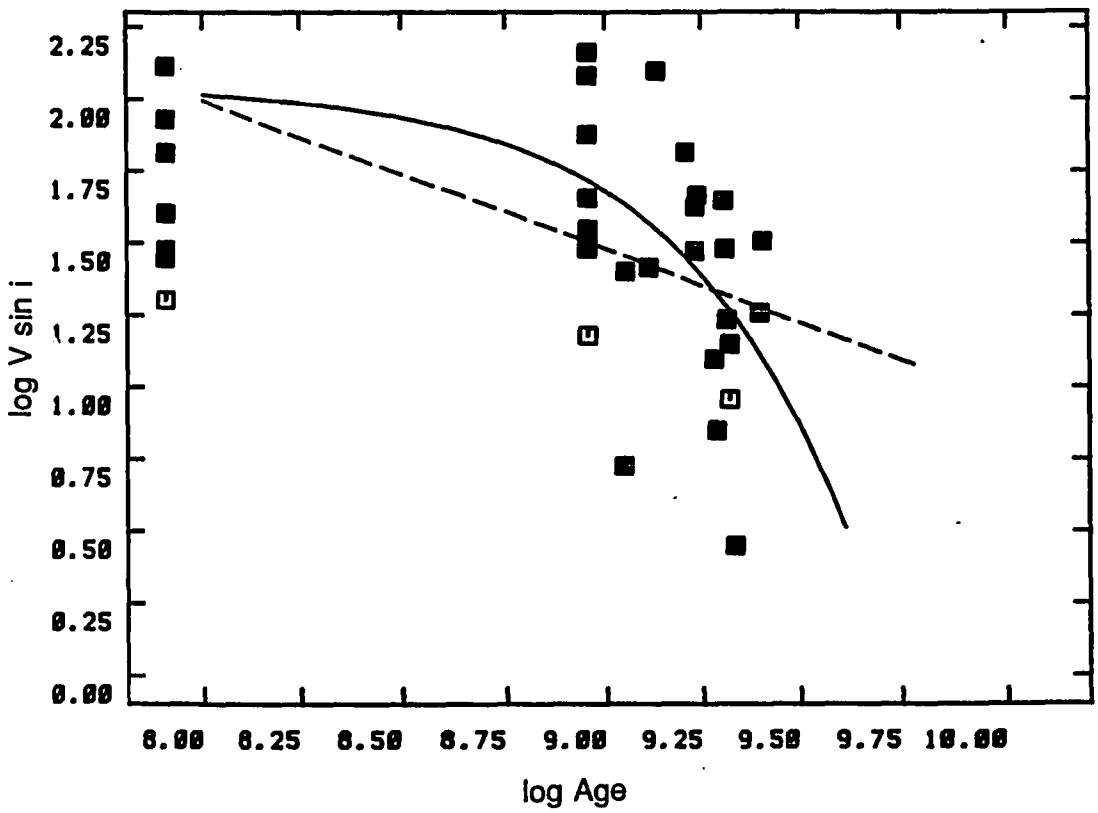

Figure 33. Plot of $\log V \sin i$ against log age for solar composition stars with $M_* \geq 1.325 M_\odot$. Only stars with measured rotations and ages are shown (no upper limits). Stars with $\sigma(V \sin i)/V \sin i < 0.5$ shown with solid symbols. Solid curve is an exponential fit. Dashed line is a power law fit.

Since all of these stars have had temperatures and luminosities estimated using the Strömgren photometric indices, radii can be calculated and values for $\Omega \sin i$ found. Plots of $\Omega \sin i$ versus age are shown in Figures 34 and 35. A least squares analysis shows that the decay of angular velocity is best modeled by an exponential law. In this case the e-folding time for $M_* < 1.325 M_\odot$ was 1.45 Gyr, while that for $M_* \geq 1.325 M_\odot$ was 1.06 Gyr. Note that the decay of $\Omega \sin i$ is faster in the high mass F stars than in the low mass F stars, contrary to what might be expected considering the overall range of $\Omega \sin i$ with spectral type or mass along the main sequence. The initial values of $\Omega \sin i$ (or at least the values at the age of the

Table 11

$V \sin i$ and $\Omega \sin i$–Age Relations

Solar Composition

Relation	Residual	a_0	a_1
	$V \sin i$ vs. age		
	$M_* < 1.325 M_\odot$		
$V \sin i = a_0 e^{-t/a_1}$	10.7	44.5 ± 3.2	1.40 ± 0.06
$V \sin i = a_0 t^{a_1}$	27.4	8.1 ± 0.5	-0.97 ± 0.05
	$M_* \geq 1.325 M_\odot$		
$V \sin i = a_0 e^{-t/a_1}$	30.7	112.7 ± 5.3	1.16 ± 0.08
$V \sin i = a_0 t^{a_1}$	29.7	30.1 ± 1.1	-0.52 ± 0.03
	$\Omega \sin i$ vs. age		
	$M_* < 1.325 M_\odot$		
$\Omega \sin i = a_0 e^{-t/a_1}$	1.36×10^{-5}	$5.75 \pm 0.41 \times 10^{-5}$	1.45 ± 0.05
$\Omega \sin i = a_0 t^{a_1}$	3.36×10^{-5}	$1.12 \pm 0.08 \times 10^{-5}$	-0.93 ± 0.05
	$M_* \geq 1.325 M_\odot$		
$\Omega \sin i = a_0 e^{-t/a_1}$	3.10×10^{-5}	$12.59 \pm 0.59 \times 10^{-5}$	1.06 ± 0.08
$\Omega \sin i = a_0 t^{a_1}$	3.18×10^{-5}	$3.02 \pm 0.14 \times 10^{-5}$	-0.56 ± 0.03

Pleiades) are much higher in the early F stars, however. This indicates that, as has been previously observed by Schatzman (1962) and by Soderblom (1983), the majority of the angular momentum difference observed between early and late F stars is generated during the pre-main-sequence phase, rather than through angular momentum loss on the main sequence.

c. The Dynamo Number and Activity

The most important recent development in the understanding of activity in solar-type stars has been the discovery that the relationship between chromospheric activity and the Rossby number (Noyes 1983, Noyes *et al.* 1984) exists. Durney and Latour (1978) suggest that in order for a solar-type dynamo to exist, the inverse Rossby number (an expression of the relative strengths of Coriolis

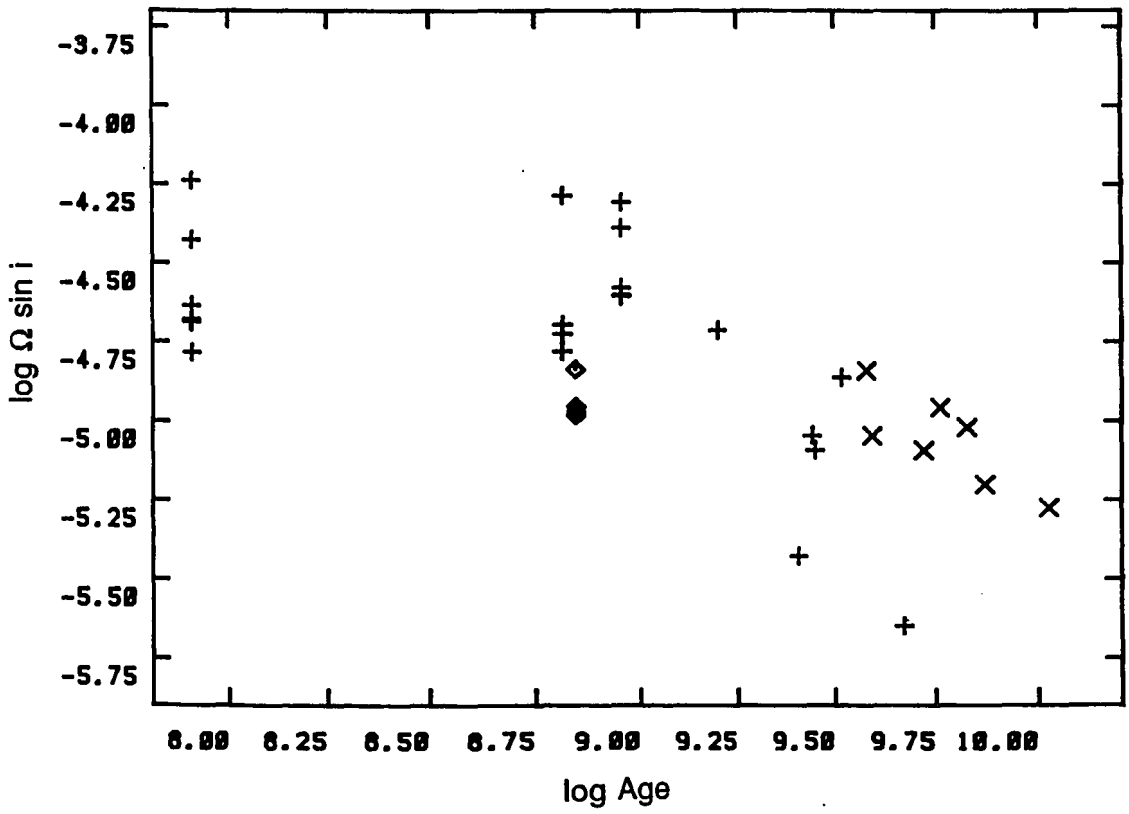

Figure 34. $\log \Omega \sin i$ versus log age for $M_* < 1.325 M_\odot$ for stars with measured ages and velocities (no upper limits are shown). Solar composition stars shown by plus signs, low-metallicity stars by X's, and Hyades stars by diamonds.

forces and those due to differential rotation) should be

$$R_o = \frac{1}{\Omega \tau_C} \leq 1. \qquad 42$$

It has been found that all solar-type and later main-sequence dwarfs appear to meet this requirement, but the best fitting relation, found by Noyes *et al.* (1984) has an exponential dependence of R' on R_o, expressed as P/τ_C, with P being the period of rotation, rather than a linear one (The Noyes *et al.* definition of R'_{HK} is slightly different from that used here; see Chapter III). In addition, the convective turnover time τ_C is only defined in terms of the $B - V$ color of the stars. This deserves some further comment. The component critically dependent

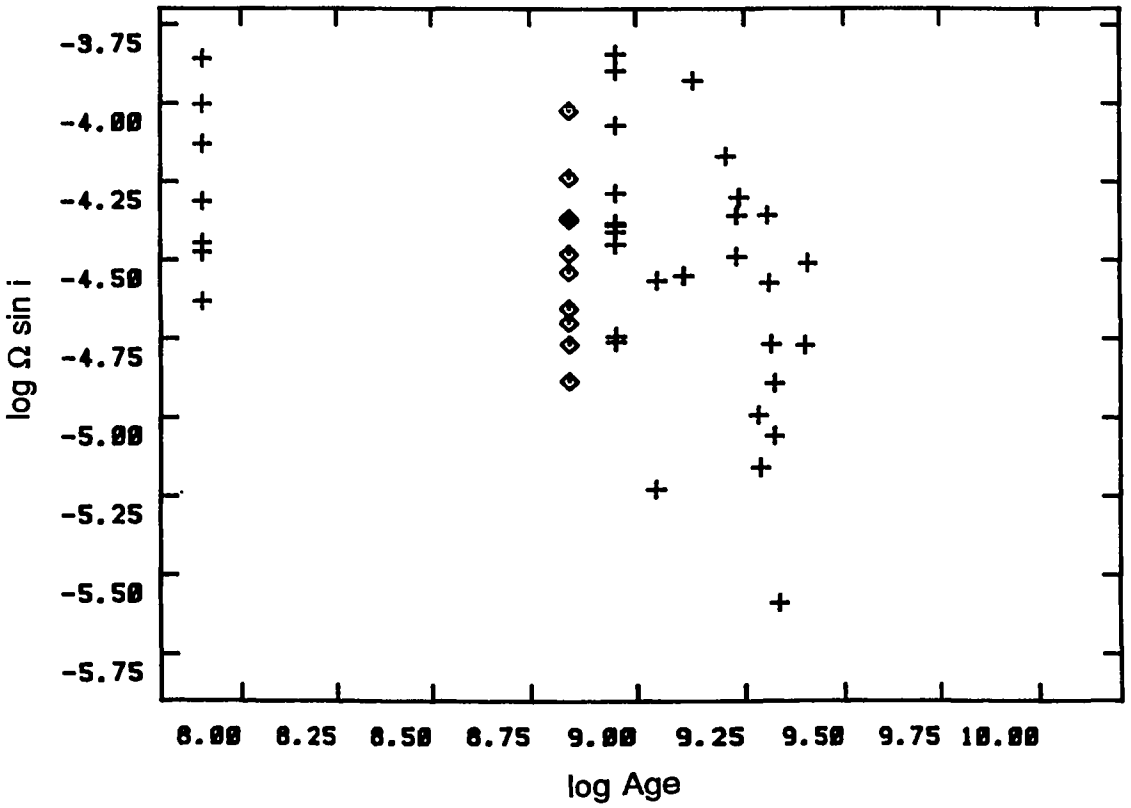

Figure 35. $\log \Omega \sin i$ versus log age for $M_* \geq 1.325 M_\odot$ for stars with measured ages and velocities (no upper limits are shown). Solar composition stars shown by plus signs, Hyads by diamonds.

on the mass of the star in the expression for the Rossby number relation is τ_C, the convective turnover time. In stars somewhat more massive than the Sun the initial value of τ_C is critically dependent on the mass of the star, as well as the convective scale height ratio α (Gilman 1979) and to an apparently lesser extent on the composition (Durney and Latour 1978). As has been shown in Chapter III, the mass of an F dwarf is not determined only by its $B-V$ color—one must also have luminosity information in order to determine the mass and age.

In terms of stellar interiors theory, the turnover time τ_C is the ratio of the average convective velocity u_C over the mixing length $L = \alpha H_P$, where H_P is the

pressure scale height, evaluated at a specific location in the star, typically (Gilman 1980) one half of one mixing length above the base of the convective zone. From hydrostatic equilibrium,

$$H_P = \frac{N_0 K T R^2}{\mu G M} \qquad 43$$

and the average velocity of the convective bubbles is

$$u_C = \frac{1}{2}\left[\frac{GM}{R^2 T}\Delta\nabla T\right]^{\frac{1}{2}} L. \qquad 44$$

Therefore,

$$\tau_C = 2\left[\frac{GM}{R^2 T}\Delta\nabla T\right]^{-\frac{1}{2}} \qquad 45$$

Here $\Delta\nabla T$ (the difference between the local temperature gradient and the adiabatic temperature gradient) must be evaluated numerically using a model atmosphere code.

Current dynamo theory (e.g. Parker 1979) does not yet provide an explicit relation between the angular velocity and the magnetic field responsible for stellar spindown. Roberts (1974) gives a plausibility argument which suggests that the poloidal field B_p, which should be the source for much of the field at large distances from the star, is proportional to the angular velocity Ω. From this conjecture and the definition of the Rossby number Durney and Latour (1978) proposed that the relationship between the surface magnetic field B_0 and angular rotation velocity is given by

$$B = B_0 \Omega \tau_C \qquad 46$$

where B_0 is a constant. Converting Ω into directly observable parameters, we get

$$B = B_0 \frac{V}{R_*} \tau_C \qquad 47$$

Since R_* varies slowly with mass, the relationship between B_0 and $\Omega\tau_C$ should be essentially the same for all late-type main-sequence stars.

Robinson and Durney (1982), using the form of the solar dynamo equations developed by Yoshimura (1975) developed a different parameter for the strength of magnetic dynamos, the dynamo number $N_D = (3/4)(\alpha_0\beta_0)^{\frac{1}{2}}\Omega\tau_C(R_C/L)^{\frac{1}{2}}$ where R_C is the radius of the base of the convective zone, the mixing length L is measured at the base of the convective zone, and the quantity $(3/4)(\alpha_0\beta_0)^{\frac{1}{2}}$ is a constant. This parameter and the assumption that $B_p \propto \Omega$ suggest a relation of the form

$$B = B_0 N_D \qquad 48$$

may be appropriate for magnetic fields (and thus activity) in late-type stars.

Several different published estimates of τ_C for solar composition stars exist. Gilman (1980) has calculated the dependence of τ_C on mass for stars with differing values of α: $\alpha = 1.0$, 2.0, and 3.0. He suggested that best agreement with observations would be found using high values of α ($\alpha \geq 2.0$).

Noyes *et al.* (1984) found that an interpolated curve for $\alpha = 1.9$ from Gilman's results provided the best fit to the Ca II activity level R'_{HK}–$B-V$ relation, particularly when the τ_C–$B-V$ relation was iterated. Noyes *et al.* obtained their initial τ_C–$B-V$ relationship using the mass–color relationship given by Allen (1973), which is not consistent with the VandenBerg models and the recent Böhm-Vitense $B-V$–T_{eff} calibration used here.

The turnover time τ_C also evolves over the main sequence lifetime of a star, as has been shown by Gilliland (1985), and this evolution can have significant effects in F stars. As described by Gilliland, this evolution occurs in essentially two phases. First, as the star evolves from the ZAMS to the main-sequence turnoff, τ_C decreases, with the amount of decrease increasing sharply with the mass of the star. A zero-age 1.25 $M_\odot$ star of solar composition takes ~2.5 Gyr to evolve

to the turnoff point. Over that time its τ_C value decreases by a factor of ~ 2. This is approximately the same decrease as is seen for zero-age stars of the same color. Stars of 1 $M_\odot$, however, show a much smaller decrease. After the main-sequence turnoff point is reached, τ_C increases rapidly, and moves farther away from the ZAMS τ_C–T_{eff} relation. Since the stars in the sample discussed here are all between the ZAMS and the main-sequence turnoff point for their masses and compositions, the actual convective turnover time for a given star should be less than that for a zero-age star of the same mass and composition. The difference between the actual and the ZAMS τ_C should increase with increasing age and mass.

Ruciński and VandenBerg (1986) have recently estimated the turnover time τ_C for main-sequence stars using the new stellar interior models of VandenBerg (1985). These calculations are the most complete set currently available, since not only the zero-age values but also evolved stellar values are found for τ_C. The models were calculated using $\alpha = 1.6$, which is consistent with standard solar models (e.g., Model 1 of Christensen-Dalsgaard 1982) and with the positions of cluster main sequences in the HR diagram (VandenBerg 1983). The evolution of τ_C up to the main sequence turnoff closely follows the values estimated for zero-age stars of the same temperature for all F stars, and is in basic agreement with the results of Gilliland. This fact allows the approximation

$$\tau_C(M_*,\ age,\ T_*) \approx \tau_C(T_{*\ ZAMS}). \qquad 49$$

Ruciński and VandenBerg (1986) also include values of the ratio $C = (R_C/H_P)^{\frac{1}{2}}$, allowing calculation of the dynamo number $N_D = \Omega\tau_C C$ for main sequence stars. This dynamo number is the same as Durney and Robinson's, except for a constant of proportionality $0.59(\alpha_0\beta_0)^{\frac{1}{2}}$.

d. Theory and Observations of the Dynamo Number

Durney and Latour (1978) computed τ_C for model envelopes with three different compositions ($Z = 0.02$, 0.03, and 0.04). The values of $\log \tau_C$ for $Z = 0.03$ are typically 0.4 less than those for $Z = 0.02$. This suggests that differing compositions can cause substantial changes in τ_C. As Durney and Latour suggest, this can most simply be explained by considering the behavior of τ_C in the Sun. If $\tau_C = u_C/L$, and in the Sun $u_C L$ is assumed to be constant, then $u_C/L \propto 1/L^2$. Now $L = \alpha H_P$, where H_P is described by equation (43) and decreases rapidly with height. Since the convective zone in a star of lower metallicity than the Sun will be shallower, L will be smaller than in the Sun and $1/L^2$ will be larger, thus τ_C should be larger in lower metallicity stars than in solar composition stars of the same mass.

It therefore appears advisable to use only stars of very nearly solar composition to compare observed activity–rotation relations with theories assuming solar composition. The effects of differing composition can be investigated later.

The number of solar-composition stars with low activity and known $V \sin i$ in the late-F sample described in section (2) is limited to four stars. Two of these have $V \sin i$ values with large uncertainties ($> 50\%$). In order to increase the sample and the precision I have included stars from Noyes *et al.* (1984) which have rotation periods obtained from measurements of periodic variations in Ca II flux. The ten late F and early G stars with observed rotation periods and $\beta \geq 2.600$ (β obtained from the Hauck and Mermilliod catalog) were combined with the solar composition low mass F stars described above. Angular rotation velocities were obtained from the measured rotation periods and multiplied by $\pi/4$ (the average value of $\sin i$

for a set of randomly oriented stars (Chandrasekhar and Munch 1950)) to match the $\Omega \sin i$ found for the rest of the stars. See Table 12.

Figure 36 shows the dependence of $\log \tau_C$ or $\log \tau_C C$ on β (where β was determined using the ZAMS temperature dependence of the VandenBerg (1983) solar composition models and the calibration discussed in section (2)) for the Ruciński-VandenBerg, Noyes *et al.*, and Gilman $\alpha = 2.0$ determinations. The Gilman τ_C curve for $\alpha = 2.0$ was based on a third degree polynomial fit to the data of Gilman (1980), and a third-degree polynomial was also fit to the Ruciński and VandenBerg (1986) calculation. The T_{eff}–color calibration given in Ruciński and VandenBerg was not used; this calibration (VandenBerg and Bell, 1985) has been shown (VandenBerg 1985) to give colors ~3% too blue for $B - V > 0.4$. The Noyes *et al.* iterated τ_C–$B - V$ relation is also shown (where the β–$B - V$ calibration of Hauck and Magnenat has also been used). Two results are immediately observed: the Ruciński and VandenBerg curve for $\alpha = 1.6$ is very similar to the Gilman curve for $\alpha = 2.0$, while the Noyes *et al.* curve is similar to both Gilman's $\alpha = 2.0$ and the Ruciński-VandenBerg $\alpha = 1.6$ curve for late F stars, but is closer to a theoretical curve for higher for the early and mid-F stars.

Table 13 shows the equations found to obtain the best fits of R'_{HK} to their respective rotation-convection parameters (either $[\Omega \sin i]\tau_C$ or $[\Omega \sin i]\tau_C C$) for the late F stars and the RMS values of the residuals in R'_{HK} in each case. Values of R'_{HK} greater than 5.0×10^{-5} were omitted from the fits. The Noyes *et al.* iterated Rossby number and the Ruciński-VandenBerg dynamo number produced fits of identical quality. As the Ruciński-VandenBerg parameter was found using $\alpha = 1.6$, identical to the stellar interiors models rather than the adjusted value used in the Noyes *et al.* iterated solution, it will be used in this dissertation. The linear

Table 12

Parameters for Stars with Photometric Rotation Periods

Name	HD	S	P_{obs} (days)	β	$B-V_c$	$\log(C_{cf})$	R_{HK}	R_{phot} ($\times 10^{-5}$)	R'_{HK}	$\log(C\tau_C)$	$\Omega\tau_C C$
(1)	(2)	(3)	(4)	(5)	(6)	(7)	(8)	(9)	(10)	(11)	(12)
	16673	0.215	5.7	2.620	0.56	0.162	4.18	2.22	1.95	6.209	20.6
50 Per	25998	0.275	2.6	2.641	0.49	0.232	6.29	2.41	3.88	5.998	27.9
	89744	0.135	12.3	2.641	0.49	0.232	3.09	2.41	0.68	5.998	5.9
	97334	0.320	7.6	2.604	0.62	0.095	5.34	2.09	3.25	6.351	21.5
α Com A	114378	0.240	3.0	2.640	0.50	0.222	5.37	2.40	2.97	6.009	24.7
β Com	114710	0.200	12.4	2.609	0.60	0.118	3.52	2.13	1.38	6.309	11.9
ι Vir	124850	0.208	7.6	2.622	0.55	0.172	4.14	2.24	1.90	6.190	14.8
λ Ser	141004	0.160	18.0	2.608	0.60	0.118	2.81	2.12	0.69	6.317	8.4
	154417	0.275	7.6	2.604	0.62	0.095	4.59	2.09	2.50	6.351	21.5
15 Sge	190406	0.190	13.5	2.615	0.58	0.140	3.51	2.18	1.33	6.255	9.7

NOTES.

Column (3): Mt. Wilson S index values from Noyes *et al.* (1984).

Column (4): Observed rotation period, days (from list of Noyes *et al.*).

Column (5): Strömgren β index from Hauck and Mermilliod (1980).

Column (6): Estimate of $B-V$ color obtained from β using the Hauck and Magnenat (1975) calibration. Used here for consistency.

Column (7): The color correction factor for Ca II flux.

Column (8), (9), and (10): The relative Ca II line core flux, the "photospheric contribution" to the Ca II flux, and the chromospheric Ca II line core flux. The calibrations of Chapter III were used.

Column (11): Ruciński and VandenBerg (1986).

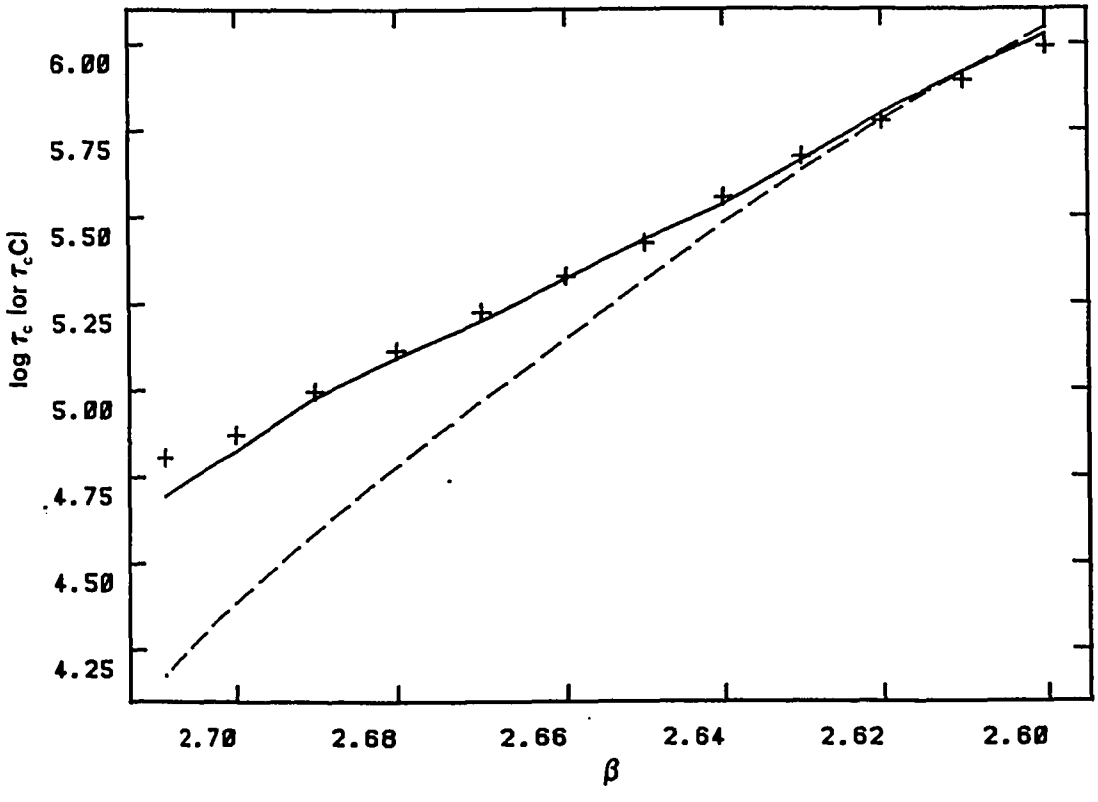

Figure 36. $\log \tau_C$(or $\tau_C C$) versus β. The line represents $\log \tau_C C - 0.45$ (Rucinski and VandenBerg [1986], $\alpha = 1.6$), the crosses $\log \tau_C$ (Noyes *et al.* 1984), the dashed line $\log \tau_C + 0.15$ (Gilman [1979], $\alpha = 2.0$). Note that the $B - V$–T_{eff} calibration given in Rucinski and VandenBerg (1986) was not used—it has been shown to be too blue (VandenBerg 1985).

relation between R'_{HK} and the Ruciński-VandenBerg parameter is consistent with dynamo theory.

Figure 37 shows R'_{HK} versus the dynamo number N_D for the low mass F stars of solar composition. The saturation above $N_D = 30$ is evident. Figure 38 considers only those low-mass F stars with $N_D < 30$. A clearly linear relationship is seen, with a linear correlation coefficient of 0.912 for 23 stars. The relation between activity and N_D in early F stars is shown in Figure 39. The rotation

Table 13

Least-Squares Fits for Rotation-Convection Parameters

$$R'_{HK} = a_0 + a_1 x$$

x	a_0	a_1	Residual
$M_* < 1.325 M_\odot$, $R'_{HK} < 5 \times 10^{-5}$			
$\Omega\tau_C C$ (RVdB)	-8.90×10^{-7}	1.83×10^{-6}	4.47×10^{-6}
$\Omega\tau_C$ (RVdB)	8.91×10^{-8}	6.07×10^{-6}	5.68×10^{-6}
$\Omega\tau_C$ (Noyes *et al.*)	-1.89×10^{-6}	5.18×10^{-6}	4.40×10^{-6}
$\Omega\tau_C$ (Gilman $\alpha = 2.0$)	2.65×10^{-6}	6.71×10^{-6}	6.94×10^{-6}
$M_* \geq 1.325 M_\odot$			
$\Omega\tau_C C$ (RVdB)	1.746×10^{-5}	6.7×10^{-7}	4.91×10^{-6}

rates of most of these objects are higher than those seen in the late F stars, but a few (those closest to the main-sequence turnoff) have low $V \sin i$ values. One feature evident from Figure 39 is that these objects do not have low activity levels. There appears to be a minimum activity level in these objects, independent of N_D.

A excess of early F stars with high equatorial rotation rates will have low apparent $V \sin i$ values because their rotation axes will be close to the line of sight (Chandrasekhar and Munch 1950). If two apparently pole-on stars in Figure 39 are omitted, an apparently linear relation for R'_{HK} with N_D can be found. For 19 stars the linear correlation coefficient of this relation is 0.873. For both early and late F stars the probability that R'_{HK} and N_D are uncorrelated is less than 0.001. The dependence of R'_{HK} on N_D, though weaker than in the late F stars, still appears to be present for the solar composition early F stars.

The low metallicity stars show a number of peculiarities in comparison to the solar-composition objects. The low metallicity stars show low activity for their Ω values, that is, their R'_{HK} values lie *below* the linear fit in Figure 38. At the same time, their $V \sin i$ values decay less rapidly than those for solar-composition stars,

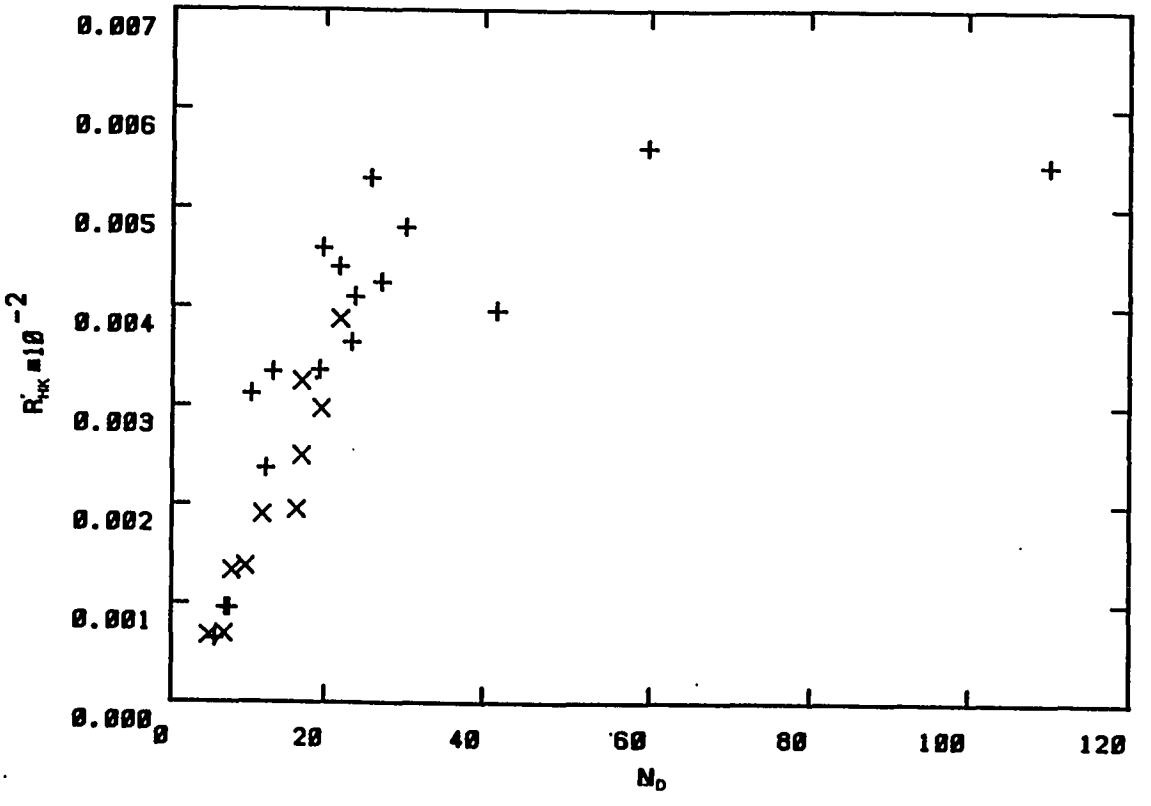

Figure 37. Ca II relative surface flux R'_{HK} versus dynamo number N_D for solar composition stars with $M_* < 1.325 M_\odot$. The saturation observed for $N_D > 30$ is evident.

as shown in Figure 30. One might at first suppose this to be due to a different $\tau_C C$–β relation for lower metallicities. Indeed, as is shown by Ruciński and VandenBerg, the $\tau_C C$–$B-V$ relation *is* different for metallicities substantially lower than solar ($\Delta\tau_C C \approx 0.05$ for $Z = 0.0017$ compared to solar $Z = 0.0169$). This is largely due to the difference in blanketing caused by the change in metallicity. However, the β–T_{eff} calibration should be nearly independent of metallicity (Crawford 1975), and so the $\tau_C C$–β relation for the low metallicity stars discussed here (which have metal abundances around one-half solar) should be little different from the solar one. The same $\tau_C C$–β relation used for the solar composition stars was used for

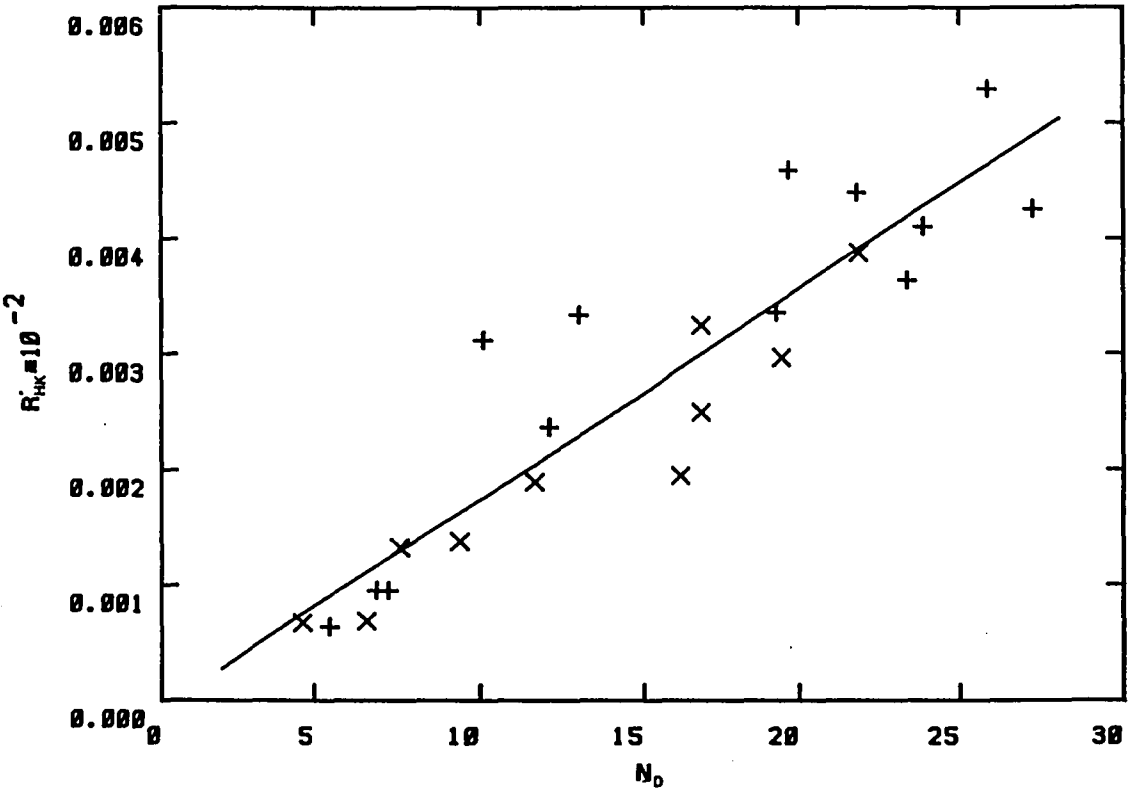

Figure 38. Ca II relative surface flux R'_{HK} versus dynamo number N_D for solar composition stars with $M_* < 1.325 M_\odot$ and $N_D < 30$. Stars from the sample used in Chapter V indicated by +, stars from Noyes *et al.* (1984) with $\beta \geq 2.60$ indicated by X. There is a correlation with $R = 0.91$ for 23 points.

the low metallicity stars. Clearly more data is needed to provide an adequate explanation for the difference between the low-metallicity and solar composition stars in the R'_{HK}–N_D diagram.

Several authors have extended the work of Noyes *et al.* to lines sampling the transition regions of both solar-type and hotter stars. Walter (1983) has collected X-ray fluxes for a sample of F stars. He found a strong relation between X-ray flux and rotational velocity for stars with $B - V > 0.52$, but only a weak relation for stars with $0.46 < B - V < 0.52$ and none for stars earlier than that. His Figure 1

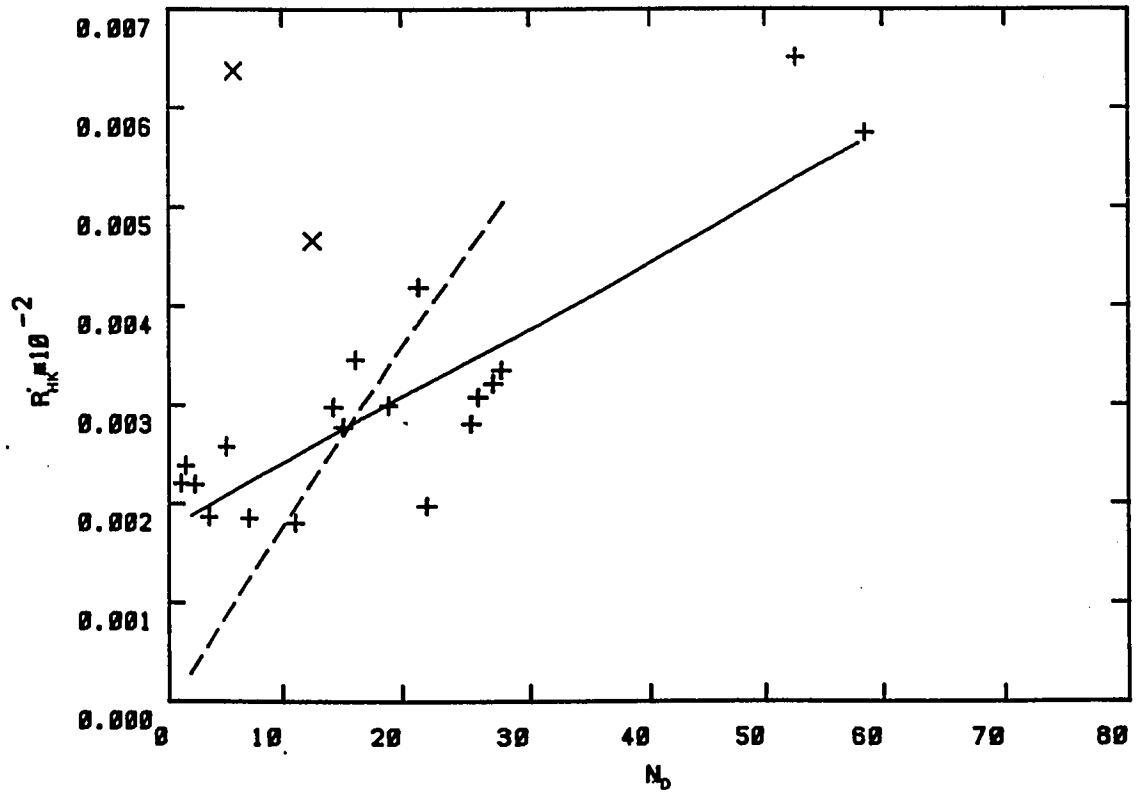

Figure 39. Ca II relative surface flux versus the dynamo number N_D for solar composition stars with $M_* \geq 1.325 M_\odot$. If the two likely pole-on stars indicated by X are excluded, there is a correlation with $R = 0.87$ for 19 points. The fit for $M_* < 1.325 M_\odot$ is shown as a dashed line. Note that no stars with $R'_{HK} < 1.8 \times 10^{-5}$ are oberved, however. This suggests an additional chromospheric heating mechanism may be involved.

does show, however, that in the $0.40 < B - V < 0.46$ group the two young cluster members have higher X-ray fluxes than the other stars. This figure, however, is contradicted by the text, which says there are no cluster members in this group. The data in the figure suggest that there is a lower limit on the X-ray flux for stars in this color range which is reached at a young age.

Walter and Linsky (1985) show a relation between emission activity in the C II and C IV transition region lines and rotation for stars with $0.42 < B - V < 0.52$

and no clear relation for stars with $B - V < 0.40$. This does not contradict the Ca II results presented here, since in the high mass solar composition sample of 19 stars only four have $B - V < 0.40$.

What all of the activity indicators agree on is that the early F stars show a narrow range of activity compared with the late F and solar type stars. Figures 23 and 24, discussed in Chapter III, as well as the X-ray data of Walter (1983), indicate that above $T_{eff} = 6600$K there appears rather suddenly as temperature increases a minimum activity level, independent of rotation. (Note the minimum level at $\sim 1.8 \times 10^{-5}$ seen in Figure 39 as well.) Several authors, including Wolff, Boesgaard, and Simon (1986) and Walter and Linsky (1985) have suggested pure acoustic heating as the cause. However, I have shown earlier that acoustic heating, at least according to the model of Renzini *et al.* (1977), when allowed to account for the non-radiative heating in early F stars, produces activity levels in older late F stars much larger than observed. The range in T_{eff} over which this "floor" activity level becomes important is extremely narrow, ~150 K or less. It is not clear what mechanism could be responsible for this additional non-radiative, and apparently non-rotationally generated heating.

In the case of solar type stars (F7 - G2V) Simon, Herbig, and Boesgaard (1985) have made an extensive series of observations of ultraviolet emission lines using *IUE* and ages based on the Duncan (1984) binary star sample. Their results show that similar relationships between activity indicators and the Rossby number to that found for Ca II H and K by Noyes *et al.* can be found for the low chromospheric lines of Mg II h and k, O I 1304Å, C I 1657Å, and Si II 1810Å. All of these lines are shown to behave as do the Ca II lines. In addition the transition region lines of N V 1240Å, C II 1335Å, Si IV 1400Å, C IV 1549Å, and He II 1640Å

were observed. These lines show a steeper dependence of emission on Rossby number than the lower chromospheric lines, suggesting that the decline in activity in solar-type transition regions is more strongly age-dependent than that in the low chromosphere. The *e*-folding time for Ca II flux was 2.7 Gyr, while that for the transition region lines was 1.4 Gyr. The age dependence of Ca II flux found by Simon, Herbig, and Boesgaard is equivalent to that found in Chapter III for F stars in general if metallicity effects are ignored. The shorter *e*-folding time for the outer-atmospheric lines suggests a possible explanation for the lack of dependence of activity on $V \sin i$ seen in the X-ray and ultraviolet activity indicators. If in early F stars there exist both a non-radiative, non-rotationally driven activity mechanism (and thus a minimum activity level independent of age and rotation) as well as a solar-type rotationally-driven activity mechanism, and the decay time for the dynamo in the outer atmosphere is shorter than for the low chromosphere as it is for solar-type stars, then one would expect the "minimum" flux level to be reached sooner in the X-ray and UV indices than it is in the chromospheric Ca II lines. Thus the effects of the solar-type generation mechanism would perhaps be observable longer there than in the corona and transition region.

4. Discussion

An approach to understanding the angular momentum history of F dwarfs can begin by examining the current results obtained for solar-type stars and scaling them to fit the F stars. The root cause of the loss of angular momentum in main-sequence solar-type stars is the transport of angular momentum away from the star by the stellar wind. Results from spherically symmetric solar wind models (Weber and Davis 1967) indicate that the torque applied to the Sun by a steady spherically

symmetric solar wind in a *radial* magnetic field is equivalent to assuming that the wind corotates with the Sun out to the Alfven radius (where the speed of magnetic disturbances equals the speed of the wind) and then flows radially away from the Sun. The velocity of the wind at the Alfven radius is nearly equal to the velocity at a very large radial distance, and can be considered a constant. Therefore, the angular momentum loss can be considered to be equivalent to that caused by a constant stellar wind flux through a corotating spherical shell at the Alfven radius, or

$$\frac{dJ}{dt} = \frac{2}{3}\Omega r_A^2 \frac{dM}{dt} \qquad 50$$

or,

$$\frac{dJ}{dt} = -\frac{2}{3}\Omega \frac{B^2}{V_A}, \qquad 51$$

where A refers to the Alfven radius r_A, where the wind speed equals the Alfven velocity $V_A = B_A/(4\pi\rho)^{\frac{1}{2}}$. If the magnetic field $B \propto \Omega$, as has been shown in section (3) to be true for low values of N_D, then it is easily shown (Durney 1976) that $\Omega \propto t^{-\frac{1}{2}}$. The previous section has shown that for late F stars of solar composition, the change of Ω with time for young stars at least is better matched by an exponential decay.

One way to adjust the theory of spindown for the F stars is by changing the geometrical configuration of the stellar magnetic field. Roxburgh (1982) examined several magnetic field configurations and the resulting equations for the angular momentum loss rate. Maintaining the assumption of corotation of the field and wind out to the Alfven radius and radial streaming beyond that point, he showed that the loss rate is given by

$$\frac{dJ}{dt} = \frac{8\pi}{3}\rho_0 V_0 \Omega r_A^{2-n} \qquad 52$$

where the magnetic field is described by $B^2 = B_0^2/r^{2n+4}$. For a radial field $n = 0$, dipole $n = 1$, quadrupole $n = 2$, etc.

The magnetic field at the Alfven radius is then given by

$$B_A = B_0/r^{n+2}, \tag{53}$$

where B_0 is the mean surface field. It can be shown that in general, $dJ/dt \propto B_0^a$, where $a = (2-n)/(2+n)$.

Gill and Roxburgh (1984) have shown, therefore that if the magnetic field of the star is quadrupole, then assuming the density at the base of the corona ρ_0 and the sound speed V_s remain constant with varying mass, the angular momentum loss is

$$\frac{d(I\Omega)}{dt} = -Kh\Omega, \tag{54}$$

where h ($h \sim 0.1$) is a nearly constant parameter depending on magnetic field strength and $K = (8\pi/3)\rho_0 V_s R^4$. That is, $d(I\Omega)/dt$ is independent of B_0. Then,

$$\Omega = \Omega_0 e^{-(Kh/I)t} \tag{55}$$

is the decay equation for rotation. This is consistent with observations for both the early and late F stars. Note that if ρ_0, V_s, and h are considered constant, and the structure of the star does not change radically over the mass range considered here, then the ratio $Kh/I \propto MR^2/R^4$. But $g = GM/R^2$, so that implies $Kh/I \propto 1/g$. Since the e-folding time is given by I/Kh, that means $t_e \propto g$. Since g is essentially constant along the main sequence, so should be t_e.

It is interesting to note that if R_* is given by the ZAMS of VandenBerg (1983) for solar composition, then the ratio of $V \sin i$ e-folding times $t_{e(M_*=1.4)}$ to $t_{e(M_*=1.2)}$ is given by $t_{e1}/t_{e2} = R_2^2 M_1/R_1^2 M_2 = 0.79$. The observed ratio of

e-folding times for the solar composition stars is $t_{e(M\geq 1.325M_\odot)}/t_{e(M<1.325M_\odot)} = 0.73$. The agreement lends confidence in the theory.

It was shown in section (3) that for late F stars of near solar composition and for $R'_{HK} < 5.0 \times 10^{-5}$,

$$R'_{HK} = A\Omega\tau_C C, \tag{56}$$

where A includes a factor of $\pi/4$, to account for the average effect of inclination, while R'_{HK} appears to saturate at a level between 5.0 and 6.0×10^{-5} for $N_D = (\pi/4)\Omega\tau_C C \gtrsim 30$ and does not increase further. Therefore, one would expect that the age dependence of R'_{HK} would be

$$R'_{HK} = A\tau_C C\Omega_0 e^{\frac{-Kh}{I}t}, \tag{57}$$

but that $R'_{HK} \gtrsim 5.0 \times 10^{-5}$ would not occur due to saturation. In other words at young ages on the main sequence R'_{HK} should be essentially constant. Of course, T Tauri stars (Simon, Herbig, and Boesgaard 1985) show activity levels (in C IV and other UV lines) roughly 100× that of the Pleiades stars. One might suppose another change in field geometry to account for this.

On the other hand, if at some later time the field changes to a dipole configuration, as suggested by Gill and Roxburgh and Roxburgh (1983), then

$$\frac{d(I\Omega)}{dt} = -F\Omega hK\left(\frac{B}{B_c}\right)^{2/3} \tag{58}$$

If the expression above is substituted for B (assuming $B \propto R'_{HK}$) then it is easily shown that

$$\frac{1}{\Omega^{2/3}} = \frac{1}{\Omega_c^{2/3}} + \frac{2FKh}{3I}(t - t_c), \tag{59}$$

where t_c is the time at which the transition occurs. Then, if $R'_{HK} = A\Omega\tau_C C$,

$$R'_{HK} = A\tau_C C \left(\frac{1}{\Omega_0^{2/3}} e^{\frac{2}{3}\frac{Kh}{I}t_c} + \frac{2FKh}{3I}(t - t_c) \right)^{-\frac{3}{2}} \qquad 60$$

Basically, for large values of t, R'_{HK} and Ω should be proportional to $t^{-\frac{3}{2}}$.

The observational results of Chapter III and of section (3) above are inconclusive concerning older late F stars of solar composition. There are insufficient data in both R'_{HK} and rotational velocity to determine whether any changes in the decay of activity or rotation occur below the Vaughan-Preston gap in the case of activity, although the $V \sin i$–age and R'_{HK}–age behavior for solar-composition stars is consistent with such a dependence.

The early F stars clearly show evidence for a decline of rotation velocity with age (see Figures 31, 33, and 35) with an e-folding time of 1.1 Gyr. The activity–age dependence is much weaker (see Figure 22), but an exponential decay appears to be likely to be present. This result is supported by the dependence of R'_{HK} on N_D observed in section (3). The lower limit of Ca II activity in the early F stars, however, appears to be independent of age or rotation rate. It should be remembered, also, that spindown will occur regardless of the source of the magnetic field so long as one is present.

It is interesting to note that the beginning of this additional non-rotational chromospheric heating mechanism occurs at $T_{eff} \sim 6600K$, just where the dip in Li abundance observed by Boesgaard and Tripicco (1986*a*, *b*, 1987) reaches its maximum size. This dip is explained by Michaud (1986) as the result of an imbalance between radiative pressure and gravitational settling at the base of the

thin convective zones in these objects. The thickness of the convective zone is rapidly changing in the early F stars (the mass contained in the zone decrease by a factor of roughly 100 between $T_{eff} = 6000$ and 6500K), and one would expect that eventually there would be too small a convective zone to support a magnetic dynamo. Golub *et al.* (1981) and Gilman and DeLuca (1985) suggest that the dynamo magnetic field is actually generated in the overshoot layer below the boundary between the convective and radiative zones, and that the convective zone actually tends to disrupt the magnetic fields as they rise to the stellar surface. A very thin convective zone may have a smaller effect on the fields generated in the overshoot region which could strengthen whatever dynamo is present. However, it appears that such fields, and the activity they generate ought still to depend on the stellar dynamo number, and thus on the rotation rate. The rapid decrease in the depth of the convective zone explains why the significance of the solar-type activity is diminished for the early F stars, but does not explain the source of the non-rotational activity noted above.

5. Conclusions

F stars of all temperatures show evidence in the Ca II H and K lines of the existence of stellar chromospheres. The F stars of solar composition show two different types of Ca II H and K activity depending on their mass or temperature. Stars with $M_*1.325 < M_\odot$ or $T_{eff} < 6600$K show activity similar to that of later-type stars. This activity depends mainly on the rotation rate of the star, and appears to be driven by a stellar dynamo. The early F stars of solar composition, those with $M_* \geq 1.325 M_\odot$ or $T_{eff} > 6600$K, have two major means of non-radiative heating in their atmospheres. One is rotationally driven, appears similar

to that found in solar-type stars, and is probably due to the presence of a magnetic dynamo. The dependence of activity upon rotation is weakened in the in the early F stars (those with solar composition and $M_* > 1.325 M_\odot$) but still appears to be present. In addition, another heating mechanism, independent of rotation, is also present. In the earliest F stars, not well sampled here but discussed by Walter (1983) and Walter and Linsky (1985), this non-rotationally driven component dominates and all such stars have a narrow range of activity, even though they still show a wide range of rotation velocities. The transition regions of F stars, as indicated by the C IV observations of Wolff, Boesgaard, and Simon (1986) and the data of Walter and Linsky (1985), indicate that the transition regions of both early and late F stars have T_{eff} dependence similar to the seen for the chromosphere in Ca II.

The age dependence of Ca II activity in the high mass F stars is similar to that of the low mass stars. The activity level measured by R'_{HK} declines only slightly in stars with ages less than $\sim$1 Gyr. but more rapidly in the older stars. The rotational velocity shows a similar increasing rate of decline with age. The range of ages in the high mass stars is of course limited by the short main-sequence lifetime in these stars. However, the decline in $V \sin i$ with age is greater than that observed in Ca II activity. Although relatively low $V \sin i$ values ($\sim$5 km s^{-1}) are attained in some older early F stars, the activity levels do not drop correspondingly. This also indicates the presence of another chromospheric heating mechanism in these objects.

The existence of the low activity mid-F stars argues against the dominance of acoustic heating as the dominant source for activity in the early F stars. A much

steeper dependence of flux on temperature than predicted by theory for acoustic heating is required for the additional heating mechanism seen in these objects.

The results here favor the dynamo number of Durney and Robinson over the Rossby number of Noyes *et al.* as a stellar activity parameter, as was found by Gilliland (1985), but not by a great deal. The relation between R'_{HK} and N_D is linear, implying that $B \propto \Omega$, as proposed by Roberts (1974). The slope is shallower for the early F stars than for the late F stars. Above $N_D \sim 30$ CaII activity in the late F stars of solar composition saturates. The lack of early F stars with $R'_{HK} < 1.8 \times 10^{-5}$, even though several stars in this temperature range were observed with low $V \sin i$ values, suggests that in these objects part of the chromospheric heating is independent of rotation. On the other hand Chapter III showed that this non-rotational heat source does not behave like pure acoustic flux as currently understood.

The exponential dependence of rotation on age seen in both the young low mass solar composition stars and in the high mass solar composition stars suggests that the angular momentum loss in these stars is independent of the magnetic field, and that in both young low mass F stars and all high mass F stars the large-scale magnetic field structure is perhaps quadrupole in form, rather than a dipole as in the solar case.

CHAPTER VI
SUMMARY

The early F stars have been somewhat neglected in previous studies of chromospheric activity. The Mt. Wilson activity survey, arguably the most important source of data on chromospheric activity nearly ignores the early F stars entirely because their Ca II flux levels, when not corrected for the increased photospheric temperature, appear to be very small when compared to later type stars. Adequate corrections, such as described here, as well as ultraviolet line fluxes from spacecraft (notably *IUE*) show that the level of chromospheric activity in F stars of all types (considered as chromospheric line flux / total stellar flux) is comparable to that observed in later type stars. This study has served to extend ideas of the relation of activity, rotation, and age developed in solar and later type stars to Ca II activity in these "warm" (Walter 1983) stars.

Observing Ca II chromospheric activity in F stars brings both benefits and additional problems in comparison to later type stars. A very significant benefit is the possibility of independent age estimates for individual stars based on Strömgren photometric indices and stellar isochrone fitting. F stars evolve rapidly enough that isochrones spanning the range between zero and several billion years can be distinguished using this approach. This allows the dependence of activity and rotation on age to be determined, at least for stars of roughly solar composition over an age range of several billion years. Some problems include the large correction required to remove the filling in of the Ca II *H* and *K* line cores at the higher photospheric temperatures found in these objects, and the lack of observed rotational modulation of the chromospheric lines. The first requires an extension

of the photospheric corrections of Middelkoop (1982), the second requires high precision $V \sin i$ measurements. The F stars generally rotate faster than later types, so that it is feasible to use additional $V \sin i$ measurements from the literature.

Over the course of this study it has been possible to adopt the recent stellar models of VandenBerg (1983) with improvements in the input physics. In addition, newer T_{eff}–color calibrations and [Fe/H]–color calibrations have allowed improved consistency between theory and observation.

Exponential decay in both Ca II activity and rotation velocity with age was observed in solar composition F stars with $M_* < 1.325 M_\odot$. The estimated angular velocity decays with an e-folding time of 1.45 Gyr, while the decay of the Ca II relative surface flux R'_{HK} has an e-folding time of 2.04 Gyr. The relation between R'_{HK} and Ω was found to be linear in the Durney-Robinson dynamo number N_D $(= \Omega \tau_C (R_C/H_P)^{\frac{1}{2}})$ up to a level of $\sim R'_{HK} = 5.0 \times 10^{-5}$. Above this activity level, corresponding to $N_D \approx 30$, activity appears to saturate. Since this level is exceeded in young late F stars, it is not surprising that the e-folding time for activity is longer that that for rotation.

The early F stars of solar composition with $M_* \geq 1.325 M_\odot$ (corresponding to $T_{eff} \geq 6600$ K) appear to show similar decay of activity and rotation with age. These stars evolve rapidly enough, however, that extremely low rotation rates (~ 2 km s^{-1}) are not reached before the stars turn onto the subgiant branch of the HR diagram. The decay of rotation with age also follows an exponential law, with an e-folding time of 1.06 Gyr, faster than the late F solar composition stars. The relation between activity and rotation is weaker than in the late F solar composition stars, but still appears to be present. In addition to the general linear relationship (which does not appear to show saturation as observed in the

late F solar composition stars) there also appears to be a "floor" activity level at $\sim 1.8 \times 10^{-5}$ which is not observed in the late F stars.

Chapter III showed that this "floor" does not correspond to chromospheric heating by pure acoustic action, as modeled by Renzini *et al.* (1977). The essential problem is that if the early F star chromospheres are dominated by acoustic heating, then the temperature dependence of acoustic flux (as determined by theory) requires that older late F stars have higher levels of chromospheric activity than actually observed. Dynamo action still appears to be a major component of chromospheric heating in early F star chromospheres.

The low mass, low metallicity ($-0.30 \lesssim$ [Fe/H] ≤ -0.12) F stars do not fit in with this picture. These stars appear bluer than solar composition stars of similar mass, and therefore the coolest in the current sample are of lower mass than the coolest solar composition stars. These stars tend to have higher $V \sin i$ than solar composition stars of similar age, and somewhat higher activity levels as well. They do not, however, fall on the same activity–N_D line as the solar type stars, and show less activity than solar composition stars of similar N_D. This problem can perhaps be solved using Li ages for cooler solar composition stars. Chapter II shows that Li and photometric ages are comparable for these objects, given similar models and temperature calibrations.

The exponential dependence of $V \sin i$ on age for both low and high mass F stars suggests that the Gill-Roxburgh theory of stellar dynamos may be correct. This theory implies a quadrupole field structure in young F stars of all masses, perhaps changing to a different configuration in old stars.

The results from this work suggest the following conclusions about stellar activity in F stars:

(1) Chromospheric activity as measured by the Ca II line in late F stars is generally similar to that observed for solar-type stars, as expected. The activity–age relation and rotational velocity–age relation are both exponential in form. The activity decays more slowly than the rotational velocity, at least for young late F stars.

(2) The difference in the rates of decay of activity and rotation in late F stars appear to be due to a change in the dependence of relative Ca II chromospheric surface flux on rotation and convection velocities. At large values of N_D the already high activity level increases only slightly with large increases of N_D.

(3) Essentially all early F stars (those with $M_* \geq 1.325 M_\odot$) show high relative Ca II flux, even though some have low rotational velocities. However, the rotational velocity shows a decay similar to that seen in the late F stars. The high initial velocity in these stars along with their short main-sequence lifetimes prevent the very low rotation velocities seen in later-type stars from being commonplace among the early F stars as well.

(4) Despite the above result, when the relative Ca II surface flux is plotted against N_D, a relationship could be observed, although it is weaker than in the late F stars. Directly comparing activity and rotation rate, without considering the convective turnover time, is much less likely to show a relation due to the wide range of turnover time present in these objects. It is possible, however, that an additional non-magnetic heating mechanism is present, since even the

lowest N_D values showed fairly strong Ca II activity. This heating mechanism does not have the temperature dependence expected for acoustic heating.

It is thus apparent that the early F stars are showing some interesting departures from solar-type magnetic activity. Further progress, however, requires that the large uncertainties present in the types of chromospheric activity and age measurements used here be reduced. Probably the greatest improvement would be made by using chromospheric activity indicators with less contamination from the photosphere. As the He D_3 equivalent width measurements have relatively large uncertainties, probably the best alternative are the ultraviolet transition region lines, which are comparatively free of photospheric effects. Reaching the older open clusters, which would provide more reliable age estimates, will require the Hubble Space Telescope.

REFERENCES

Allen, C. W. 1973, *Astrophysical Quantities* (3 ed., London: Athlone).

Ayres, T. R. 1975, *Ap. J.*, **201**, 799.

Ayres, T. R., Linsky, J. L., and Shine, R. A. 1974, *Ap. J.*, **192**, 93.

Baliunas, S. L. 1985, in *Cool Stars, Stellar Systems, and the Sun*, ed. M. Zeilik and D. M. Gibson (Berlin: Springer) p. 3.

Baliunas, S. L., Vaughan, A. H., Hartmann, L., Middelkoop, F., Mihalas, D., Noyes, R. W., Preston, G. W., Frazer, J., and Lanning, H. 1983, *Ap. J.*, **275**, 752.

Baliunas, S. L. and Vaughan, A. H. 1985, *Ann. Rev. Astr. Ap.*, **23**, 379.

Baliunas, S. L., Vaughan, A. H., Hartmann, L., Middelkoop, F., Mihalas, D., Noyes, R. W., Preston, G. W., Frazer, J., and Lanning, H. 1983, *Ap. J.*, **275**, 752.

Baranne, A., Mayor, M., and Poncet J. L. 1979, *Vistas in Astronomy*, **23**, 279.

Barnes, T. G. and Evans, D. D. 1976, *M.N.R.A.S.*, **174**, 489.

Barry, D. C., Cromwell, R. H., Hege, K., and Schoolman, S. A. 1981, *Ap. J.*, **247**, 210.

Barry, D. C., Hege, K., and Cromwell, R. H. 1984, *Ap. J. (Letters)*, **277**, L65.

Benz, W. and Mayor, M. 1981,*Astr. Ap.*, **93**, 235.

Benz, W. Mayor, M., and Mermilliod, J. C. 1984, *Astr. Ap.*, **138**, 93.

Bessell, M. S. 1979, *Pub. A.S.P.*, **91**, 589.

Boesgaard, A. M. 1976, *Ap. J.*, **210**, 466.

Boesgaard, A. M. and Tripicco, M. J. 1986*a*, *Ap. J. (Letters)*, **302**, L49.

Boesgaard, A. M. and Tripicco, M. J. 1986*b*, *Ap. J.*, **303**, 724.

Boesgaard, A. M. and Tripicco, M. J. 1987, *Ap. J.*, **313**, 389.

Böhm-Vitense, E. 1981, *Ann. Rev. Astr. Ap.*, **19**, 295.

Böhm-Vitense, E. and Dettman, T. 1980, *Ap. J.*, **236**, 560.

Brault, J. W. and White, O. R. 1971, *Astr. Ap.*, **13**, 169.

Carroll, J. A. 1933, *M.N.R.A.S.*, **93**, 478.

Chandrasekhar S. and Munch G. 1950, *Ap. J.*, **111**, 142.

Christensen-Dalsgaard, J. 1982, *M.N.R.A.S.*, **199**, 735.

Ciardullo, R. B. and Demarque, P. 1977, *Trans. Yale Univ. Obs.* **33**.

Ciardullo, R. B. and Demarque, P. 1979, *Dudley Obs. Report* **14**, 317.

Collins, G. W. and Sonneborn, G. H. 1977, *Astr. Ap. Suppl.*, **34**, 41.

Crawford, D. L. 1975, *A.J.*, **80**, 955.

Crawford, D. L. and Barnes, J. V. 1969 *A.J.*, **74**, 407.

Crawford, D. L., and Barnes, J. V. 1970, *A.J.*, **75**, 946.

Crawford, D. L., and Perry, C. L. 1976, *Pub. A.S.P.*, **88**,454.

Danks, A. C. and Lambert, D. L. 1985, *Astr. Ap.*, **148**, 293.

Danziger, I. J. and Faber, S. M. 1972, *Astr. Ap.*, **18**, 428.

Duncan, D. K. 1981, *Ap. J.*, **248**, 651.

Duncan, D. K. 1983, *Ap. J.*, **271**, 663.

Duncan, D. K. 1983, private communication.

Duncan, D. K. 1984, *A.J.*, **89**, 515.

Duncan, D. K. 1985, private communication.

Duncan, D. K. and Jones, B. F. 1983, *Ap. J.*, **271**, 663.

Duncan, D. K., Baliunas, S. L., Noyes, R. W., Vaughan, A. H., Frazer, J., and Lanning, H. H. 1984, *Pub. A.S.P.*, **96**, 707.

Durney, B. R. and Latour, J. 1978, *Geophys. Astrophys. Fluid Dyn.* **9**, 241.

Durney, B. R., Mihalas, D., and Robinson, R. D. 1982, *Pub. A.S.P.*, **93**, 537.

Durney, B. R. and Robinson, R. D. 1982, *Ap. J.*, **253**, 290.

Feigelson, E. D. and Nelson, P. I. 1985, *Ap. J.*, **293**, 192.

Giampapa, M. S. and Rosner, R. 1984, *Ap. J. (Letters)*, **286**, L19.

Gill, R. S. and Roxburgh, I. W. 1984, in *Space Research Prospects in Stellar Activity and Variability*, ed. A. Mangeney and F. Praderie (Paris: Meudon Obs.) p. 335.

Gilman, P. A. 1979, in *Stellar Turbulence*, (I.A.U. Colloq. #51), ed. D. F. Gray and J. L. Linsky (Berlin: Springer) p. 19.

Gilman, P. A. and DeLuca, E. E. 1985, in *Cool Stars, Stellar Systems,and the Sun*, ed. M. Zeilik and D. M. Gibson (Berlin: Springer) p. 163.

Gliese, W. 1969, *Veröffentlichungen des Astronomischen Rechen-Instituts Heidelberg* No. 22.

Golub, L., Rosner, R., Vaiana, G. S., and Weiss, N. O. 1981, *Ap. J.*, **243**, 309.

Gray, D. F. 1973, *Ap. J.*, **184**, 461.

Gray, D. F. 1976, *The Observation and Analysis of Stellar Photospheres* (New York: Wiley) p. 400.

Gray, D. F. 1981, *Ap. J.*, **251**, 152.

Gray, D. F. 1978, *Solar Phys.*, **59**, 193.

Gray, D. F. 1984*a* *Ap. J.*, **277**, 640.

Gray, D. F. 1984*b* *Ap. J.*, **281**, 719.

Griffin, R. and R. 1979, *A Photometric Spectral Atlas of Procyon λλ 3140–7470 Å*, available from the authors at the Institute of Astronomy, The Observatories, Madingley Road, Cambridge CB3 0HA England.

Hartmann, L., Soderblom, D. R., Noyes, R. W., Burnham, N., and Vaughan, A. H. 1984, *Ap. J.*, **276**, 254.

Hauck, B. and Magnenat, P. 1975, in *Multicolor Photometry and the Theoretical HR Diagram*, ed. A. G. D. Philip and D. S. Hayes, *Dudley Obs. Report* #9, p. 171.

Hauck, B. and Mermilliod, M. 1980, *Astr. Ap. Suppl.*, **40**, 1.

Heasley, J. N. and Milkey, R. W. 1978, *Ap. J.*, **221**, 677.

Heinemann, K. 1926, *Astron. Nachr.* **227**, 193.

Hejlesen, P. M. 1980, *Astr. Ap. Suppl.*, **39**, 347.

Herbig, G. H. 1965, *Ap. J.*, **141**, 588.

Hertzsprung, E. 1947, *Ann. Leiden Obs.*, **19**, No. 1A.

Hlivak, R. J., Henry, J. P., and Pilcher, C. B. 1984, *S.P.I.E. Proceedings*, **445**,122.

Hlivak, R. J., Pilcher, C. B., Howell, R. R., Colucci, A. J., and Henry, J. P. 1982, *S.P.I.E. Proceedings*, **331**,96.

Hoffleit, D. 1964, *Catalogue of Bright Stars*, 3rd. ed. (New Haven: Yale Univ. Obs.).

Huang, S. S. 1953, *Ap. J.*, **118**, 285.

Janes, K. A. 1979, *Ap. J. Suppl.*, **39**, 135.

Joy, A. H. and Wilson, R. E. 1949, *Ap. J.*, **109**, 231.

Kelch, W. L., Linsky, J. L., and Worden, S. P. 1979, *Ap. J.*, **229**, 700.

Klein Wassink, W. J. 1927, Groningen Publ. No. 41.

Kraft, R. P. 1965, *Ap. J.*, **142**, 681.

Kraft, R. P. 1967, *Ap. J.*, **150**, 551.

Kurucz, R. L. 1979, *Ap. J. Suppl.*, **40**, 1.

LaBonte, B. J. and Rose, J. A. 1985, *Pub. A.S.P.*, **97**,790.

Linsky, J. L., Worden, S. P., McClintock, W., and Robertson, R. M. 1979, *Ap. J. Suppl.*, **41**, 47.

Lockwood, G. W., Thompson, D. T., Radick, R. R., Osborn, W. H., Baggett, W. E., Duncan, D. K., and Hartmann, L. W. 1984, *Pub. A.S.P.*, **96**, 714.

Mandel, J. 1964, *The Statistical Analysis of Experimental Data*, (New York: Dover), p. 288.

Marcy, G. W. 1982, in *Solar and Stellar Magnetic Fields: Origins and Coronal Effects* ed. J. O. Stenflo (Dordrecht: Reidel) p. 3.

Maeder, A. and Peytremann, E. 1972, *Astr. Ap.*, **21**, 279.

McGee, J. D., Khogali, I. A., Braun, W. A., and Kraft, R. P. 1967, *M.N.R.A.S.*, **137**, 303.

Mendoza V., E. E. 1967, *Bol. Obs. Tonanzintla y Tacubaya*, **4**, 149.

Michaud, G. 1986, *Ap. J.*, **302**, 650.

Middelkoop, F. 1982, *Astr. Ap.*, **107**, 31.

Morel, M., Bentollia, C., Cayrel, G., and Hauck, B. 1976, in *Abundance Effects in Classification*, I.A.U. Symposium No. 72, ed. B. Hauck and P. C. Keenan (Dordrecht: Reidel), p. 223.

Nissen, P. E. 1980, in *Star Clusters*, I.A.U. Symposium No. 85, ed. J. Hesser (Dordrecht: Reidel), p. 51.

Norris, J. 1971, *Ap. J. Suppl.*, **23**, 193.

Noyes, R. W. 1981, in *Solar Phenomena in Cool Stars and Stellar Systems*, ed. R. M. Bonnet and A. K. Dupree (Dordrecht: Reidel), p. 1.

Noyes, R. W., Hartmann, L. W., Baliunas, S. L., Duncan, D. K., and Vaughan, A. H. 1984, *Ap. J.*, **279**, 763.

O'Connell, R. W. 1973, *A.J.*, **78**, 1074.

Oke, J. B. and Conti, P. S. 1966, *Ap. J.*, **143**, 134.

Oranje, B. J. 1983, *Astr. Ap.*, **124**, 43.

Parker, E. N. 1979, *Cosmical Magnetic Fields* (Oxford: Clarendon Press).

Perrin, M.-N., Hejlesen, P. M., Cayrel de Strobel, G., and Cayrel, R. 1977, *Astr. Ap.*, **54**, 779.

Radick, R. R., Hartmann, L., Mihalas, D., Worden, S. P. 1982, *Pub. A.S.P.*, **94**, 934.

Radick, R. R., Lockwood, G. W., Thompson, D. T., Warnock, A., Hartmann, L., Mihalas, D., Worden, S. P., Henry, G. W., and Sherlin, J. M. 1983a, *Pub. A.S.P.*, **95**,621.

Radick, R. R., Wilkerson, M. S., Worden, S. P., Africano, J. L., Klimke, A., Ruden, S., Rogers, W., Armandroff, T. E., and Giampapa, M. S. 1983*b*, *Pub. A.S.P.*, **95**, 300.

Relyea, L. J. and Kurucz, R. L. 1978, *Ap. J. Suppl.*, **37**, 45.

Roberts, P. H. 1974, in *Solar Winds Three*, ed. C. T. Russell (Los Angeles: U.C.L.A. Institute of Geophysics and Planetary Physics), pg. 231.

Robinson, R. D. and Durney, B. R. 1982 *Astr. Ap.*, 108, 322.

Robinson, R. D., Worden, S. P., and Harvey, J. W. 1980, *Ap. J. (Letters)*, **236**, L155.

Rowse, D. P. and Roxburgh, I. W. 1981, *Solar Physics*, **74**, 165.

Roxburgh, I. W. 1983, in *Solar and Stellar Magnetic Fields: Origins and Coronal Effects* (I.A.U. Symp. 102), ed. J. O. Stenflo (Dordrecht: Reidel), p. 449.

Ruciński, S. M. and VandenBerg, D. A. 1986, *Pub. A.S.P.*, **98**, 669.

Rutten, R. G. M. 1984, *Astr. Ap.*, **130**, 353.

Rutten, R. G. M. 1985, *Cool Stars, Stellar Systems, and the Sun*,ed. M. Zeilik and D. M. Gibson (Berlin: Springer) p. 116.

Rutten, R. G. M. and Schrijver, C. J. 1985, *Cool Stars, Stellar Systems,and the Sun*, ed. M. Zeilik and D. M. Gibson (Berlin: Springer) p. 120.

Schatzman, E. 1962, *Ann. d'Ap.*, **25**, 18.

Schatzman, E. 1977, *Astr. Ap.*, **56**, 211.

Schlesinger, B. M. 1969, *Ap. J.*, **157**, 533.

Schmitz, F. and Ulmschneider, P. 1980, *Astr. Ap.*, **84**,191.

Schwarzschild, K. and Eberhard, G. 1913, *Ap. J.*, **38**, 292.

Simon, T., Herbig, G., and Boesgaard, A. M. 1985, *Ap. J.*, **293**, 551.

Skumanich, A. 1972, *Ap. J.*, **171**, 565.

Smith, M. A. 1976 *Ap. J.***203**, 603.

Smith, M. A. 1981 *Ap. J.***246**, 905.

Soderblom, D. R. 1982, *Ap. J.*, **263**, 239.

Soderblom, D. R. 1983, *Ap. J. Suppl.*, **53**, 1.

Soderblom, D. R. 1985, preprint.

Spite, F. and Spite, M. 1982, *Astr. Ap.*, **115**, 357.

Stauffer, J. R., Hartmann, L., Soderblom, D. R., and Burnham, N. 1984, *Ap. J.*, **280**, 202.

Stauffer, J. R. and Hartmann, L. 1986, *Ap. J. Suppl.*, **61**, 531.

Stein, R. F. 1981, *Ap. J.*, **246**, 966.

Strömgren, B. 1966, *Ann. Rev. Astr. Ap.*, **4**, 433.

Tonry, J. and Davis, M. 1979, *A.J.*, **84**, 1511.

Trumpler, R. J. 1938, *Lick Obs. Bull.*, **18**, 167.

Twarog, B. A. 1980, *Ap. J.*, **242**, 242.

Twarog, B. A. 1983, *Ap. J.*, **267**, 207.

van Bueren, H. G. 1952, *Bull. Astr. Inst. Netherl.*, **11**, 385.

van den Heuvel, E. P. J. 1969, *Pub. A.S.P.*, **81**, 815.

van den Heuvel, E. P. J. and Conti, P. S. 1971, *Science*, **171**, 895.

VandenBerg, D. A. 1983, *Ap. J. Suppl.*, **51**, 29.

VandenBerg, D. A. 1985, *Ap. J. Suppl.*, **58**, 711.

VandenBerg, D. A. and Bridges, T. J. 1984, *Ap. J.*, **278**, 679.

VandenBerg, D. A. and Bell R. A. 1985 *Ap. J. Suppl.*, **58**, 561.

Vaughan, A. H. 1980, *Pub. A.S.P.*, **92**, 392.

Vaughan, A. H. and Preston, G. W. 1980, *Pub. A.S.P.*, **92**, 385.

Vaughan, A. H., Preston, G. W., and Wilson, O. C. 1978, *Pub. A.S.P.*, **90**, 267.

Walter, F. M. 1983, *Ap. J.*, **274**, 794.

Walter, F. M. and Linsky, J. L. 1985, *Bull. A.A.S.*, **17**, 879.

Wilson, O. C. 1963, *Ap. J.*, **138**, 832.

Wilson, O. C. 1966, *Ap. J.*, **144**, 695.

Wilson, O. C. 1968, *Ap. J.*, **153**,221.

Wilson, O. C. 1978, *Ap. J.*, **226**,379.

Wolff, S. C. 1983, *The A-Type Stars: Problems and Perspectives* NASA SP-463.

Wolff, S. C., Boesgaard, A. M., and Simon, T. 1986, *Ap. J.*, **310**,360.

Wolff, S. C., Heasley, J. N., and Varsik, J. 1985, *Pub. A.S.P.*, **97**, 707.